Max Planck Graduate Center
mit der Johannes Gutenberg-Universität

JOHANNES GUTENBERG UNIVERSITÄT MAINZ

Synoptic Regimes and $\delta^{18}O$: A Model-Based Approach to Climate Variability

Dissertation

zur Erlangung des akademischen Grades

Doctor rerum naturalium (Dr. rer. nat.)

der Fachbereiche

08 - Physik, Mathematik und Informatik
09 – Chemie, Pharmazie, Geographie und Geowissenschaften
10 - Biologie
Universitätsmedizin

der

Johannes Gutenberg-Universität Mainz

vorgelegt von

Tim Martin Liesenhoff

Mainz, 06. Oktober 2025

Betreuer:
Prof. Dr. Denis Scholz

Zweitbetreuer:
Prof. Dr. Holger Tost

Tag der mündlichen Prüfung:
25.11.2025

Declarations Regarding the Dissertation

in accordance with the MPGC Doctoral Regulations

Institutionelle Zugehörigkeit / Affiliation

Deutsch: Speläothemforschung, Hochauflösende Paläoklimaforschung, Institut für Geowissenschaften, Fachbereich 09 Chemie, Pharmazie, Geographie und Geowissenschaften, Johannes Gutenberg-Universität Mainz.

English: Speleothem Research, Exogenous and Environmental Geosciences, Institute of Geosciences, Faculty 09: Chemistry, Pharmaceutical Sciences, Geography and Geosciences, Johannes Gutenberg University Mainz.

Förderung / Funding

Deutsch: Gefördert durch das Max Planck Graduate Center mit der Johannes Gutenberg-Universität Mainz (MPGC).

English: Funded by the Max Planck Graduate Center with the Johannes Gutenberg University Mainz (MPGC).

Declaration of Authorship

I hereby declare that I wrote the dissertation submitted without any unauthorized external assistance and used only sources acknowledged in the work. All textual passages which are appropriated verbatim or paraphrased from published and unpublished texts as well as all information obtained from oral sources are duly indicated and listed in accordance with bibliographical rules. In carrying out this research, I complied with the rules of standard scientific practice as formulated in the statutes of Johannes Gutenberg-University Mainz to insure standard scientific practice.

Place, Date: _____ Signature: _____

Acknowledgements

I would like to extend my sincere gratitude to the Max Planck Graduate Center (MPGC) for their financial support through a doctoral fellowship and for the invaluable networking opportunities and professional development seminars provided throughout my PhD. My deepest thanks go to my supervisors at the Johannes Gutenberg University Mainz for their expert guidance, insightful discussions, and numerous contributions to study design and data analysis. I also gratefully acknowledge the members of my working group for their constant support and collegial collaboration. I am indebted to the developers of the EMAC model for making their general circulation model publicly available, and to Johannes Gutenberg University Mainz for granting me access to the MOGON2 supercomputing infrastructure, which was essential for my high-resolution simulations. Finally, I owe my heartfelt appreciation to my family, especially my parents and my brother, for their unconditional encouragement and support in both the best of times and the most challenging moments.

Zusammenfassung der Dissertation

Diese Dissertation entwickelt einen innovativen, modellgestützten Ansatz zur physikalisch konsistenten Interpretation stabiler Sauerstoffisotope (δ^{18}O) in Speläothemen mit dem Ziel, großskalige atmosphärische Zirkulationsmuster und Niederschlagsprozesse vergangener Klimaperioden belastbar zu rekonstruieren. Zentral ist die Verknüpfung eines isotopenfähigen globalen Zirkulationsmodells (EMAC/H_2OISO) mit einer objektiven dynamischen Klassifikation großskaliger Wetterregimes (Diagnostic Synoptic Regime Model, DSRM). Ergänzt wird dieser Ansatz durch vier differenzierte Isotopengewichtungen: ungewichtete δ^{18}O-Werte des Niederschlags sowie niederschlags-, infiltrations- und kalzitgewichtete δ^{18}O, die jeweils unterschiedliche Prozesse der Signalentstehung abbilden. Für das heutige Klima wurden 30-jährige AMIP-konforme Simulationen durchgeführt und anhand von 12 deutschen GNIP-Stationen validiert. Dabei zeigte sich eine systematische Überschätzung der ungewichteten δ^{18}O-Werte um etwa 1 ‰ bis 3 ‰, welche durch Niederschlagsgewichtung weitgehend korrigiert werden konnte. Eine Hauptkomponentenanalyse ergab, dass Temperatur, Niederschlag und das vorherrschende synoptische Regime gemeinsam rund 50 % der Variabilität zwischen den Stationen erklären und somit deren zentrale Rolle bei der Steuerung isotopischer Signale unterstreichen. Unter Bedingungen des Letzten Glazialen Maximums (LGM) verändert sich die atmosphärische Zirkulation über Europa und dem Mittelmeerraum deutlich: Zonale Flüsse und zyklonale Regime nehmen ab, während meridionale Muster und antizyklonale Regime zunehmen. Der Abgleich modellierter δ^{18}O-Signale mit 14 mediterranen Speläothem-Datensätzen aus dem SISAL-Archiv zeigt, dass insbesondere infiltrations- und kalzitgewichtete Signale die beobachtete Proxy-Variabilität am besten reproduzieren. Im mediterranen LGM-Szenario führen zyklonale Regime zu ausgeprägter isotopischer Abreicherung, antizyklonale Hochdrucklagen hingegen zu Anreicherung. Eine markante Ost-West-Differenzierung spiegelt die unterschiedlichen Feuchtigkeitsquellen wider, welche für europäisch atlantische bzw. mediterrane Regionen charakteristisch sind. Die Ergebnisse belegen, dass die Kombination aus dynamischer Regimeklassifikation und physikalisch fundierter Isotopengewichtung eine robuste Rekonstruktion atmosphärischer Dynamik aus terrestrischen Speläothem-Archiven ermöglicht. Der Ansatz eignet sich sowohl für die Analyse heutiger Klimabedingungen als auch für komplexe glaziale Szenarien und liefert wertvolle Einblicke in die Kopplung von großskaliger Zirkulation, regionalem Hydroklima und isotopischer Signaturbildung in terrestrischen Sedimenten.

Abstract

This dissertation develops an innovative, model-based framework for the physically consistent interpretation of stable oxygen isotopes ($\delta^{18}O$) in speleothems, with the aim of robustly reconstructing large-scale atmospheric circulation patterns and precipitation processes of past climate periods. Central to this approach is the integration of an isotope-enabled general circulation model (EMAC/H_2OISO), an objective and dynamic classification of large-scale weather regimes (Diagnostic Synoptic Regime Model, DSRM), and four differentiated isotope weighting schemes (unweighted $\delta^{18}O$ in precipitation, precipitation-, infiltration-, and calcite-weighted $\delta^{18}O$), each representing distinct processes of signal formation. For present-day climate, 30-year AMIP-style simulations were conducted and validated against 12 German GNIP stations. These revealed a systematic overestimation of unweighted $\delta^{18}O$ values by approx. 1 ‰ to 3 ‰, which can largely be mitigated by applying precipitation weighting. A principal component analysis confirmed that temperature, precipitation, and the prevailing synoptic regime together explain approximately 50 % of the variability, underscoring their importance as key drivers of isotopic signals. Under Last Glacial Maximum (LGM) conditions, atmospheric circulation over Europe and the Mediterranean region shifts significantly: the frequency of zonal flows and cyclonic regimes decreases, while meridional patterns and anticyclonic regimes become more prevalent. A comparison of modeled $\delta^{18}O$ signals with 14 Mediterranean speleothem records from the SISAL database shows that infiltration- and especially calcite-weighted signals best reproduce observed proxy variability. In the Mediterranean LGM scenario, cyclonic regimes lead to pronounced isotopic depletion, while anticyclonic regimes result in isotopic enrichment. A pronounced east–west gradient reflects the contrasting moisture sources characteristic of the Atlantic and Mediterranean domains. The results demonstrate that the methodological combination of DSRM classification and physically motivated isotope weighting enables a robust and reproducible reconstruction of atmospheric dynamics from terrestrial speleothem archives. This framework is applicable to both modern climate analysis and complex glacial conditions, offering valuable insights into the coupling between large-scale circulation, regional hydroclimate variability, and isotopic signal formation in terrestrial sediments.

Contents

List of Figures

List of Tables

List of Abbreviations

2 m	2-meter air temperature
AMIP-IIc	Atmospheric Model Intercomparison Project, phase II
CFC	Chlorofluorocarbon
CH_4	Methane
CO_2	Carbon dioxide
$\delta^{18}O$	Delta notation for the isotope ratio $\frac{^{18}O}{^{16}O}$ (‰)
ζ	Shear–vorticity term in Lamb–type diagnostics
DSRM	Diagnostic Synoptic Regime Model
DWD	*Deutscher Wetterdienst* (German Weather Service)
EMAC	ECHAM5/MESSy Atmospheric Chemistry model
GCM	General Circulation Model
GNIP	Global Network of Isotopes in Precipitation
GWL	*Großwetterlagen*
H2OISO	EMAC submodel for stable water–isotopologues
ICS	International Commission on Stratigraphy
KMO	Kaiser–Meyer–Olkin test (sampling adequacy for factor analysis)
LGM	Last Glacial Maximum
MOGON2	MOGON2 supercomputer cluster (JGU Mainz)
MPI-OM	Max Planck Institute Ocean Model
NAO	North Atlantic Oscillation
PCA	Principal Component Analysis
PCP	Prior Calcite Precipitation
PET	Potential Evapotranspiration
PSM	Proxy System Model
RCM	Regional Climate Model
SIC	Sea Ice Concentration
SISAL	Speleothem Isotope Synthesis and Analysis database
SST	Sea Surface Temperature
STR	Straight Flow Regime (near–uniform zonal drift)
T106	Spectral truncation T106 (approx. 1.1° horizontal grid)
VPDB	Vienna Pee Dee Belemnite (carbonate isotope standard)
VSMOW	Vienna Standard Mean Ocean Water (water–isotope standard)

Editorial and Linguistic Abbreviations

e.g.	for example (Latin: *exempli gratia*)
i.e.	that is, in other words (Latin: *id est*)
etc.	and so on (Latin: *et cetera*)
cf.	compare (Latin: *confer*)
vs.	versus, in contrast to
approx.	approximately
et al.	and others (Latin: *et alii*)
p.	page
pp.	pages
Fig.	Figure
Eq.	Equation
Sec.	Section
Ch.	Chapter
No.	Number
Vol.	Volume
ka	thousand years (*kiloannum*)
BP	before present

1 Background and Motivation

Understanding how past climates varied and which atmospheric processes drove those changes remains a cornerstone of Earth-system science. Speleothems (stalagmites and flowstones) preserve high-resolution records of stable oxygen isotopes ($\delta^{18}O$) that integrate temperature, moisture source, and rainout history. Yet interpreting these signals demands a clear grasp of large scale circulation regimes. For example, in Europe, the *Großwetterlagen* (GWL) classification was developed as a framework to categorize synoptic regimes and their influence on regional hydroclimatic patterns [52]. Until now, links between different circulation regimes and $\delta^{18}O$ in precipitation have remained qualitatively acknowledged but quantitatively unexplored. Recent advances in isotope-enabled climate modeling help to bridge this gap. For instance, the ECHAM5/MESSy Atmospheric Chemistry (EMAC) model, when coupled with the H2OISO module, is capable of simulating $\delta^{18}O$ in precipitation under varying boundary conditions, including Pleistocene glacial and interglacial periods as well as the modern era. The quantification of the imprint of distinct weather regimes on speleothem isotopes remains largely unexplored and represents a rather niche area of research. This is primarily due to speleothem studies often relying on simplified climatic interpretations based on $\delta^{18}O$, such as one-dimensional relationships between $\delta^{18}O$ in precipitation and temperature or precipitation. This dissertation presents an effort to integrate isotope-enabled simulations with an objective synoptic classification, employing the Diagnostic Synoptic Regime Model (DSRM), which was specifically developed for this study series and is grounded in the Hess-Brezowsky *Großwetterlagen* (HB-GWL) framework. It comprises three comprehensive studies that build upon each other, tracing the progressive development and refinement of the DSRM.

The first study utilizes the EMAC model to investigate contemporary climate conditions. An objective classification of daily *Großwetterlagen* (GWL) types is applied using the Diagnostic Synoptic Regime Model (DSRM). Observational $\delta^{18}O$ in precipitation data from Global Network of Isotopes in Precipitation (GNIP) stations across Germany serve as a reference dataset for evaluating the simulated isotopic signatures [61]. Statistical analyses are employed to assess the relationships between simulated isotopes and relevant climatic and synoptic variables.

Building on this, the second study reconstructs *Großwetterlagen* (GWL) frequencies under Last Glacial Maximum (LGM) boundary conditions. To better represent karst recharge processes, an infiltration model was developed and incorporated into the Diagnostic Synoptic Regime Model (DSRM). This integration facilitates a more compre-

hensive evaluation of synoptic influences on regional hydroclimate. Comparison with European and Mediterranean δ^{18}O speleothem records from the Speleothem Isotope Synthesis and Analysis (SISAL) database [20] underscores the importance of weighted δ^{18}O representations in accurately capturing proxy variability and highlights the critical role of karst recharge dynamics under glacial forcing.

The third study applies the DSRM classification to an isotope-enabled EMAC simulation under Last Glacial Maximum (LGM) conditions, supplemented with isotope data from ten Mediterranean speleothems sourced from the Speleothem Isotope Synthesis and Analysis (SISAL) database [20]. The infiltration model is incorporated into the DSRM framework to facilitate regime-specific calculations, enabling a detailed examination of potential direct links between atmospheric circulation patterns and speleothem isotopic signals. This approach seeks to improve the interpretation of proxy records by accounting for the complex interplay of synoptic and hydrological processes that influence isotopic variability.

Together, these studies establish a unified framework for interpreting speleothem δ^{18}O in the context of dynamic synoptic processes; advancing our ability to reconstruct both interglacial and glacial climates.

2 Research Questions

Understanding the atmospheric controls on the stable oxygen isotope ratio $\delta^{18}O$ is essential for interpreting paleoclimate records and validating climate model simulations. This dissertation addresses key questions regarding the synoptic mechanisms that influence $\delta^{18}O$ variability across different climatic epochs, with a focus on both glacial and interglacial periods.

Application of the DSRM

The first study evaluates the performance of isotope-enabled climate simulations under modern conditions. It asks:

> *To what degree can EMAC/H2OISO simulations accurately reproduce observed $\delta^{18}O$ values in precipitation across Germany, and in what ways are these isotopic signatures influenced by objectively classified Großwetterlagen (GWL) circulation types?*

This question is addressed through linear regression and principal-component analyses comparing simulation output to GNIP observations, and by quantifying the joint influence of temperature, precipitation, and synoptic regime on isotopic variability.

Infiltration Submodel Integration within DSRM

The second study explores how glacial boundary conditions reshape circulation regimes and their isotope signatures. It asks:

> *Which mechanisms control $\delta^{18}O$ variability in precipitation during the Last Glacial Maximum, and to what extent can speleothem proxy records be reconstructed using unweighted, precipitation-weighted, infiltration-weighted, and calcite-weighted $\delta^{18}O$?*

This investigation uses LGM simulations classified by the DSRM, compares regime frequencies to modern analogues, and evaluates multiple isotope-weighting schemes against SISAL speleothem records.

Model Application to Speleothem Archives

Building on the LGM circulation diagnostics, the third study drills down into regional speleothem archives. It asks:

> *How do distinct synoptic regime types imprint on δ^{18}O signals in Mediterranean speleothems during the LGM, and which isotope-weighting scheme (precipitation-, infiltration-, or calcite-weighted δ^{18}O) best captures these regime-dependent variations?*

This question is addressed by compositing simulated δ^{18}O under each regime with three weighting approaches and comparing them directly to speleothem records to disentangle different isotopic fractionation effects.

Overarching Research Question

Synthesizing insights from modern and glacial climates, the dissertation addresses a single, unifying question:

> *How can synoptic-scale circulation diagnostics and isotope-enabled modeling be integrated into a consistent framework for interpreting speleothem δ^{18}O?*

Answering these questions provides a robust basis for improving paleoclimate reconstructions and deepening our understanding of atmospheric controls on δ^{18}O in precipitation.

3 Theoretical Foundations and Concepts

3.1 Stable Isotope Systems

Stable isotope systems refer to naturally occurring isotopes of chemical elements that do not undergo radioactive decay. These isotopes differ in mass but exhibit nearly identical chemical behavior, allowing them to participate in physical and chemical processes in predictable ways. The most commonly studied stable isotopes in climate and environmental sciences include those of hydrogen, oxygen, carbon, and nitrogen [89]. Isotopic fractionation occurs when physical processes such as evaporation, condensation, diffusion, or biological activity cause a preferential partitioning of lighter or heavier isotopes. This leads to measurable variations in isotope ratios between different reservoirs (e.g., atmosphere, ocean, biosphere) or phases (e.g., vapor, liquid, solid).

3.1.1 Stable Oxygen Isotope Systems

Stable oxygen isotopes, particularly ^{18}O and ^{16}O, are naturally occurring variants of oxygen that differ primarily in mass while exhibiting nearly identical chemical properties. However, their slight mass difference leads not only to subtle but significant variations in physical behavior but also affects isotopic fractionation processes during mineral formation. For example, different isotopes are preferentially incorporated into crystal structures such as calcite, resulting in measurable isotope-specific partitioning despite the chemical similarity. These mass-dependent effects influence how the isotopes participate in phase transitions such as evaporation and condensation, resulting in isotope fractionation that is sensitive to temperature and environmental conditions [24]. These properties make oxygen isotopes valuable tracers in hydrology, climatology, and paleoclimatology [102]. The ratio of ^{18}O to ^{16}O in water is commonly expressed using the delta notation $\delta^{18}O$, which quantifies the deviation of a sample's isotopic ratio from a standard reference material. This ratio is sensitive to environmental conditions and can be preserved in natural archives such as ice cores, lake sediments, and speleothems [49, 73, 80].

3.1.2 Oxygen Isotopes in the Global Water Cycle

The global water cycle governs the distribution and transformation of oxygen isotopes. During evaporation, lighter ^{16}O isotopes preferentially enter the vapor phase, leaving the residual water enriched in ^{18}O. As moist air masses move and cool, condensation occurs, and the heavier ^{18}O isotope is more likely to precipitate out. This leads to

Table 1: Overview of key fractionation processes affecting δ^{18}O in the global water cycle [71].

Process	**Effect on δ^{18}O (in precipitation)**
Evaporation	^{16}O preferentially evaporates; residual enriched in ^{18}O.
Condensation	^{18}O condenses more readily.
Rayleigh distillation	Progressive ^{18}O depletion.
Precipitation amount	Higher rainfall yields more depleted δ^{18}O.
Temperature	Lower temperatures correspond to more depleted δ^{18}O.
Altitude	^{18}O depletion with increasing elevation.
Latitude	Higher latitudes show more depleted δ^{18}O.
Moisture source	Vapor origin affects initial δ^{18}O.
Infiltration	Fractionation during infiltration alters δ^{18}O.
Mineralization	Temperature-dependent fractionation in minerals.

progressive depletion of ^{18}O in precipitation along the moisture trajectory; a process known as Rayleigh distillation [24]. Table 1 provides a conceptual overview of how climatic and environmental factors shape $\delta^{18}O$ signatures in precipitation and surface waters, offering a valuable framework for interpreting isotopic records in paleoclimate studies. These fractionation effects are modulated by climatic and geographic factors such as latitude, altitude, seasonality, and synoptic-scale atmospheric circulation [42]. Understanding these mechanisms is essential for interpreting isotopic signals in proxy archives and for developing physically consistent climate models that simulate isotope dynamics under varying boundary conditions.

3.2 Delta Notation and δ^{18}O

In geosciences, stable isotope ratios are typically expressed in delta notation (δ), which quantifies the relative difference between a sample and a standard reference material [21]. These ratios serve as powerful tracers for reconstructing environmental conditions, tracking water and carbon cycles, and interpreting paleoclimate signals preserved in natural archives such as ice cores, sediments, and speleothems.

3.2.1 Fundamentals of Oxygen Isotopes

The $\delta^{18}O$ value is calculated as shown in Equation 1:

$$\delta^{18}O = \left(\frac{R_{\text{sample}}}{R_{\text{standard}}} - 1 \right) \times 1000 \tag{1}$$

where R is the ratio $^{18}O/^{16}O$, and the standard is typically VSMOW (Vienna Standard Mean Ocean Water) [6]. Positive $\delta^{18}O$ values indicate enrichment in ^{18}O, often associated with evaporation or warmer conditions, while negative values reflect depletion, typically linked to condensation, colder or wetter conditions [24, 116]. In climate science, $\delta^{18}O$ serves as a proxy for reconstructing past temperature and precipitation patterns. Its interpretation requires an understanding of the processes that influence isotopic fractionation, including temperature gradients, moisture sources, and atmospheric transport pathways.

3.2.2 Standards and Reference Materials

The interpretation of stable isotope ratios requires comparison to internationally recognized reference materials. For oxygen isotopes in water, the most commonly used standard is VSMOW (Vienna Standard Mean Ocean Water), which provides a consistent baseline for reporting $\delta^{18}O$ values [6]. In carbonate-based archives such as speleothems, the VPDB (Vienna Pee Dee Belemnite) standard is often used, and values can be converted to VSMOW for intercomparison [30]. These standards ensure comparability across laboratories and studies, allowing for the integration of observational datasets and simulation outputs. Accurate calibration against reference materials is essential for assessing environmental signals and for validating climate reconstructions based on isotopic proxies.

3.2.3 Applications in Climate Science

The isotopic ratio $\delta^{18}O$ is extensively used in climate science as a proxy to reconstruct past variations in temperature, precipitation, and atmospheric circulation patterns. $\delta^{18}O$ in precipitation reflects the integrated effects of moisture source, transport history, and local meteorological conditions [24]. In speleothems, the isotopic composition of calcite records the $\delta^{18}O$ of infiltrating water, modulated by cave temperature and hydrological filtering [71, 112] [81]. These applications span both modern observational networks and paleoclimate archives. In contemporary settings, $\delta^{18}O$ measurements in

precipitation (e.g., Global Network of Isotopes in Precipitation (GNIP)) provide insights into seasonal and synoptic variability [61]. In paleoclimate research, speleothem records offer high-resolution reconstructions of hydroclimatic conditions over millennial timescales [20].
Isotope-enabled climate models simulate $\delta^{18}O$ dynamics within the hydrological cycle, allowing for direct comparison with proxy data. This integration supports the interpretation of isotopic signals in terms of physical climate processes and enhances the robustness of climate reconstructions across different temporal and spatial scales [117].

3.3 Speleothems

Speleothems, also known as cave carbonates, are among the most important terrestrial archives for reconstructing past climate conditions. Their layered growth, mineral composition, and geochemical signatures provide high-resolution records of environmental variability over timescales ranging from decades to hundreds of thousands of years [20, 80]. In particular, speleothems are widely used in paleoclimatology due to their ability to preserve stable isotope signals, especially $\delta^{18}O$ and $\delta^{13}C$ [100].

3.3.1 Formation and Mineralogy

Speleothems form through the precipitation of calcium carbonate ($CaCO_3$) from drip water in karst caves [33]. This water originates from meteoric precipitation that infiltrates through soil and carbonate bedrock, dissolving minerals along its path. Upon entering the cave atmosphere, CO_2 degasses from the water, leading to supersaturation and the precipitation of calcite or, less commonly, aragonite. The mineralogical composition of speleothems is influenced by cave-specific factors such as temperature, humidity, CO_2 concentration, and drip rate. These conditions also affect the incorporation of stable isotopes and trace elements into the calcite matrix, making speleothems sensitive indicators of past environmental conditions [34].

3.3.2 Geographical Occurrence

Speleothems are found in karst regions worldwide, where soluble carbonate rocks such as limestone and dolomite dominate the geology. Their occurrence spans a wide range of climatic zones, from tropical to temperate and even semi-arid environments, thus making them suitable for reconstructing regional climate variability across diverse settings [33]. The SISAL database, which compiles speleothem $\delta^{18}O$ records, reveals a particularly high density of speleothem datasets in Europe, with key concentrations in

the Alps, the Balkans, and the Mediterranean basin. These regions provide well-dated and high-resolution archives that span glacial and interglacial periods, offering insights into hydroclimatic changes over long timescales [20].

3.3.3 Speleothems and Stable Isotope Systems

Speleothems preserve stable isotope signals, especially δ^{18}O and δ^{13}C, which are widely used in paleoclimate research. The δ^{18}O value in speleothem calcite reflects the isotopic composition of infiltrating water, modulated by cave temperature and hydrological processes such as evaporation, mixing, and residence time in the karst system [112]. Interpreting speleothem isotope records requires consideration of seasonal biases, moisture source variability, and synoptic-scale atmospheric dynamics. Weighting schemes, such as precipitation-weighted or infiltration-weighted δ^{18}O, help approximate the effective signal recorded in the calcite. These records thus serve as integrative proxies linking surface climate variability with subsurface hydrology [33, 34].

3.4 Synoptic Classification

Synoptic classification systematically categorizes large-scale atmospheric circulation patterns based on pressure, wind, and vorticity. This approach is key to understanding weather dynamics and their impact on regional climate variability [52]. By grouping recurring circulation types, it facilitates long-term climate analysis and aids meteorological and hydrological data interpretation [67, 72].

3.4.1 Pressure Systems

Atmospheric pressure systems are fundamental components of synoptic meteorology. High-pressure systems (anticyclones) are typically associated with descending air, clear skies, and stable weather conditions. In contrast, low-pressure systems (cyclones) involve ascending air, cloud formation, and precipitation. The spatial distribution and movement of these systems govern the transport of air masses and moisture, influencing local and regional climate.

Pressure systems are identified through surface pressure fields and geopotential height maps. Their evolution is driven by thermal gradients, planetary wave dynamics, and interactions with topography and oceanic conditions. Understanding pressure systems is crucial for interpreting weather patterns and for classifying synoptic regimes [67, 72].

3.4.2 Synoptic Patterns in Europe and Mid-Latitudes

In the mid-latitudes, including Central and Western Europe, synoptic patterns are dominated by westerly flow, frontal systems, and seasonal shifts in jet stream position. These regions experience a wide range of circulation types, from zonal (west–east) to meridional (north–south) flows, each with distinct impacts on temperature and precipitation. As an example, distinct synoptic regimes, such as zonal and meridional flows, generate markedly different precipitation patterns across southern Europe, underscoring the climatic significance of circulation type classification [26].

Synoptic variability in Europe is further influenced by large-scale modes such as the North Atlantic Oscillation (NAO), which modulates both the strength and latitudinal position of the westerlies. The prevailing westerlies in the mid-latitudes facilitate the regular eastward movement of cyclones from the North Atlantic toward Europe, contributing significantly to regional precipitation and temperature variability. Cyclonic regimes are generally associated with ascending air masses, enhanced cloud formation, and increased precipitation, often resulting in mild and humid conditions. In contrast, anticyclonic regimes are characterized by descending air and atmospheric stability, leading to dry conditions that may be accompanied by either cold or hot temperatures depending on the season. These circulation patterns play a crucial role in shaping the hydrological cycle and in modulating the distribution of climate-sensitive variables across Europe.

3.4.3 Classification Systems in Europe

Several objective classification systems have been developed to categorize synoptic regimes in Europe. The most widely used is the *Großwetterlagen* (GWL) system, established by Hess and Brezowsky in the 1960s [52]. It defines 29 circulation types based on surface pressure patterns, geopotential height configurations, and flow directions over Central Europe, grouped into zonal, meridional and mixed categories. Another prominent classification is the Lamb Weather Type (LWT) system, developed by Lamb in the 1970s [72], which derives flow direction and vorticity parameters from sea-level pressure data over the British Isles. Both systems are applied in climatological studies to analyze the frequency and variability of circulation types and their relationship to temperature, precipitation, and other climate indicators [53, 66, 67]. Synoptic classification provides a framework for linking atmospheric dynamics to observed climate signals. It enables the identification of regime shifts, seasonal patterns, and long-term trends in circulation behavior, contributing to a deeper understanding of regional climate variability.

Lamb Weather Type (LWT) Classification

The Lamb Weather Type (LWT) classification is an objective system originally developed by Lamb for the British Isles [72]. It categorizes daily atmospheric circulation based on sea-level pressure data at predefined grid points. The classification uses parameters such as flow direction, vorticity, and pressure gradients to determine the prevailing weather type. LWT types are divided into directional flows (e.g., northerly, westerly, easterly), cyclonic, anticyclonic, and unclassified patterns. This system allows for high-resolution analysis of daily weather regimes and is particularly useful for studying regional climate variability and the impact of circulation types on meteorological conditions. The LWT classification has been widely adopted in climatological research across Europe due to its flexibility and objectivity [66, 67]. It supports the identification of dominant circulation patterns, seasonal shifts, and long-term changes in atmospheric behavior, making it a key tool in synoptic climatology. An overview of the individual LWT types and their abbreviations is provided in Table 2.

Table 2: Lamb Weather Type (LWT) classification system, categorizing synoptic-scale weather patterns over the British Isles into anticyclonic (A), directional, and cyclonic (C) types based on prevailing wind direction and pressure characteristics.

Base Direction	**Types**
Northeasterly (NE)	ANE, CNE
Easterly (E)	AE, CE
Southeasterly (SE)	ASE, CSE
Southerly (S)	AS, CS
Southwesterly (SW)	ASW, CSW
Westerly (W)	AW, CW
Northwesterly (NW)	ANW, CNW
Northerly (N)	AN, CN
No direction	A, C

Großwetterlagen (GWL) Classification

The *Großwetterlagen* (GWL) classification is a traditional synoptic system developed by Hess and Brezowsky [52] to categorize large-scale circulation patterns over Central Europe. It defines 29 distinct weather types based on surface pressure configurations and prevailing flow directions. These circulation types are classified into three principal categories: zonal (westerly flow), meridional (north–south or easterly flow), and mixed regimes. Each GWL type reflects characteristic atmospheric conditions and typically

persists for several days. The classification is widely used in climatology and meteorology to analyze long-term trends, seasonal variability, and the influence of circulation types on temperature, precipitation, and other climate variables. By linking surface pressure fields to regional weather outcomes, the GWL system provides a valuable framework for understanding synoptic-scale climate dynamics in Central Europe; an overview of the individual GWL types and their definitions is provided in Table 3.

3.5 Climatological Parameters

Climatological parameters are essential variables used to describe and analyze the state and variability of the Earth's atmosphere and surface conditions. They provide quantitative insights into temperature, precipitation, pressure, and moisture dynamics, which are fundamental for understanding weather patterns, climate processes, and environmental interactions. These parameters are typically derived from observational datasets and climate models, and they serve as the basis for evaluating seasonal trends, long-term changes, and the impacts of atmospheric circulation on regional climates.

3.5.1 2m Temperature

The 2-meter air temperature is a standard meteorological variable representing the ambient temperature measured approximately two meters above the ground surface. It is influenced by factors such as solar radiation, cloud cover, surface albedo, and atmospheric circulation. This parameter is crucial for assessing thermal conditions near the surface and is widely used in climate monitoring, weather forecasting, and impact studies related to agriculture, health, and energy demand [48, 76, 105].

3.5.2 Precipitation

Precipitation encompasses all forms of water, liquid or solid, that fall from the atmosphere to the Earth's surface, including rain, snow, sleet, and hail. It is a key component of the hydrological cycle and directly affects soil moisture, river discharge, and vegetation dynamics. Precipitation patterns are governed by atmospheric moisture content, vertical motion, and synoptic-scale circulation. Long-term precipitation data are essential for evaluating droughts, floods, and climate variability [29, 98, 109].

Table 3: Classification of European synoptic-scale weather patterns according to the *Großwetterlagen* (GWL) system. Each code represents a distinct circulation type, characterized by dominant pressure systems and prevailing wind directions.

GWL Code	**Definition**
Zonal	
WA	Anticyclonic westerly
WZ	Cyclonic westerly
WS	Southern westerly
WW	Angled westerly (Eastern European blocking)
Mixed	
SWA	Anticyclonic southwesterly
SWZ	Cyclonic southwesterly
NWA	Anticyclonic northwesterly
NWZ	Cyclonic northwesterly
HM	High pressure over Central Europe
BM	Ridge across Central Europe
TM	Low pressure over Central Europe
Meridional	
NA	Anticyclonic northerly
NZ	Cyclonic northerly
HNA	Icelandic high, anticyclonic
HNZ	Icelandic high, cyclonic
HB	High pressure over the British Isles
TRM	Trough over Central Europe
NEA	Anticyclonic northeasterly
NEZ	Cyclonic northeasterly
HFA	Scandinavian high, ridge over Central Europe
HFZ	Scandinavian high, trough over Central Europe
HNFA	High Scandinavia–Iceland, anticyclonic
HNFZ	High Scandinavia–Iceland, cyclonic
SEA	Anticyclonic southeasterly
SEZ	Cyclonic southeasterly
SA	Anticyclonic southerly
SZ	Cyclonic southerly
TB	British Isles cyclonic system
TRW	Trough over Western Europe
Unclassified	
U	Unclassified

3.5.3 Surface Pressure

Surface pressure refers to the atmospheric pressure exerted at the Earth's surface, typically measured in hectopascals (hPa). It reflects the weight of the air column above a given location and is a fundamental variable in synoptic meteorology. Variations in surface pressure are associated with the development and movement of high- and low-pressure systems, which in turn influence wind patterns, temperature, and precipitation. Surface pressure maps are used to identify weather fronts and track cyclones and anticyclones [5, 38].

3.5.4 Evaporation

Evaporation is the process by which water is transformed from liquid to vapor and transferred from the Earth's surface to the atmosphere. It is driven by solar radiation, air temperature, wind speed, and humidity. Evaporation plays a vital role in the water balance and energy exchange between the surface and the atmosphere. It affects soil moisture, plant transpiration, and the formation of clouds, making it a key variable in both hydrological and climatological studies [41, 77, 78].

3.5.5 Isotope Ratios

Isotope ratios, particularly of oxygen (δ^{18}O) and hydrogen (δ^{2}H), are used as tracers in climatology and hydrology to study the origin and transformation of water masses. These ratios vary with temperature, altitude, and precipitation processes, providing insights into past and present climate conditions. Isotopic composition in precipitation and surface waters can reveal information about moisture sources, evaporation rates, and atmospheric circulation patterns. Isotope analysis is a valuable tool in paleoclimatology and environmental monitoring [42, 71, 80, 89].

3.6 Climate Modeling

Climate modeling is a fundamental tool in atmospheric science used to simulate and understand the behavior of the Earth's climate system. Models integrate physical, chemical, and biological processes to represent interactions between the atmosphere, oceans, land surface, and cryosphere. They are essential for studying past climate variability [13], projecting future climate scenarios [107], and assessing the impacts of anthropogenic influences [64].

3.6.1 History of Climate Modeling

The development of climate models began in the mid-20th century with simple energy balance models [16, 101] and gradually evolved into complex general circulation models (GCMs) [118]. Early models focused on radiative transfer and global temperature equilibrium, while later generations incorporated dynamic representations of atmospheric and oceanic circulation. Advances in computational power and observational data have enabled the creation of Earth system models (ESMs), which include biogeochemical cycles and feedback mechanisms [19, 23]. Today, climate models are central to international assessments such as those conducted by the Intergovernmental Panel on Climate Change (IPCC) [54, 62].

3.6.2 Isotope-Enabled Climate Modeling

Isotope-enabled climate models simulate the transport and fractionation of stable isotopes, such as δ^{18}O and δ^{2}H, within the hydrological cycle [83]. These models allow researchers to link climate dynamics with isotopic signatures found in natural archives like ice cores [40], tree rings [10], and speleothems [57]. By incorporating isotopic tracers, models can improve the interpretation of paleoclimate records and validate hydrological processes [117]. Isotope-enabled modeling also helps to identify moisture sources, track precipitation pathways, and assess evaporation and condensation effects under varying climate conditions [18, 69].

3.6.3 Advantages and Limitations

Climate models offer powerful insights into the functioning of the climate system and its response to external forcings. They enable scenario-based projections, sensitivity analyses, and the evaluation of mitigation strategies. However, models are subject to limitations due to uncertainties in parameterizations, spatial resolution, and initial conditions [97]. Simplifications of complex processes and incomplete knowledge of feedbacks can affect model accuracy [55]. Isotope-enabled models add further complexity but provide valuable constraints for validating hydrological and climatic processes [117]. Continuous model development and comparison with observational data are essential for improving reliability and robustness.

3.7 Geological Time Scale

The geological time scale is a hierarchical system used to describe the timing and relationships of events in Earth's history [47]. It is divided into eons, eras, periods, epochs, and ages, based on significant changes in Earth's geology, climate, and life forms. This framework is essential for interpreting paleoclimate records and understanding long-term environmental evolution [47]. The most recent era, the Cenozoic Era, began about 66 million years ago and is subdivided into three periods: the Paleogene, Neogene, and Quaternary. The Quaternary Period, which started approximately 2.6 million years ago and continues to the present, is particularly relevant for climate research due to its pronounced variability and the availability of high-resolution climate archives.

Quaternary Period

The Quaternary Period is the most recent geological period, spanning from approximately 2.6 million years ago to the present. It is part of the Cenozoic Era and is subdivided into two formally recognized epochs: the Pleistocene and the Holocene. The Quaternary is characterized by dramatic climatic fluctuations, including repeated glacial-interglacial cycles, and the emergence and expansion of human civilizations. It provides a crucial framework for paleoclimate research, as it encompasses the most detailed and accessible climate archives.

3.7.1 Pleistocene Epoch

The Pleistocene epoch extends from about 2.6 million to 11,700 years ago. It is defined by the presence of extensive glaciations, with large ice sheets periodically covering much of the Northern Hemisphere. These cycles of glacial advance and retreat significantly influenced global climate, sea levels, and ecosystems [87]. The Pleistocene also saw the evolution and dispersal of Homo sapiens and other hominins [106]. Climate variability during this epoch is well documented in ice cores [115], marine sediments [56], and terrestrial records [3], offering insights into natural climate drivers and feedback mechanisms.

Last Glacial Maximum (LGM)

The Last Glacial Maximum occurred around 21,000 years ago, during the late Pleistocene. It marks the peak of the last glacial cycle, when ice sheets reached their maximum extent. Global temperatures were significantly lower, and sea levels were

approximately 120 meters below present levels. The LGM is a key reference point in paleoclimate studies, used to validate climate models [86] and understand the Earth's response to changes in orbital forcing and greenhouse gas concentrations [103].

3.7.2 Holocene Epoch

The Holocene began approximately 11,700 years ago, following the end of the last glaciation. It is characterized by relatively stable and warm climatic conditions, which facilitated the development of agriculture, urbanization, and complex societies. The Holocene includes notable climate events such as the Holocene Thermal Maximum, the Medieval Warm Period, and the Little Ice Age. This epoch provides the baseline for understanding pre-industrial climate variability and serves as a reference for assessing modern anthropogenic climate change.

Anthropocene (Informal Epoch)

The Anthropocene is a proposed informal epoch that describes the period from the late 19th century to the present, during which human activities have become the dominant influence on Earth's climate and ecosystems [22]. Although not yet formally recognized within the geologic time scale, the Anthropocene concept highlights the unprecedented rate of environmental change driven by industrialization, fossil fuel combustion, deforestation, and urban expansion. This period is marked by rising greenhouse gas concentrations, global warming, and biodiversity loss, and is central to discussions on sustainability and climate policy [74].

4 Summary

Over the course of three interconnected studies, a unified framework has been developed, validated, and applied to link large-scale atmospheric circulation to the oxygen-isotope composition (δ^{18}O) of precipitation and speleothem calcite. At its core, the methodology combines an isotope-enabled general circulation model (EMAC/H_2OISO), an objective synoptic-classification algorithm (Diagnostic Synoptic Regime Model, DSRM, based on Lamb parameters and the Hess–Brezowsky *Großwetterlagen* catalog) [52, 72], and a suite of isotope-weighting schemes (unweighted averages, precipitation- and infiltration-weighted signals, plus a memory-based calcite model with temperature-dependent fractionation). This stepwise approach advances from modern-day validation (*Investigation of the Links Between Weather Patterns and Climate Parameters Including $\delta^{18}O$ Using Simulation Data*), through Last Glacial Maximum (LGM) diagnostics (*Synoptic Regime Shifts and $\delta^{18}O$ Variability During the Last Glacial Maximum: Insights from Isotope-Enabled Climate Simulations and Speleothem Proxy Comparisons*), to regime-specific cave-site interpretations (*Synoptic Controls on Speleothem $\delta^{18}O$ During the Last Glacial Maximum*).

In the first study, the Diagnostic Synoptic Regime Model (DSRM) classification was employed to identify circulation types, and the EMAC/H_2OISO model was evaluated using 30 years of AMIP-style modern simulations covering Germany. Daily sea-level pressure fields were sorted into 29 Hess–Brezowsky weather types via an automated DSRM procedure sampling six subgrids (British Isles, Iceland, Azores, Eastern Europe, Scandinavia, Central Europe). Monthly anomalies of simulated temperature, precipitation and δ^{18}O in precipitation were systematically compared to observations from 12 GNIP stations [61]. The simulated climatologies successfully captured the broad spatial patterns of temperature and precipitation but consistently overestimated δ^{18}O values by approximately 1 ‰ to 3 ‰. Principal component analysis showed that the leading component (accounting for roughly 50 % of variance) couples temperature, precipitation and δ^{18}O in precipitation, while subsequent components isolate circulation frequency and the NAO index. These results validated the ability of our framework to capture modern synoptic–isotope linkages and established a baseline for paleoclimate proxy evaluation.

Building on that foundation, the second study applied the identical DSRM–EMAC setup to the LGM (30-year runs under glacial boundary conditions including reduced greenhouse gases, altered SST/SIC). Comparing simulated GWL frequencies between present day and LGM revealed a pronounced migration away from zonal cyclonic

regimes toward more persistent anticyclonic and meridional regimes, accompanied by a decrease in transitional flows. Spatial analyses of δ^{18}O in precipitation, temperature, precipitation, and sea-level pressure revealed coherent gradients, while also indicating a persistent model bias over the Bay of Biscay, suggestive of a localized discrepancy in simulation performance. Regression was performed against fourteen speleothem δ^{18}O records from the SISAL database [20], testing four isotope-weighting schemes: unweighted δ^{18}O in precipitation, precipitation-weighted δ^{18}O, infiltration-weighted δ^{18}O, and calcite-weighted δ^{18}O. Calcite-weighted δ^{18}O exhibits the closest agreement with observational data, characterized by a negligible mean difference of -0.0065 ‰ and an insignificant t-test result ($t = -0.0086$, $p = 0.9933$). This close agreement underscores the robustness of calcite-weighting in capturing the isotopic signature recorded in speleothems, highlighting its value for accurately linking simulated isotopic signals with proxy records under glacial conditions.

The third study then focused on regime-dependent isotope signatures at ten Mediterranean cave sites during the LGM. Daily DSRM classification of LGM sea-level pressure fields was used to produce regime composites for each cave, from which monthly δ^{18}O anomalies were computed via unweighted, precipitation-, infiltration-, and calcite-weighted approaches. It was found that pronounced δ^{18}O depletion in precipitation is produced by strongly cyclonic regimes, marked by intense, amount-driven rainfall, whereas δ^{18}O enrichment in precipitation is generated by anticyclonic patterns characterized by low rainfall, high evaporation, and water-vapor recycling. Eastern and western Mediterranean cave sites exhibit distinct moisture source characteristics. Western locations are influenced by enhanced cyclonic activity and substantial moisture input via westerly Atlantic flow, which reinforces the isotopic amount effect in δ^{18}O records. In contrast, eastern sites are predominantly shaped by recycled and locally sourced Mediterranean moisture, resulting in enriched δ^{18}O values.

Taken together, these three studies chart a coherent research trajectory: calibrating an isotope-enabled synoptic framework in the modern climate, diagnosing circulation and isotope shifts during the LGM, and resolving cave-site isotope signals in a regime-specific context. This progressive workflow demonstrates that large-scale atmospheric regimes, hydrological filtering and speleothem growth dynamics must all be accounted for to yield reliable paleoclimate reconstructions.

5 Application of the DSRM

Investigation of the Links Between Weather Patterns and Climate Parameters Including $\delta^{18}O$ Using Simulation Data (manuscript in preparation)

Specific Contribution Summary

The foundational concept of the study was developed by Holger Tost and Denis Scholz. All simulation data were processed by Tim Liesenhoff and Holger Tost. Tim Liesenhoff carried out the regime classification across all datasets and developed the source code for the DSRM. The interpretation of results was a joint effort by Tim Liesenhoff, Holger Tost, and Denis Scholz, with Tim Liesenhoff assuming a leading role. He also coordinated and led the writing of the manuscript.

5.1 Background and Objectives

Large-scale atmospheric circulation patterns exert a fundamental influence on the spatial and temporal variability of meteorological conditions across Central Europe [72, 91, 92]. These synoptic-scale regimes govern not only surface temperature and precipitation dynamics, but also the isotopic composition of precipitation, particularly the ratio of stable oxygen isotopes (δ^{18}O in precipitation). The latter serves as a critical proxy in paleoclimatology, offering insights into past hydroclimatic conditions through its preservation in natural archives such as speleothems, ice cores, and lake sediments [8, 20, 112].

The interpretation of δ^{18}O signals in precipitation, however, is inherently complex. It requires a nuanced understanding of the atmospheric processes that modulate isotopic fractionation, including moisture source variability, transport pathways, condensation temperature, and the influence of synoptic-scale circulation [31, 65]. In mid-latitude regions, such as Central Europe, the interplay between westerly flow regimes, frontal systems, and seasonal shifts in jet stream position introduces substantial variability in both meteorological and isotopic parameters [58, 60]. Despite the recognized importance of synoptic dynamics, the relationship between specific circulation types, such as those defined by the Hess-Brezowsky *Großwetterlagen* (GWL) system, and δ^{18}O variability in

precipitation remains insufficiently quantified. Traditional GWL classifications, though widely applied, depend on subjective interpretation and lack the objective framework needed for seamless integration with climate model outputs [52, 53]. To address this gap, the present study introduces a novel classification framework: the Diagnostic Synoptic Regime Model (DSRM). This model builds upon the GWL system by applying objective criteria derived from regional sea-level pressure fields, enabling reproducible and automated classification of daily weather regimes [12, 63].
Using a 30-year simulation dataset generated by the isotope-enabled ECHAM5/ MESSy Atmospheric Chemistry (EMAC) model [68, 117], this study applies the DSRM framework to classify synoptic regimes and analyze their associations with climate parameters including temperature, precipitation, and δ^{18}O in precipitation. Observational data from 12 GNIP stations across Germany [61] serve as a validation benchmark, allowing for a robust comparison between simulated and measured values. The overarching objectives of this study are as follows:

1. To develop and apply an objective classification scheme (DSRM) for synoptic regimes based on GWL principles and regional SLP diagnostics.

2. To quantify the statistical relationships between circulation types and climate parameters (T, P, δ^{18}O), including seasonal variability and regime-specific anomalies.

3. To evaluate the performance of the EMAC model in reproducing observed modern isotopic and meteorological patterns, with emphasis on precipitation-weighted δ^{18}O.

4. To identify the dominant drivers of climate variability through principal component analysis (PCA), distinguishing between physical interactions and synoptic influences, such as the North Atlantic Oscillation (NAO).

This study integrates synoptic classification with isotope-enabled modeling and observational validation to establish a physically consistent framework for interpreting δ^{18}O in precipitation under modern climate conditions. The findings will inform the use of speleothem-based proxies in paleoclimate reconstruction and contribute to the broader understanding of atmospheric controls on stable isotope variability.

5.2 Methods and Data

Table 4: Atmospheric forcing parameters applied in the simulation dataset. Modern Day values follow Wackerbarth et al. [112].

Simulation Parameter	Description
Base Parameters	
Simulation Interval	0-40 / 10-30 (excluding spin-up)
Horizontal Resolution	T106 (1.12° at the equator)
Vertical Resolution	L31ECMWF (31 vertical levels up to 0.01 hPa)
Orbital Forcing	
Orbital Parameters	Keplerian orbital configuration
Atmospheric Forcing	
CO_2	348 ppm
CH_4	1.650 ppm
NO_x	0.306 ppm
CFCs	262 ppt (CFC1) / 540 ppt (CFC2)
Oceanic Forcing	
SST	Prescribed modern SST climatology (AMIP2)
SIC	Prescribed modern SIC climatology (AMIP2)

5.2.1 Simulation Configuration

To investigate the relationship between synoptic-scale circulation patterns and climate parameters, this study employs a 40-year simulation dataset, excluding a 10-year spin-up phase to ensure equilibrium conditions. The simulations were conducted using the isotope-enabled ECHAM5/MESSy Atmospheric Chemistry (EMAC) model [68, 117], which integrates the H2OISO module for tracking stable water isotopologues throughout the hydrological cycle [31]. The model operates at T106 spectral resolution, corresponding to a horizontal grid spacing of approximately 1.1°, and includes 31 vertical layers (L31ECMWF) extending from the surface to the stratosphere (0.01 hPa). Boundary conditions are prescribed using climatological datasets from AMIP-IIc [43], including sea surface temperature (SST) and sea ice concentration (SIC). Orbital parameters follow Keplerian dynamics consistent with present-day configurations. Atmospheric trace gases such as CO_2, CH_4, NO_x, and CFCs are prescribed based on observational records representative of the simulation period [112]. A detailed overview of all applied forc-

ing parameters, including orbital, atmospheric, and oceanic components, is provided in Table 4. These settings ensure physical consistency with the modern climate state and allow for direct comparison with observational datasets.

Validation of the model output is performed using data from 12 GNIP (Global Network of Isotopes in Precipitation) stations distributed across Germany [61]. These stations provide high-resolution records of temperature, precipitation, and δ^{18}O in precipitation, enabling robust evaluation of the model's performance. The H2OISO module plays a central role in this setup, enabling the explicit simulation of fractionation processes during evaporation, condensation, and transport. By resolving the behavior of $H_2^{16}O$ and $H_2^{18}O$ across all phases of the water cycle, the model facilitates direct comparison between simulated δ^{18}O values in precipitation and empirical isotope data, thereby linking atmospheric dynamics with geochemical proxies.

5.2.2 Synoptic Classification

A central methodological innovation of this study is the development and application of the Diagnostic Synoptic Regime Model (DSRM). This model builds upon the Lamb Weather Type (LWT) classification system [66, 72] and the Hess-Brezowsky *Großwetterlagen* (HB-GWL) framework [52, 53], adapting and extending them to objectively classify daily synoptic regimes over Central Europe. The classification begins with the definition of six regional subgrids spanning key areas across the North Atlantic and Europe; namely Western Europe, Iceland, the Azores, Eastern Europe, Scandinavia, and Central Europe. Each subgrid contains 16 systematically arranged reference points used for extracting daily sea-level pressure (SLP) values from climate model output. The spatial configuration of these subgrids and reference points is illustrated in Figure 1, which provides a visual overview of the diagnostic framework applied in this study. The color-coded subgrids help distinguish regional circulation influences and ensure spatial coverage of dominant pressure centers.

Using the Lamb methodology, geostrophic flow components are calculated from the pressure fields, specifically the zonal (westerly) and meridional (southerly) components [66, 72]. These are combined to determine the resultant flow direction and magnitude. In parallel, shear vorticity is derived to assess whether the flow exhibits cyclonic or anticyclonic curvature. Based on these diagnostics, each day is assigned a circulation type according to the extended Lamb scheme, which includes 27 distinct types such as pure directional flows (e.g., N, NE, SW), cyclonic (C), anticyclonic (A), and hybrid forms (e.g., CNW, ASW). To ensure regional applicability, the Lamb-type diagnostics were recalibrated for Central Europe [63]. The underlying classification logic is visualized in

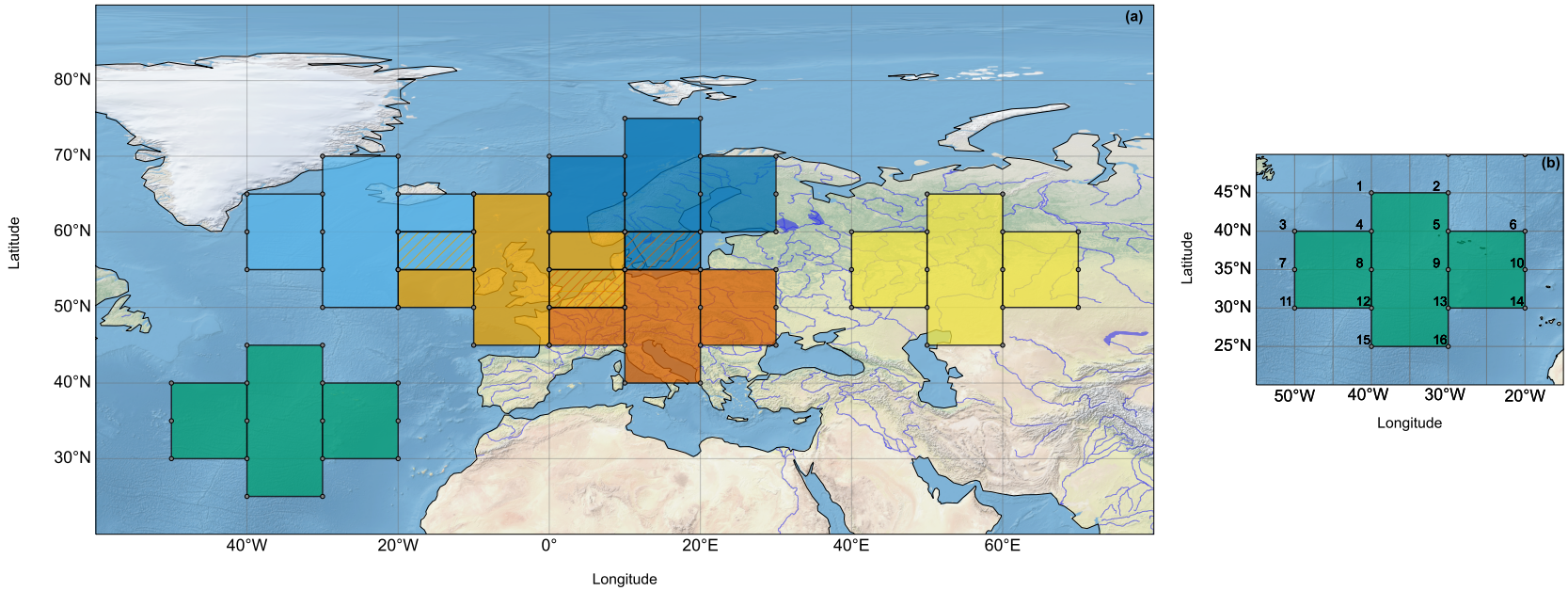

Figure 1: (a) Geographic distribution of sub-grids across the North Atlantic and Europe used in this study. Colors represent distinct regions: Western Europe (light orange), Iceland (light blue), Azores (green), Eastern Europe (yellow), Scandinavia (blue), and Central Europe (orange). (b) Grid points over the Azores employed in the calculations following the methodology of [66]. The numbered nodes correspond to the computational scheme illustrated in Figure 2.

Figure 2, which presents the diagnostic flowchart used in the DSRM. This schematic outlines the stepwise calculation of key parameters (westerly (W) and southerly (S) flow components, resultant flow magnitude (F), flow direction (θ), and shear vorticity (ζ)) based on SLP gradients. Threshold criteria are applied to these diagnostics to assign each day a specific circulation type within the extended Lamb framework.

To bridge the gap between regional Lamb-type diagnostics and continental-scale synoptic interpretation, the DSRM incorporates a hierarchical aggregation scheme that translates subgrid-level circulation types into composite *Großwetterlagen* (GWL) [52, 53]. Each of the six subgrids (Western Europe, Iceland, Azores, Eastern Europe, Scandinavia, and Central Europe) produces a daily Lamb classification based on local pressure gradients and flow parameters [66, 72]. These regional types are then evaluated collectively to determine the dominant synoptic regime for Central Europe. As illustrated in Table 5 and 6, the aggregation scheme follows a rule-based logic that emphasizes spatial coherence and dynamical consistency. For example, if multiple subgrids simultaneously exhibit cyclonic types (C or hybrid forms with positive vorticity), and the Central European grid confirms a cyclonic curvature with enhanced southerly flow, the day is classified as a cyclonic GWL (e.g., *Tief Mitteleuropa*). Conversely, widespread anticyclonic signatures across the Azores, Western Europe, and Central Europe, combined with suppressed vorticity, support the assignment of an anticyclonic GWL (e.g., *Hoch Mitteleuropa* or *Brücke Mitteleuropa*). By synthesizing the Lamb classifications across all subgrids, the DSRM framework reconstructs GWLs in a reproducible and physically grounded manner. This approach preserves the diagnostic strengths of the Lamb scheme while enabling direct comparison with traditional synoptic climatologies and proxy-based reconstructions. Unlike traditional GWL classification, which relies on manual interpretation of synoptic charts, the DSRM enables reproducible and automated regime identification directly from climate model output [12, 63]. This objectivity is particularly valuable when comparing simulated and observed circulation patterns across different climate states, such as modern and glacial conditions. The model demonstrates the capability to differentiate between cyclonic, anticyclonic, and transitional regimes, and offers a promising basis for exploring links between atmospheric circulation and isotopic variability in precipitation.

5.2.3 Validation Data

To evaluate the performance of the EMAC model and the DSRM classification, observational data from 12 GNIP (Global Network of Isotopes in Precipitation) stations distributed across Germany were used [61]. These stations provide high-resolution records

Figure 2: Diagnostic flowchart for Lamb-type weather classification used in the DSRM. The schematic illustrates the spatial arrangement of 16 sea-level pressure (SLP) reference points and the calculation of key flow parameters: westerly (W) and southerly (S) components, resultant flow magnitude (F), flow direction (θ), and shear vorticity (ζ). These diagnostics are used to assign daily circulation types within the extended Lamb scheme, including directional, cyclonic (C), anticyclonic (A), hybrid, and unclassified (U) regimes.

Table 5: Schematic representation (Part A) of the individual circulation modes across the reference grids used to determine the European atmospheric circulation regime, based on the GWL catalog by Gerstengarbe (2010) [45]. The table lists the dominant circulation type for each mode and region. Abbreviations denote: C – cyclonic (low-pressure influence), AC – anticyclonic (high-pressure influence), H – hybrid (mixed or transitional state). Region abbreviations: WE – Western Europe, IC – Iceland, AO – Acores, EE – Eastern Europe, SC – Scandinavia, CE – Central Europe.

Index	**WE**	**IC**	**AO**	**EE**	**SC**	**CE**
Zonal						
WA	H / AC	C	AC	H / C	H / C	H / AC
WZ	H / C	H / C	AC	H / AC	H / C	H / C
WS	H / AC	H / AC	H / AC	H / C	AC	H / C
WW	H / C	C	AC	AC	H / C	H / C
Mixed						
SWA	H / C	H / C	H	H / C	C	H / AC
SWZ	H / C	H / C	H / C	H / AC	C	H / C
NWA	H / AC	H / C	H	H / C	C	H / AC
NWZ	H	C	AC	H / C	H / C	H / C
HM	H	H / C	H / AC	H / C	H / C	AC
BM	AC	H / C	H / AC	H / C	H / AC	AC
TM	H / C	H / AC	H / AC	H / AC	H	C

of essential climatic variables, including daily and monthly mean air temperature (T), daily precipitation totals (P), and oxygen isotope ratios in precipitation (δ^{18}O). In addition, monthly precipitation-weighted δ^{18}O values were calculated to account for the influence of precipitation amount on isotopic composition [112], as shown in Equation 2:

$$\delta^{18}\mathrm{O}_{\mathrm{weighted}} = \frac{\sum_{i=1}^{n} \delta^{18}\mathrm{O}_i \cdot P_i}{\sum_{i=1}^{n} P_i} \tag{2}$$

where $\delta^{18}\mathrm{O}_i$ is the daily isotope ratio and P_i the corresponding daily precipitation.

Figure 3 shows the geographic distribution of the GNIP stations used in this study. The network spans a broad latitudinal and longitudinal range within Germany, encompassing inland and alpine regions and capturing a range of subclimatic conditions that support meaningful validation of model output. The location of Mainz is shown for reference only and does not represent a GNIP station with available isotope data. In addition to local parameters, synoptic-scale indicators were incorporated to contextu-

Table 6: Schematic representation (Part B) of the individual circulation modes across the reference grids used to determine the European atmospheric circulation regime, based on the GWL catalog by Gerstengarbe (2010) [45]. The table lists the dominant circulation type for each mode and region. Abbreviations denote: C – cyclonic (low-pressure influence), AC – anticyclonic (high-pressure influence), H – hybrid (mixed or transitional state). Region abbreviations: WE – Western Europe, IC – Iceland, AO – Acores, EE – Eastern Europe, SC – Scandinavia, CE – Central Europe.

Index	**WE**	**IC**	**AO**	**EE**	**SC**	**CE**
Meridional						
NA	AC	H / C	AC	H / C	H / AC	H / C
NZ	AC	AC	H / AC	H / C	H / C	H
HNA	H / AC	AC	AC	C	H / C	H / AC
HNZ	H / C	AC	AC	H / C	H / C	H
HB	AC	H / C	H / C	H / C	H / C	H
TRM	H / C	C	AC	H / AC	H / C	C
NEA	AC	H / C	AC	H / AC	AC	H / AC
NEZ	AC	H / C	AC	H / AC	AC	H / C
HFA	H / C	H / C	H / C	H / AC	AC	H / AC
HFZ	H	H / C	H / AC	H / AC	AC	H
HNFA	H / AC	H / C	AC	AC	AC	H / C
HNFZ	H / AC	H / AC	H / AC	H / AC	AC	H / C
SEA	H / AC	C	H / AC	H	H / AC	AC
SEZ	H / C	C	H / C	H / AC	AC	H / C
SA	H / C	C	H / C	H / C	AC	H
SZ	C	H / C	AC	H / AC	H / C	H / C
TB	C	H / AC	AC	H / C	H / AC	H / C
TRW	C	H / AC	H / AC	H / AC	C	/
Miscellaneous						
U	/	/	/	/	/	/
STR	H	H	H	H	H	H

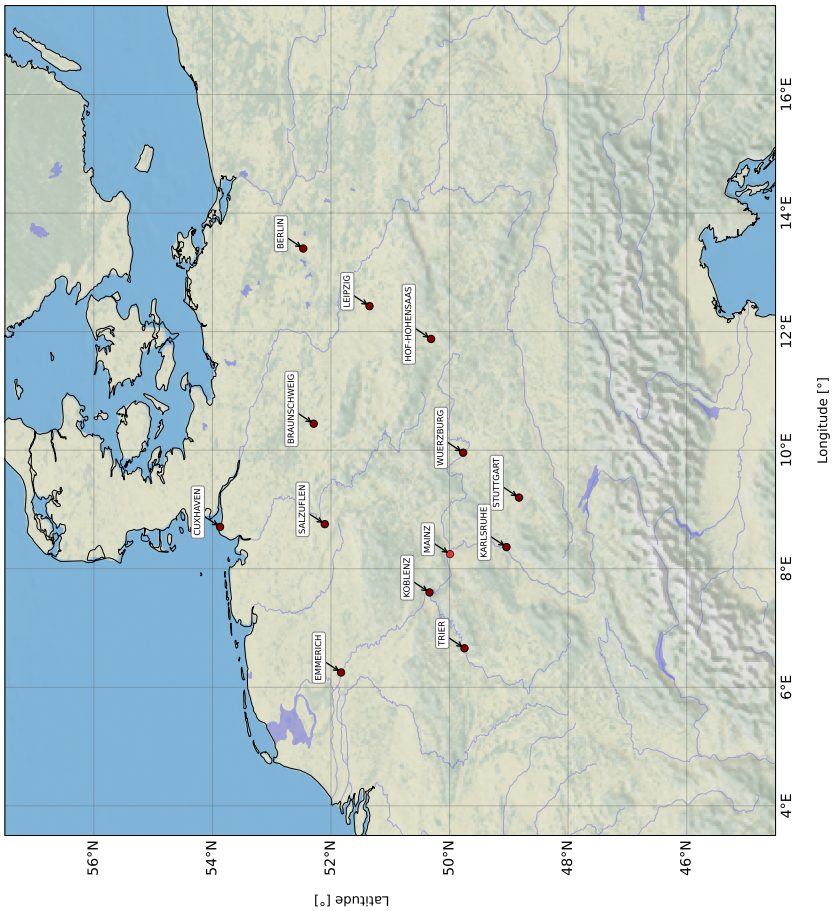

Figure 3: Geographic distribution of GNIP stations used for model validation. The selected network includes 12 stations across Germany.

alize isotopic variability. These include monthly frequencies of GWL circulation types derived from the DSRM classification [52, 53], as well as the North Atlantic Oscillation (NAO) index [58, 60], which captures large-scale pressure anomalies influencing European climate. To ensure comparability across stations with differing climatological baselines, station-specific anomalies were computed. The anomalies were standardized by removing the spatial mean across all GNIP stations and dividing by the standard deviation calculated from these spatial means. The resulting anomaly dataset serves as the basis for principal component analysis (PCA) and GWL-dependent trend analyses to identify dominant circulation–isotope relationships.

5.3 Results

5.3.1 GWL Frequency Distributions

Figure 4 presents the simulated frequency distributions of *Großwetterlagen* (GWL) derived from the DSRM classification and from observational data provided by the *Deutscher Wetterdienst* (DWD) [28, 45]. The DWD is Germany's national meteorological service, responsible for the acquisition and dissemination of standardized weather and climate observations [27]. Each segment in the charts represents a specific GWL type and its relative frequency. Color codes are defined as follows: blue and dark blue indicate zonal regimes (e.g., W, WA, WZ), green denotes mixed regimes, orange represents meridional regimes (e.g., N, S, E), and grey corresponds to transitional or undefined regimes, including days with ambiguous or shifting synoptic conditions. The DSRM classification additionally introduces the Straight Flow (STR) regime to account for days with minimal pressure gradients over Central Europe and the North Atlantic. These cases are not explicitly represented in traditional HB-GWL schemes.

In the simulation, zonal and straight-flow regimes account for 14.0 % and 5.6 % respectively. Mixed regimes comprise 26.9 %, with HM (10.9 %) and NW (8.3 %) representing the largest shares, followed by TM (5.1 %) and SW (2.6 %). Meridional regimes total 39.1 %, with E (16.3 %) and S (14.7 %) contributing most, and N (8.1 %) less frequently. Unclassified regimes constitute 14.4 % of the total. The DWD reference data show the following distribution: zonal regimes account for 26.9 %, mixed regimes for 32.6 %, and meridional regimes for 39.6 %. Within the mixed category, HM (16.6 %) and NW (8.5 %) are most frequent, while TM (2.5 %) and SW (5.0 %) are less represented. Meridional regimes are distributed among E (15.5 %), N (15.8 %), and S (8.3 %). The proportion of unclassified regimes is 0.9 %.

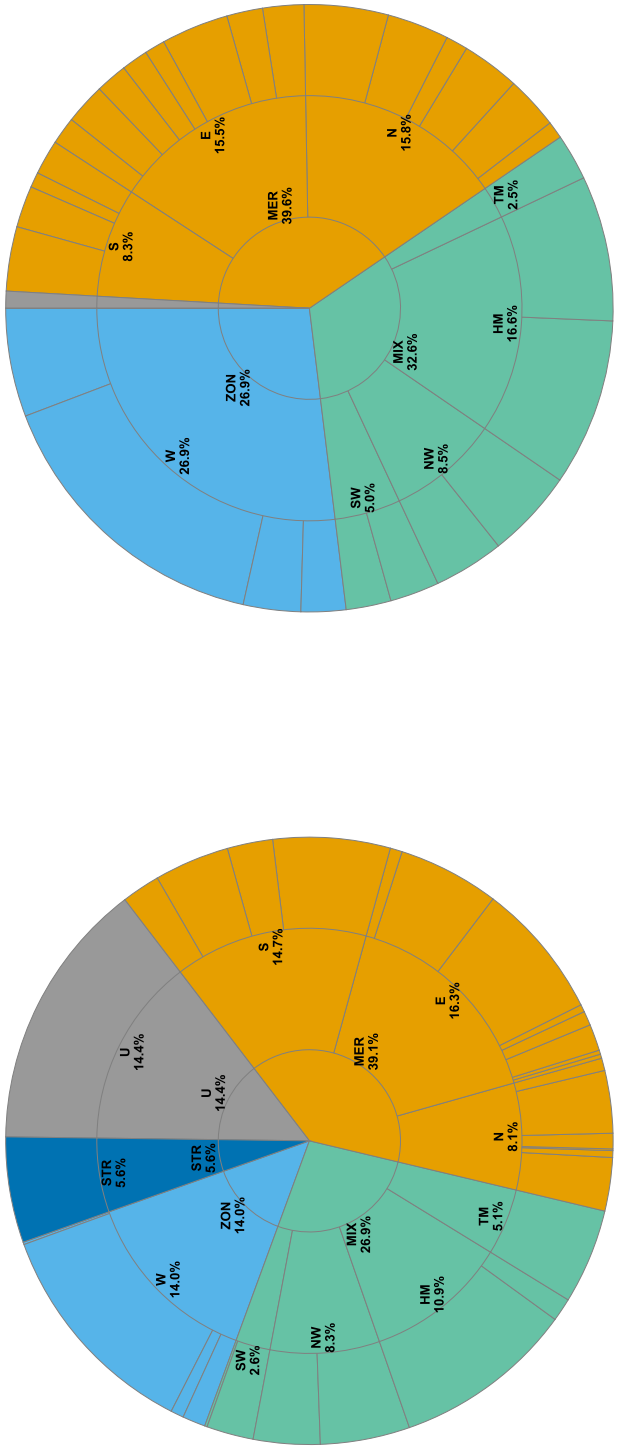

Figure 4: Comparison of GWL frequency distributions derived from simulation (left panel) and DWD reference data (right panel). Each segment represents a specific synoptic regime, color-coded as follows: blue and dark blue indicate zonal regimes (pure westerly flow), green denotes mixed regimes, orange represents meridional regimes, and grey corresponds to transitional or undefined regimes.

The simulation reproduces the general structure of the synoptic frequency distribution. Differences are primarily observed in the frequency of zonal and unclassified regimes, as well as in the detailed composition of mixed and meridional categories. The DSRM classification applies an objective diagnostic scheme, which results in a higher proportion of unclassified cases. In contrast, the DWD classification is based on manual assignment, typically allocating ambiguous patterns to established regime types.

5.3.2 Evaluation of Simulation Accuracy

Figure 5 presents four scatter plots comparing simulated values with experimentally measured data. Each panel includes a 1:1 reference line to indicate ideal agreement between simulation and observation. All statistical comparisons between simulated and observed values were evaluated using a one-sample t-test, testing whether the mean difference significantly deviates from zero. Across all panels, the error bars reflect a range of uncertainties in the measurements.

Panel (a) shows the oxygen isotope signal (δ^{18}O in precipitation, expressed in ‰ VSMOW), with data points clustering near the reference line but generally exhibiting a positive offset. The associated error bars reflect varying levels of measurement uncertainty. On average, the simulated values are higher than the observations, with a mean difference of -0.8676 ‰ ($t = -2.5317$, $p = 0.0279$). Panel (b) shows the modified precipitation-weighted isotopic oxygen signal ($\delta^{18}O_{wp}$, in ‰ VSMOW), where most data points align closely with the 1:1 line, although some deviations are present. The mean difference is 0.3953 ‰, indicating slightly lower simulated values, but the deviation is not statistically significant ($t = 0.8627$, $p = 0.4067$). Panel (c) presents temperature data (in °C), with a broader distribution of points around the reference line and most measurements falling above it. The simulated temperatures are significantly lower than the observed ones, with a mean difference of 2.037 °C ($t = 3.0893$, $p = 0.0103$). Notably, three observed values are substantially underestimated by the simulation, with discrepancies reaching up to 6 °C. Panel (d) illustrates monthly precipitation values (in mm per month), with approximately half of the data points lying near the 1:1 line, while several others exhibit more pronounced positive deviations. The simulation substantially overestimate precipitation, with a mean difference of -21.1344 mm per month ($t = -3.6665$, $p = 0.0037$).

Overall, the results highlight strengths and limitations of the EMAC model: while isotopic signals, especially when precipitation-weighted, are reasonably well captured, temperature and precipitation simulations show greater variability and reduced statistical agreement.

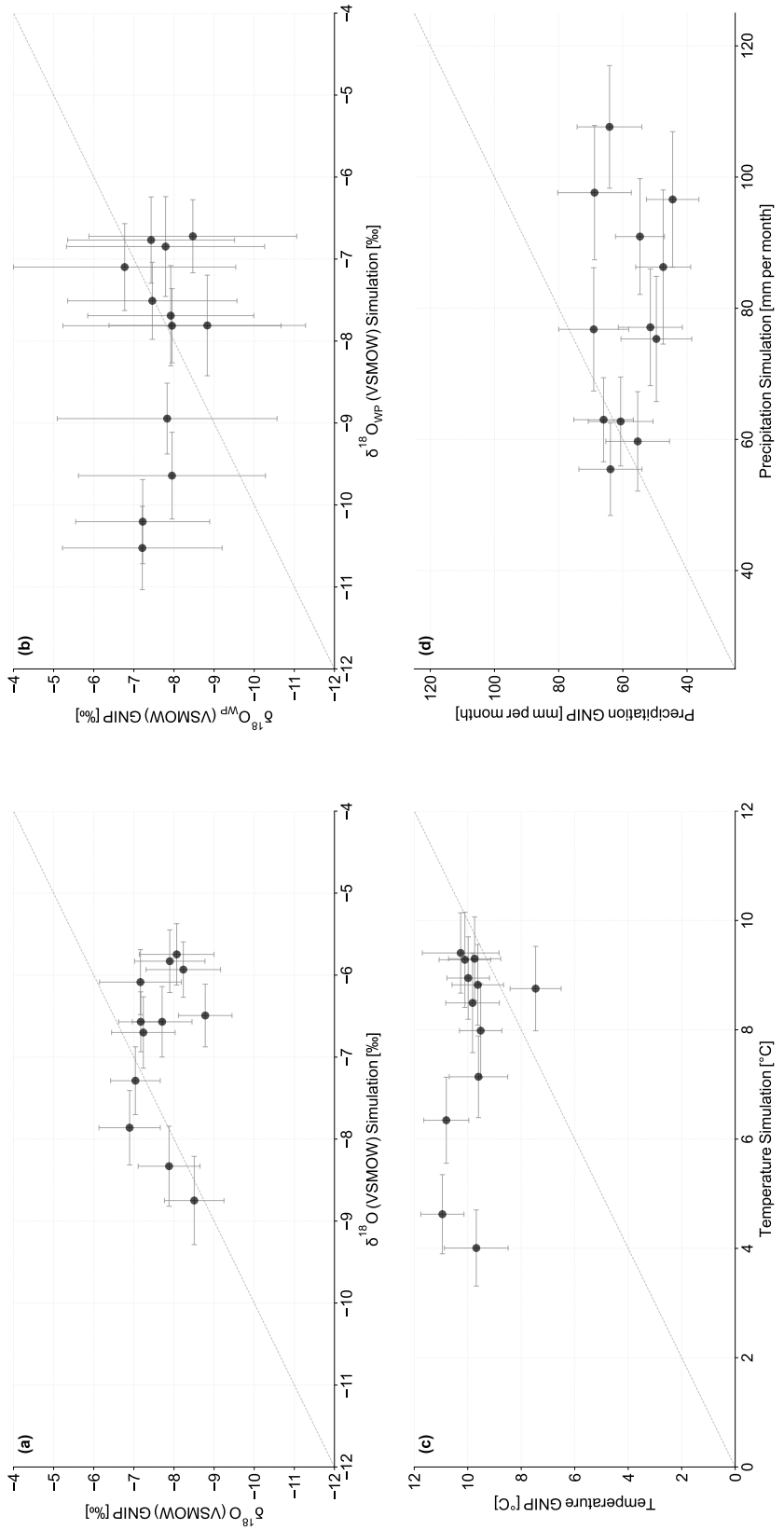

Figure 5: Regression plots comparing simulated and observed values for (a) δ^{18}O in precipitation, (b) precipitation-weighted δ^{18}O, (c) temperature, and (d) precipitation across 12 GNIP stations.

5.3.3 Climate Parameter Anomalies by Circulation Type

Figure 6 presents four boxplots showing station-specific anomalies for precipitation-weighted δ^{18}O, unweighted δ^{18}O in precipitation, temperature, and precipitation. These anomalies are expressed as deviations in units of standard deviation (σ) relative to the station-wide mean and grouped by circulation type. The color scheme follows the convention established earlier: blue and dark blue indicate zonal regimes (e.g., W, WA, WZ), green denotes mixed regimes (e.g., SW, NW, HM, TM), red represents meridional regimes (e.g., N, E, S), and grey corresponds to transitional or undefined regimes.

Circulation types W, SW, NW, HM, and TM display elevated median σ values and wider interquartile ranges across all parameters. Circulation types N, E, S, U, and STR show lower median values and narrower interquartile ranges. Whisker lengths are comparable across all circulation types. Panel (a) shows precipitation-weighted $\delta^{18}O_{wp}$ anomalies. Positive anomaly values are observed in the following order: STR, W, SW, NW, and HM. TM shows the most negative anomaly. N, E, S, and U are centered near zero, with N, E, and S exhibiting narrow boxplot widths. Panel (b) displays raw δ^{18}O anomalies. STR, W, SW, NW, HM, TM, and N show negative shifts. S shows a positive shift. U and E remain near baseline. Panel (c) presents precipitation anomalies by circulation type. Positive anomalies are observed in SW, S, and TM. Negative anomalies are recorded in HM, E, N, and W. STR, NW, and U are near the climatological baseline. Panel (d) shows temperature anomalies by circulation type. Positive anomalies are observed in SW, NW, and S. Negative anomalies are recorded in TM, E, and N. W, HM, STR, and U remain near zero.

Overall, these results highlight the influence of synoptic circulation on local climate parameter anomalies. Standardizing the anomalies using σ units enables meaningful comparisons across parameters with different natural scales and variabilities.

5.3.4 Principal Component Analysis (PCA)

Principal component analyses (PCAs) were conducted separately for summer and winter on standardized monthly anomalies of temperature (T), δ^{18}O in precipitation, precipitation (P), the NAO index, and circulation types (GT). Components with eigenvalues ≥ 1 were retained, yielding four principal components (PC1–PC4) in each season. In the summer season, PC1 was heavily loaded on T, δ^{18}O, and P. PC2 showed strong loadings on the NAO index and GT, with a moderate loading on P. PC3 was dominated by GT and NAO, while PC4 was primarily influenced by P and NAO. Together, these four components explained 90.5 % of the total variance, with individual contri-

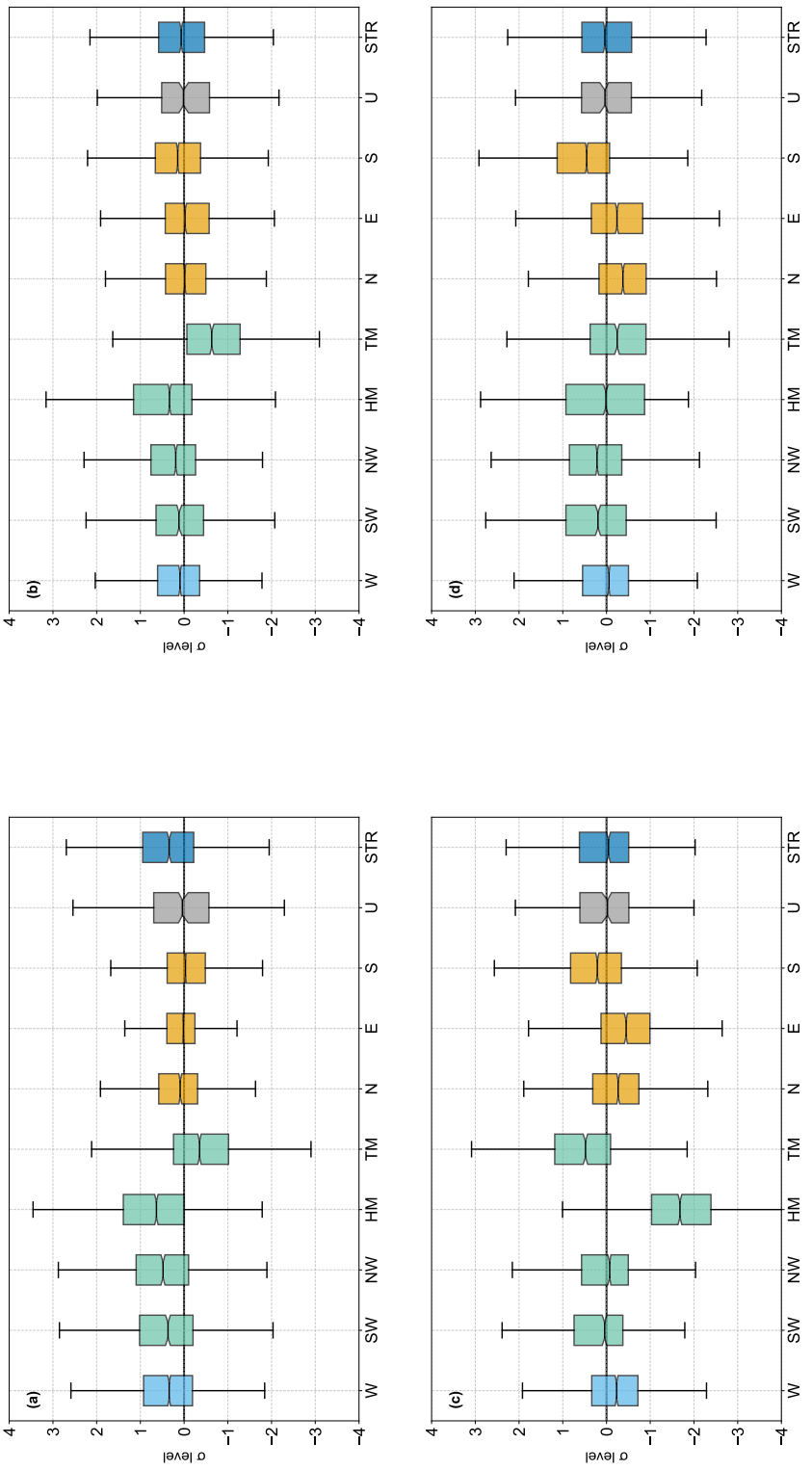

Figure 6: Boxplots of station-specific standardized anomalies expressed as deviations in units of standard deviation (σ) relative to the overall station-wide mean for (a) Precipitation-weighted δ^{18}O, (b) δ^{18}O in precipitation, (c) Precipitation, and (d) Temperature. The circulation types are color-coded as follows: blue and dark blue indicate zonal regimes, green denotes mixed regimes, orange represents meridional regimes, and grey corresponds to transitional or undefined regimes.

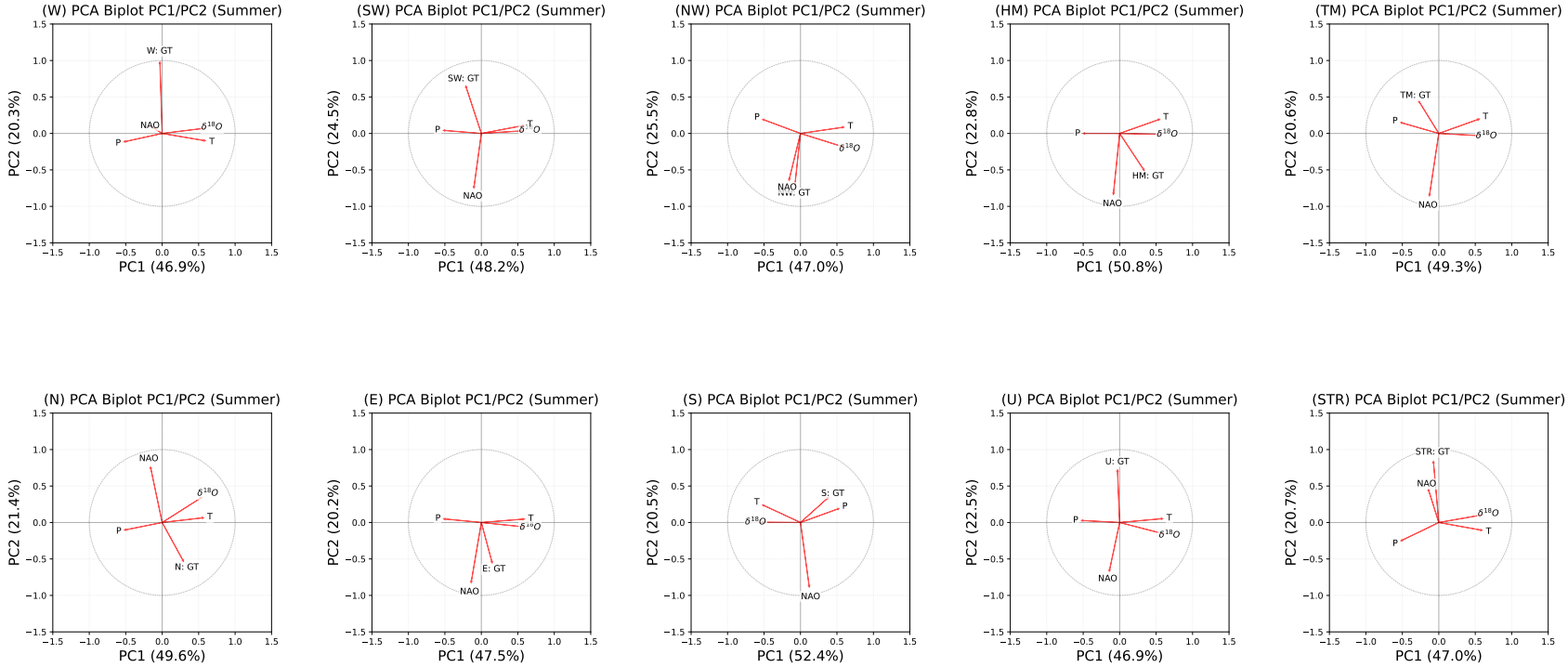

Figure 7: PCA biplot of summer anomalies showing the distribution of PC1 and PC2. PC1 is dominated by temperature, δ^{18}O in precipitation, and precipitation, while PC2 reflects variability in the NAO index and circulation types (GT).

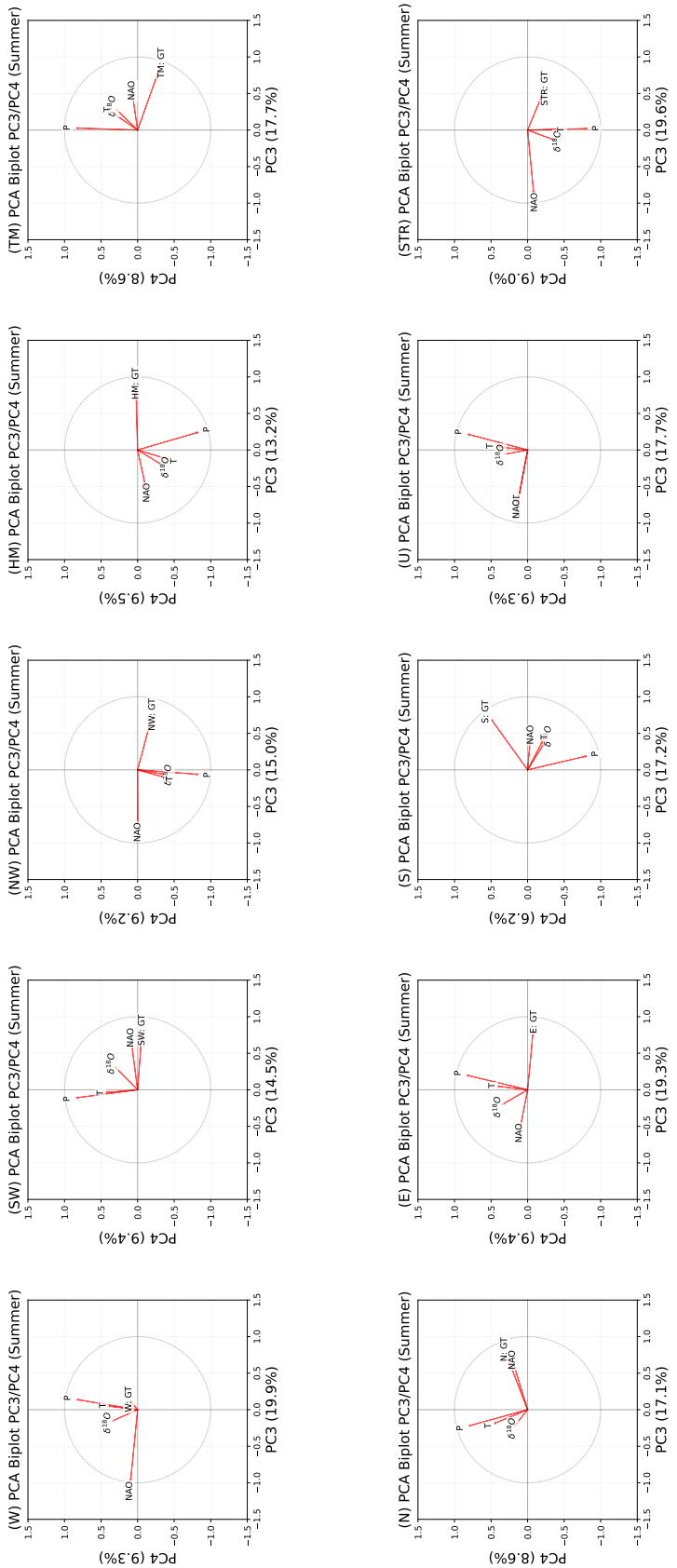

Figure 8: PCA biplot of PC3 and PC4, highlighting secondary patterns shaped by GT, NAO, and precipitation.

butions of 40.5 %, 21.3 %, 16.3 %, and 12.4 %, respectively. The corresponding loading structures are illustrated in Figure 7 and Figure 8. In the winter season, PC1 was strongly associated with T, P, and δ^{18}O, and moderately with GT. PC2 was dominated by GT, with additional moderate loadings on NAO and δ^{18}O. PC3 was heavily loaded on GT and NAO, and PC4 showed strong associations with P, including moderate associations with δ^{18}O and GT. The cumulative variance explained by these four components was 90.3 %, with individual contributions of 41.1 %, 22.6 %, 15.3 %, and 11.3 %, respectively. These patterns are visualized in Figure 9 and Figure 10. The cumulative explained variance of the first four principal components exceeded 90 % in both seasons. To assess the dataset's suitability for factor analysis, Bartlett's test of sphericity and the Kaiser–Meyer–Olkin (KMO) measure were applied across all GTs. The average Bartlett's χ^2 value of 139.04 indicated sufficient intercorrelations, while the mean KMO value of 0.602, which is slightly above the recommended threshold, suggested moderate limitations in sampling adequacy. All p-values were highly significant ($\overline{p} = 5.06 \times 10^{-16}$), confirming the statistical robustness of the results.

5.4 Discussion

The comparison between simulated and observed *Großwetterlagen* (GWL) frequencies demonstrates that the EMAC model captures the overall structure of large-scale circulation patterns over Central Europe. However, systematic biases are evident. Zonal regimes are underrepresented, likely due to the model's difficulty in classifying weak pressure gradients over Europe, which often leads to misclassification as Unclassified (U) or Straight (STR) [53]. Mixed regimes including SW, NW, HM, and TM are also underrepresented, suggesting limitations in distinguishing transitional synoptic states. In contrast, meridional regimes (N, E, S) are well represented, reflecting the model's ability to reproduce strong north–south advection patterns. The introduction of the Straight Flow (STR) regime helps account for days with minimal pressure gradients, which are not adequately captured by traditional HB-GWL schemes [63]. These findings underscore the importance of classification methodology and demonstrate that objective schemes like the DSRM offer improved reproducibility and diagnostic clarity [12].

The accuracy of the EMAC model was further evaluated by comparing simulated values of δ^{18}O in precipitation, precipitation-weighted δ^{18}O, temperature, and precipitation against observational data from 12 GNIP stations [61]. The scatter plots reveal systematic deviations across all parameters. Simulated δ^{18}O in precipitation consistently overestimates observed values by approximately 1 ‰ to 3 ‰, highlighting limitations

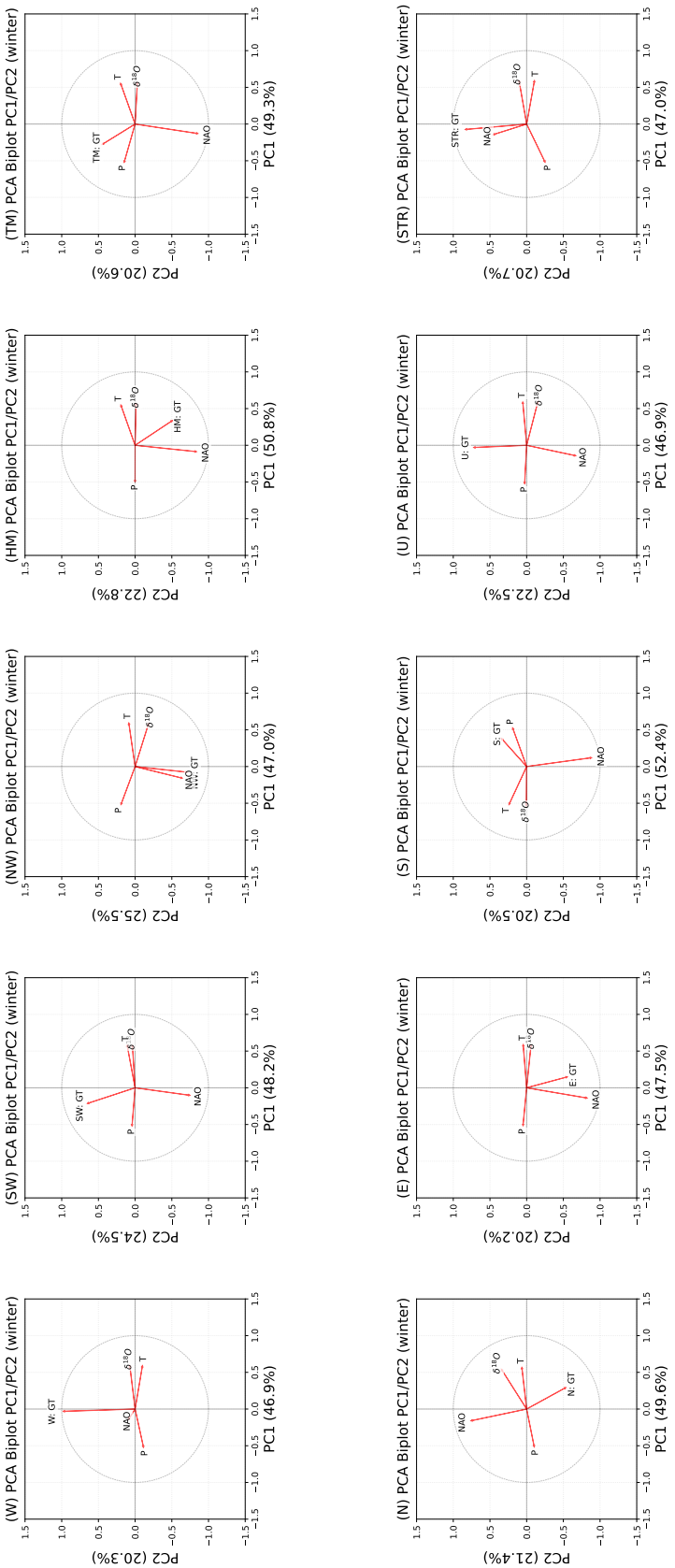

Figure 9: PCA biplot of winter anomalies showing the distribution of PC1 and PC2. PC1 is shaped by temperature, precipitation, and $\delta^{18}O$, with moderate GT influence; PC2 reflects precipitation variability and contributions from GT and $\delta^{18}O$

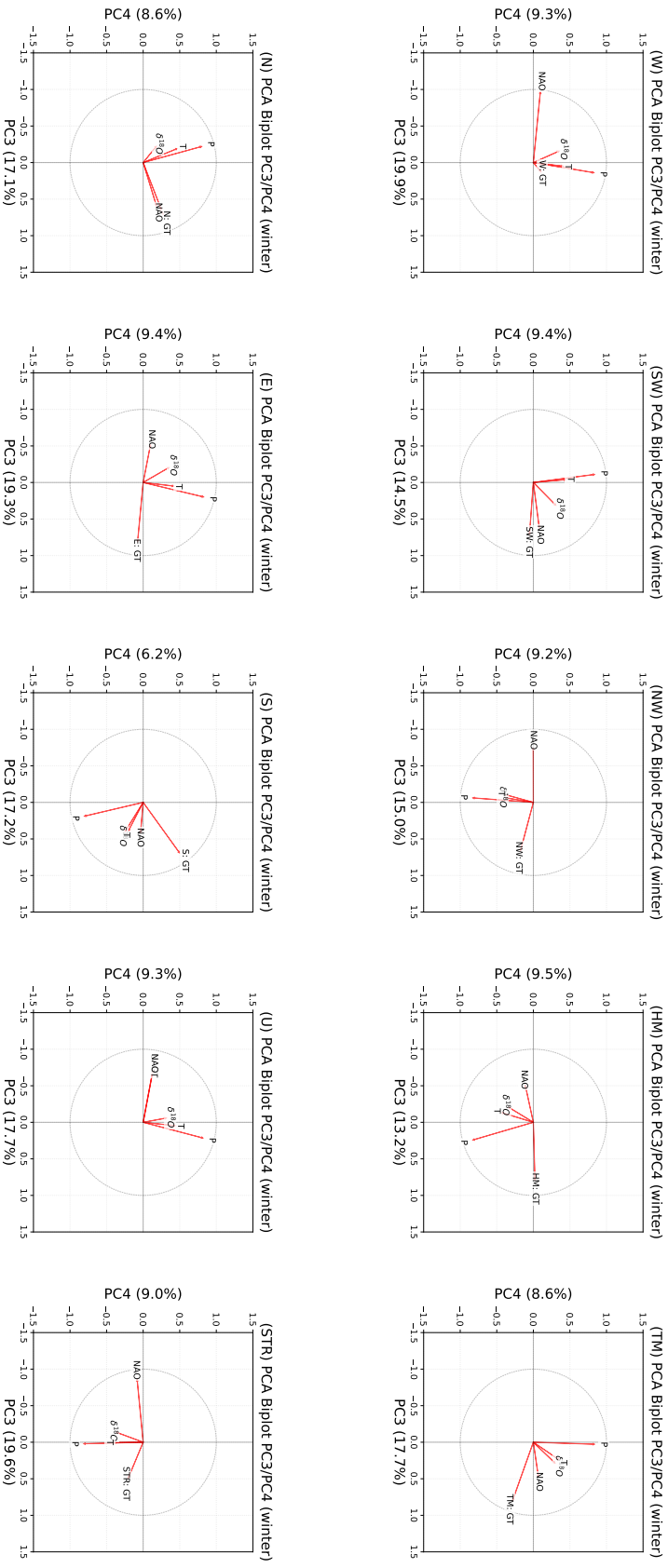

Figure 10: PCA biplot of winter anomalies showing the distribution of PC3 and PC4, highlighting secondary patterns shaped by GT, NAO, and precipitation.

in the model's representation of isotope fractionation processes [31]. Precipitation-weighted δ^{18}O improves agreement with observations, suggesting that accounting for the amount of precipitation enhances the isotopic signal [112]. Simulated temperatures are systematically underestimated across most stations, likely due to missing topographic detail and simplified representations of greenhouse gas concentrations and radiative forcing in the simulation setup. Precipitation simulations exhibit high variability, with a tendency to overestimate extreme events, reflecting challenges in modeling convective processes and moisture transport [36]. While the simulation reproduces broad climatic patterns, these biases highlight areas for refinement in future simulations. Station-specific anomalies grouped by circulation type reveal distinct patterns in climate variability. Cyclonic and mixed regimes (W, SW, NW, HM, TM) are associated with higher median anomalies and broader interquartile ranges, indicating stronger deviations from the station-wide mean and greater variability. In contrast, meridional and undefined regimes (N, E, S, STR, U) exhibit lower median anomalies and narrower distributions, suggesting more stable conditions. Despite differences in general tendency, the overall spread remains consistent across circulation types, implying that deviations occur under all regimes. Notably, HM shows the highest positive anomalies in precipitation-weighted δ^{18}O and unweighted δ^{18}O in precipitation, while TM exhibits the strongest negative anomalies. Temperature and precipitation anomalies also vary significantly by circulation type, underscoring the role of synoptic patterns in modulating local climate conditions [58, 60].

Principal Component Analysis (PCA) was performed separately for summer and winter seasons using standardized monthly anomalies of temperature, precipitation, δ^{18}O in precipitation, NAO index, and circulation type frequency (GT). Components with eigenvalues ≥ 1 were retained, yielding four principal components (PC1–PC4) per season. Notably, the first four components explained a high cumulative variance: approximately 90 % in both summer and winter season. PC1 alone accounted for nearly 45 % of the variance, highlighting its dominant role in climate variability. In summer, PC1 showed strong loadings on temperature (T), δ^{18}O, and precipitation (P), reflecting their interconnected seasonal influence. PC2 was primarily driven by NAO and GT, with a moderate contribution from P, indicating links between atmospheric circulation and precipitation patterns. PC3 was associated mainly with GT and NAO, while PC4 was dominated by P and NAO. During winter, PC1 was strongly loaded on T and δ^{18}O, with a moderate influence from GT, emphasizing the persistent importance of temperature and isotopic composition. PC2 showed strong loadings on P, alongside moderate associations with GT and δ^{18}O, capturing seasonal moisture variability. PC3

was influenced predominantly by GT and NAO, whereas PC4 exhibited strong loadings on P, NAO, and GT, underscoring the combined effects of atmospheric circulation and precipitation variability in winter climate dynamics. Bartlett's test of sphericity ($\chi^2 = 139.04$) and the Kaiser-Meyer-Olkin measure (KMO = 0.602) indicated sufficient intercorrelations and moderate sampling adequacy. Highly significant p-values ($\overline{p} = 5.06 \times 10^{-16}$) confirmed the robustness of the factorability.
In summary, the study highlights the strengths and limitations of the EMAC model in reproducing observed climate variability and isotopic signals. The integration of synoptic-scale classifications with local diagnostics provides a nuanced understanding of how circulation regimes influence temperature, precipitation, and δ^{18}O dynamics in precipitation across seasons.

5.5 Conclusion

This study demonstrates that combining long-term simulations from the ECHAM5/ MESSy Atmospheric Chemistry (EMAC) model [68, 117] with an objective synoptic classification via the Diagnostic Synoptic Regime Model (DSRM) approach [12, 63] provides a robust framework for investigating the links between large-scale atmospheric circulation and local climate parameters, particularly the variability of δ^{18}O in precipitation over Central Europe. The EMAC model qualitatively reproduces the general distributions of temperature and precipitation, although systematic biases are evident under specific synoptic conditions [36]. Cyclonic regimes are associated with enhanced moisture advection and lower δ^{18}O values, while anticyclonic regimes tend to produce enriched isotopic signals [58, 60]. The precipitation-weighted δ^{18}O metric ($\delta^{18}O_{wp}$) improves the agreement between simulated and observed values, effectively compensating for the model's tendency to overestimate unweighted δ^{18}O in precipitation [112]. Principal Component Analysis (PCA) reveals that nearly 50 % of the total variance is explained by the combined behavior of temperature, precipitation, and δ^{18}O in precipitation, highlighting the strong physical coupling among these variables. The circulation type frequency (GT) does not act as a primary driver but contributes significantly to secondary components, indicating that synoptic-scale dynamics modulate local isotopic signals indirectly through their influence on temperature and moisture availability. A similar pattern is observed in winter, with temperature and δ^{18}O in precipitation remaining dominant, and GT contributing meaningfully to later components. The study also emphasizes the value of the DSRM classification, which enables reproducible and automated identification of circulation regimes, facilitating large-scale analysis of weather patterns and their climatic impacts [53].

The integration of synoptic-scale classifications with local climate diagnostics significantly advances the understanding of the processes governing variability in temperature, precipitation, and δ^{18}O in precipitation. The results demonstrate that atmospheric circulation patterns influence isotopic signals regionally, while the model framework is capable of realistically reproducing spatial and seasonal variations. Notably, accounting for precipitation-weighted δ^{18}O enhances the agreement between simulations and observations. These findings provide a robust basis for capturing the complex interactions between large-scale circulation regimes and local climate conditions, which is essential for applications in paleoclimate reconstructions. To further improve the fidelity and predictive capability of isotope-enabled climate simulations, future efforts should prioritize higher spatial resolution, more comprehensive seasonal analyses, and the inclusion of ocean–atmosphere feedback mechanisms. Additionally, the current simulation setup relies on prescribed sea surface temperature (SST) and sea ice concentration (SIC) [43], future work should incorporate a coupled ocean model such as MPI-OM [120] to better represent ocean–atmosphere interactions and improve the simulation of hydrological processes.

6 Infiltration Submodel Integration within DSRM

Synoptic regime shifts and $\delta^{18}O$ variability during the Last Glacial Maximum: Insights from isotope-enabled climate simulations and speleothem proxy comparisons (manuscript in preparation)

Specific Contribution Summary

The foundational concept of the study was developed by Holger Tost and Denis Scholz. All simulation data were processed by Tim Liesenhoff and Holger Tost. Tim Liesenhoff carried out the regime classification across all datasets and developed the source code for the DSRM and the infiltration model. The interpretation of results was a joint effort by Tim Liesenhoff, Holger Tost, and Denis Scholz, with Tim Liesenhoff assuming a leading role. He also coordinated and led the writing of the manuscript.

6.1 Background and Objectives

Large-scale atmospheric circulation patterns exert a central influence on regional climate and isotopic variability across Europe [72, 91, 92]. During the Last Glacial Maximum (LGM) reorganized boundary conditions such as expanded ice sheets reduced greenhouse gas concentrations and altered sea surface temperatures resulted in significantly different climate conditions across Europe. This shift is traditionally associated with more persistent high-pressure systems and a more stable atmospheric configuration over the European continent [52, 53]. As a key paleoclimate proxy, stable oxygen isotope ratios (δ^{18}O) preserved in speleothems integrates signals from moisture source trajectories, rainout histories, and synoptic-scale dynamics [8, 20]. However, interpreting these signals remains complex due to the interplay of local meteorological conditions and large-scale atmospheric circulation [65, 112]. To address these challenges, this study applies the Hess-Brezowsky *Großwetterlagen* (GWL) classification [52] to objectively characterize synoptic regimes using output from the isotope-enabled EMAC model. The HB-GWL framework, which defines 29 circulation types and has undergone multiple revisions [45, 53], provides a robust basis for analyzing the daily dynamics of European weather regimes. The Diagnostic Synoptic Regime Model (DSRM) framework,

developed by the authors of this study, is employed to assign daily weather types based on regional sea-level pressure fields, enabling reproducible identification of circulation types under glacial boundary conditions. In addition, this study employs a multi-tiered isotope modeling approach to derive monthly δ^{18}O values in precipitation from climate model output. Three distinct weighting schemes are applied to account for different hydrological and geochemical processes: (i) precipitation-weighted δ^{18}O values emphasize the contribution of effective rainfall to the isotopic signal, (ii) infiltration-weighted values incorporate hydrological filtering mechanisms such as evapotranspiration and karstic recharge dynamics, and (iii) calcite-weighted δ^{18}O values simulate speleothem formation by applying temperature-dependent isotopic fractionation to the infiltrated water during mineral precipitation. Together, these methods offer a refined framework for linking climate model output with speleothem-based proxy records. By combining synoptic diagnostics with isotope-enabled modeling and proxy integration, this study aims to improve the interpretability of paleoclimate signals and contribute to a deeper understanding of glacial climate dynamics.

The specific objectives of this study are:

1. To characterize spatial patterns and statistical relationships between simulated δ^{18}O values in precipitation and key climate parameters (temperature (T), precipitation (P), sea-level pressure (SLP), and evaporation(E)) during the LGM.

2. To reconstruct LGM circulation regimes through an objective, pattern-based classification of model output using the HB-GWL framework.

3. To apply an infiltration-weighted isotope modeling approach that enables direct comparison between simulated δ^{18}O in precipitation and European speleothem records.

By combining synoptic diagnostics with isotope-enabled modeling and proxy validation, this study refines our understanding of glacial climate dynamics and improves the interpretation of speleothem-based δ^{18}O records. The findings underscore the value of circulation-based frameworks in paleoclimate reconstruction and offer new insights into the mechanisms driving isotopic variability under glacial boundary conditions.

6.2 Methods and Data

6.2.1 Simulation Configuration

To investigate the influence of synoptic-scale circulation on δ^{18}O variability in precipitation during the Last Glacial Maximum (LGM), this study utilizes a 30-year simulation dataset generated with the isotope-enabled ECHAM5/MESSy Atmospheric Chemistry (EMAC) model [68, 117]. The H2OISO submodel is employed to simulate the transport and fractionation of stable water isotopologues ($H_2^{18}O$, $H_2^{16}O$) across all phases of the hydrological cycle [31]. This includes explicit resolution of fractionation processes during evaporation, condensation, and atmospheric transport, enabling direct comparison between simulated δ^{18}O in precipitation and speleothem-derived proxy records. The simulation setup is informed by glacial boundary conditions consistent with PMIP3 recommendations [1], while allowing for scenario-specific adjustments. It ensures equilibrium in both isotopic and hydrological components. Observational data from 14 European and Mediterranean cave sites are used for validation, extracted from the SISAL database v2.0 [20]. All simulations are performed at high spatial resolution (T106), allowing for detailed regional analysis of isotopic variability across Europe. A comprehensive overview of the applied forcing parameters is provided in Table 7.
Daily synoptic regimes during the Last Glacial Maximum (LGM) are identified using the same Diagnostic Synoptic Regime Model (DSRM) framework described in Section 5.2.2. In short, sea-level pressure (SLP) fields are extracted from six regional subgrids covering Western Europe, Iceland, Azores, Eastern Europe, Scandinavia, and Central Europe (see Figure 1 for subgrid layout). Geostrophic flow diagnostics are then computed, including zonal and meridional components (W, S), resultant flow magnitude (F), flow direction (θ), and shear vorticity (ζ), following the classification logic illustrated in Figure 2. Based on threshold criteria shown in Table 5 and Table 6, each simulation day is assigned to one of 27 circulation types: zonal, mixed, meridional, straight, or unclassified. Monthly *Großwetterlagen* (GWL) frequencies are derived from these daily labels, enabling direct comparison with climate simulations and observational datasets.

6.2.2 Infiltration Model and δ^{18}O Weighting

To complement the synoptic classification and isotope diagnostics, this study implements a physically based infiltration model designed to estimate effective karst aquifer recharge from daily climate model output. The model integrates surface temperature, relative humidity, and precipitation to compute potential evapotranspiration (PET) using the Haude method [51], which relies on saturation vapor pressure derived via

Table 7: Atmospheric forcing parameters applied in the simulation dataset. The forcing parameters for the LGM scenario are determined by the authors of this paper.

Simulation Parameter	**Description**
Base Parameters	
Simulation Interval	0–40 / 10–40 (excluding spin-up)
Horizontal Resolution	T106 (1.12° at the equator)
Vertical Resolution	L31ECMWF (31 vertical levels up to 0.01 hPa)
Orbital Forcing	
Orbital Parameters	Keplerian orbital configuration
Atmospheric Forcing	
CO_2	149 ppm
CH_4	162 ppb
NO_x	196 ppb
CFCs	0 ppt (CFC1) / 0 ppt (CFC2)
Oceanic Forcing	
SST	Prescribed LGM sea surface temperatures (T106)
SIC	Prescribed LGM sea ice concentrations (T106)

the Magnus formula [15]. Infiltration is then calculated as the residual between precipitation and PET, constrained to non-negative values to reflect realistic hydrological conditions and prevent artificial recharge during dry periods. The resulting infiltration time series forms the basis for calculating monthly δ^{18}O values using four distinct weighting schemes, as illustrated in Equations 3 to 7:

Unweighted $\delta^{18}\mathbf{O}_{mean}$ in precipitation:

$$\delta^{18}\mathrm{O}_{\mathrm{mean}} = \frac{1}{n}\sum_{i=1}^{n}\delta^{18}\mathrm{O}_i \tag{3}$$

where n is the number of days in the month and $\delta^{18}\mathrm{O}_i$ is the daily isotope value.

Precipitation-weighted $\delta^{18}\mathbf{O}_{wp}$:

$$\delta^{18}\mathrm{O}_{\mathrm{wp}} = \frac{\sum_{i=1}^{n}\delta^{18}\mathrm{O}_i \cdot P_i}{\sum_{i=1}^{n} P_i} \tag{4}$$

where P_i is the daily precipitation amount. This weighting emphasizes the contribution of wetter days to the isotopic signal.

Infiltration-weighted $\delta^{18}\mathbf{O}_{wi}$:

$$\delta^{18}\mathrm{O_{wi}} = \frac{\sum_{i=1}^{n} \delta^{18}\mathrm{O}_i \cdot I_i}{\sum_{i=1}^{n} I_i} \tag{5}$$

where I_i is the daily infiltration rate, accounting for hydrological filtering processes such as evapotranspiration and recharge seasonality.

Calcite-weighted $\delta^{18}\mathbf{O}_{wc}$:

Simulated speleothem calcite values derived from the infiltration-weighted δ^{18}O signal using a memory-based mixing model and temperature-dependent fractionation [112]. The reservoir mixing follows:

$$R_t = R_{t-1} + \alpha \cdot (\delta^{18}\mathrm{O}_{\mathrm{inflow},t} - R_{t-1}) \quad \text{with} \quad \alpha = \frac{1}{\tau} \tag{6}$$

where R_t is the monthly reservoir value and τ is the mixing time in months. The calcite isotope value is then calculated as:

$$\delta^{18}\mathrm{O}_{\mathrm{wc},t} = \left(\frac{R_t + 1000}{1.03086}\right) \cdot \exp\left(\frac{2780}{T_{\mathrm{year}}^2} - \frac{2.89}{1000}\right) - 1000 \tag{7}$$

with T_{year} as the annual mean site temperature in Kelvin.

All calculations are conducted at the grid-cell level for each speleothem site using bilinear interpolation of the simulation output. This ensures spatial consistency between simulated climate variables and proxy locations. The resulting time series (comprising unweighted δ^{18}O in precipitation, precipitation-weighted δ^{18}O, infiltration-weighted δ^{18}O, and calcite-weighted δ^{18}O) are subsequently compared to speleothem records from the SISAL database [20] to evaluate simulation–proxy agreement and to explore the climatic controls on isotopic variability.

6.2.3 Speleothem Cave Sites

To validate the simulated δ^{18}O signals under glacial conditions, this study utilizes speleothem records from 14 well-dated cave sites across Europe and the Mediterranean region, as compiled in the SISAL database [20]. These sites span a broad range of climatic zones and karst environments, offering a diverse and spatially representative proxy network for simulation–data comparison.

The selected speleothems provide high-resolution records of stable oxygen isotope ratios ($\delta^{18}O$), which are used to benchmark the simulated infiltration-weighted and calcite-weighted isotope signals. Each cave site is treated as a grid-cell reference point within the EMAC model simulation domain, enabling direct comparison between simulated and observed values. Analytical precision of the speleothem records is approximately ± 0.15 ‰, and values are converted from VPDB to VSMOW for consistency with model output [6, 21]. The geographic distribution of the cave sites used in this study is shown in Figure 11. This distribution allows for assessment of regional coherence, site-specific anomalies, and the influence of synoptic regimes on isotopic variability.
Sites such as Villars Cave, Katerloch Cave, Sofular Cave, and Soreq Cave are particularly well-documented and serve as key anchors for evaluating model fidelity [7, 8, 121]. The combination of high-resolution proxy data and isotope-enabled climate simulations provides a robust framework for interpreting speleothem $\delta^{18}O$ signals in the context of glacial climate dynamics.

6.3 Results

6.3.1 Synoptic Regime Shifts

A comparative analysis of *Großwetterlagen* (GWL) frequencies between the Last Glacial Maximum (LGM) and the Modern Day (MD) reveals substantial shifts in synoptic-scale circulation patterns (Figure 12). Under LGM conditions, westerly types WA (-20 %), WS (-15 %), SWZ (-10 %), and NWZ (-15 %) occur less frequently, whereas WZ (+5 %), WW (+20 %), SWA (+30 %), and NWA (+20 %) become more frequent. Northerly and northeasterly types NZ (-70 %), NEA (-35 %), and NEZ (-40 %) show decreased frequency, while NA remains unchanged (0 %) and NWA increases (+20 %). Southern and southeastern types exhibit mixed trends: SEA (-15 %) decreases, SEZ and SZ remain stable (0 %), and SA (+15 %) increases. Stationary high-pressure systems HM and BM both increase in frequency (+10 %), with TM unchanged (0 %). Hybrid and transitional regimes HNA (-100 %), HNZ (-35 %), HNFA (-55 %), HFZ (-30 %), and HFA (-25 %) occur more frequently under MD conditions, as do TRM (-5 %) and TB (-5 %), while TRW (+7.5 %) and HB (+15 %) increase in frequency in the LGM scenario. Finally, the occurrence of unclassified flow types (U) decreases under LGM conditions (-15 %), whereas STR becomes more frequent (+10 %). These observed shifts are statistically significant, as confirmed by a Pearson chi-squared test ($\chi^2 = 80.30$, $p < 0.0001$), underscoring a robust reorganization of synoptic-scale dynamics under glacial boundary conditions.

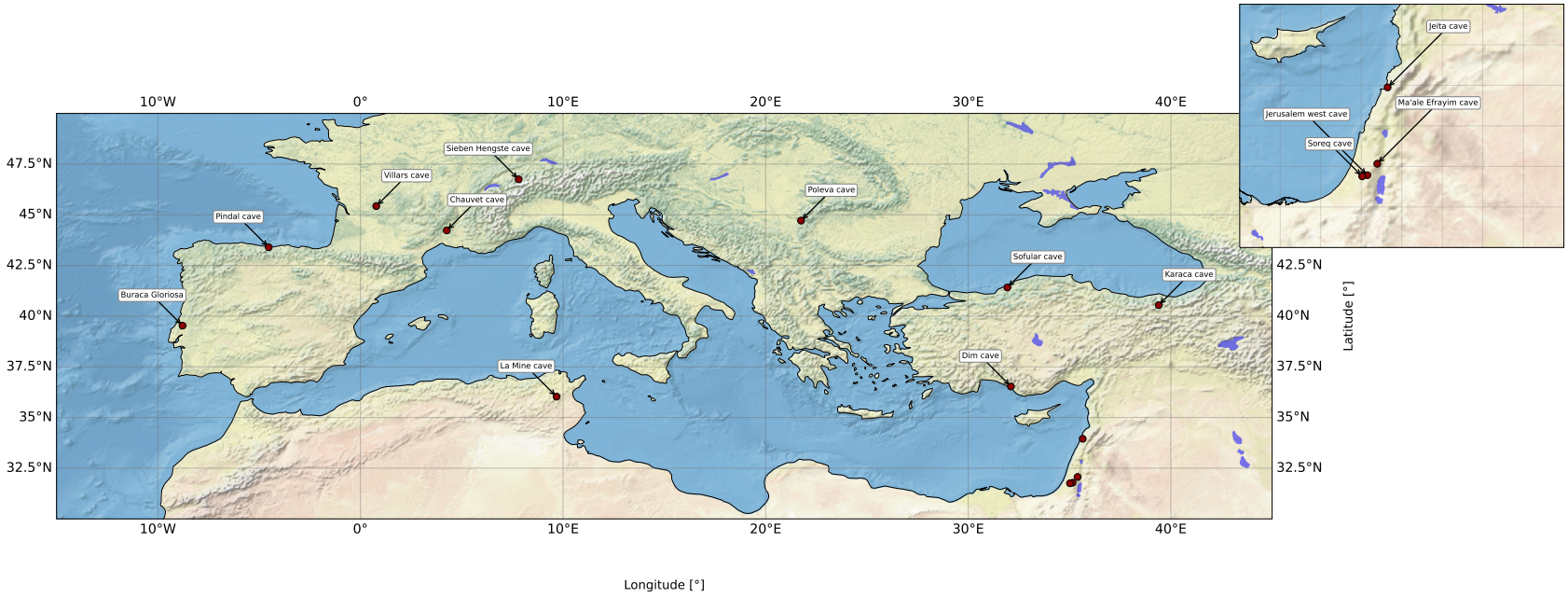

Figure 11: Geographic distribution of speleothem cave sites from the SISAL database across Europe and the Mediterranean region, serving as reference points for comparing simulated δ^{18}O values with the SISAL dataset.

Figure 12: Comparison of synoptic regime frequencies between the Last Glacial Maximum (LGM) and the Modern Day (MD) based on DSRM-classified *Großwetterlagen* (GWL). The plot shows the relative change in regime abundance from MD to LGM, with positive percentages (green) indicating increased frequency during glacial conditions, and negative percentages (red) indicating decreased frequency.

6.3.2 Spatial Climate Parameter Fields

Figure 13 shows climatological mean fields averaged over 30 years from the isotope-enabled EMAC model, highlighting four key climate parameters under Last Glacial Maximum boundary conditions.

Simulated δ^{18}O in precipitation (Panel (a)) exhibits a clear north–south gradient: strongly depleted values appear over high-latitude regions (Scandinavia, the Baltic, British Isles), while enriched signatures occur in southern zones (Levant, North Africa, southern Arabian Peninsula, Azores). A secondary depletion extends from Eastern Europe into Siberia and Central Asia. A pronounced minimum in δ^{18}O values in precipitation extends across the Bay of Biscay and the Iberian Peninsula, with the lowest values situated northwest of Galicia. Simulation resolution limits topographic detail, leading to only approximate reproduction of cave site isotopic values. Comparison with SISAL speleothems shows close agreement in the Western Mediterranean (Chauvet Cave), slight overestimates in the Eastern Mediterranean (Jeita Cave, Jerusalem West Cave), and larger biases at mountainous sites (Sieben Hengste Cave, Poleva Cave, Sofular Cave, Karaca Cave). Precipitation totals (Panel (b)) form wave-like spatial patterns. Maximum rainfall concentrates over the Bay of Biscay and Iberian Peninsula (peak northwest of Galicia), with additional high-precipitation belts in Central Europe, the British Isles, the Sahel, the Arabian Peninsula, and the Persian Plateau. Conversely, western North Africa, the Azores, Western Europe, Central Asia, and the Eastern European Plain receive relatively low precipitation. Annual mean temperature (Panel (c)) shows a steep latitudinal gradient, with coldest conditions in northern Europe and progressively warmer values toward the south. Western Europe remains marginally warmer than Central Europe under LGM forcing. The British Isles exhibit notably lower temperatures compared to surrounding regions, and the coldest temperatures align again over the Bay of Biscay and Iberia, with a local minimum near Galicia. Surface pressure (Panel (d)) exhibits a meridional dipole pattern, with cyclonic circulation dominating Central and Northern Europe, and anticyclonic highs prevailing over the Mediterranean–Middle East region, extending westward to the Azores. Weak yet discernible cyclonic influences are also evident over the Southern Sahara and the Red Sea. North of the Alps, sea level pressure (SLP) steadily drops with latitude, reinforcing a strong meridional gradient.

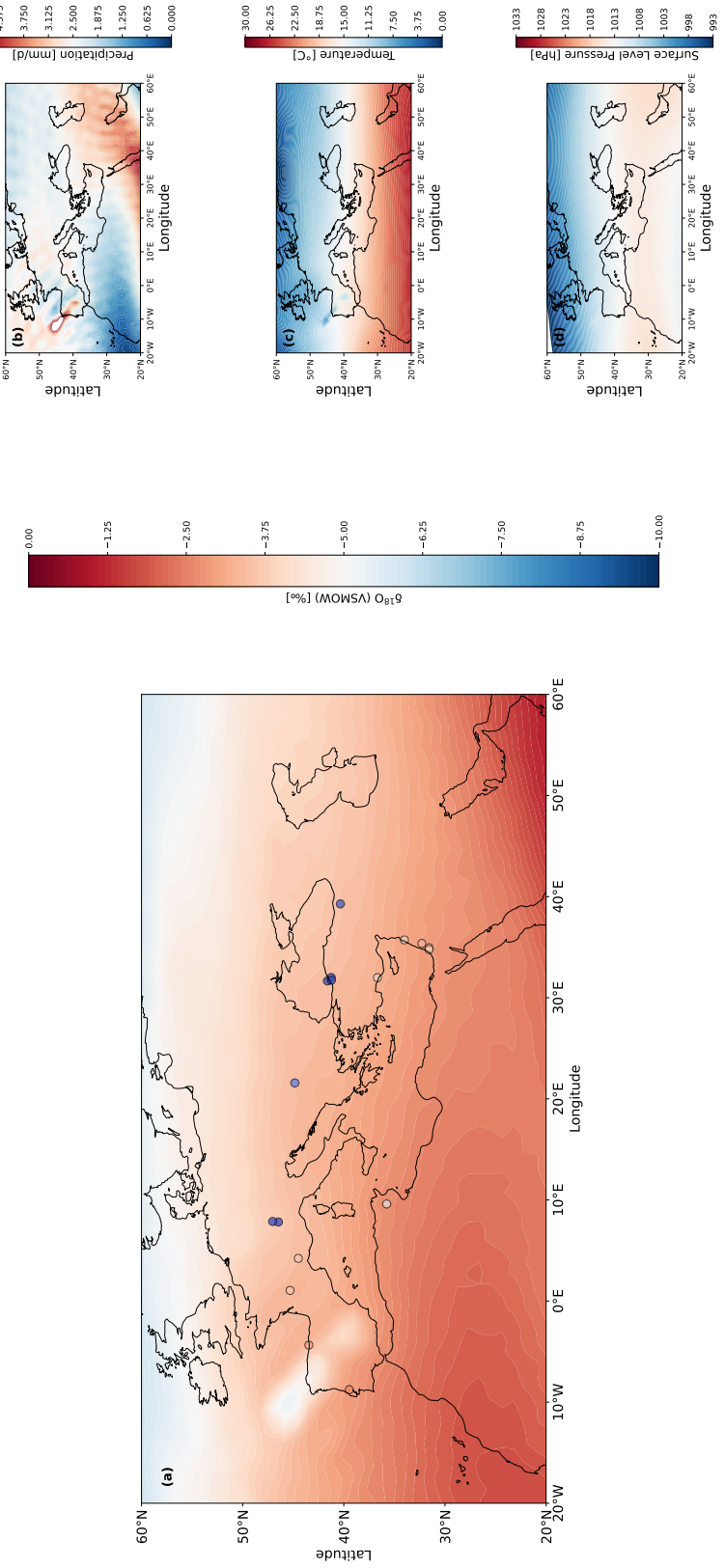

Figure 13: Spatial distribution of simulated climate parameters during the Last Glacial Maximum (LGM) over Europe and adjacent regions, based on 30-year mean values from the isotope-enabled EMAC model. Panels show (a) δ^{18}O in precipitation, (b) precipitation totals, (c) annual mean temperature, and (d) surface-level pressure. The δ^{18}O panel presents cave sites with proxy data, comparing simulated δ^{18}O values against SISAL reference records to illustrate regional model performance across the Mediterranean and Southern Europe.

6.3.3 δ^{18}O–Climate Parameter Correlations

Figure 14 presents the coefficient of determination (R) between simulated monthly mean δ^{18}O in precipitation and four climatic drivers (temperature (Panel (a)), precipitation (Panel (b)), sea-level pressure (Panel (c)), and evaporation (Panel (d))) across Europe and adjacent regions during the Last Glacial Maximum.

The temperature–δ^{18}O relationship (Panel (a)) is generally weak and positive across the domain, with correlation coefficients ranging from $0 < R < 0.3$, except over the Sahara and Arabian Peninsula where negative correlations ($R < 0$) occur. A localized maximum is observed northwest of Galicia, spanning the Bay of Biscay and the Iberian Peninsula. Statistically insignificant correlations appear north of the British Isles and within narrow bands across North Africa and the Middle East. Panel (b) illustrates weak to moderate correlations between δ^{18}O and precipitation, with R values between 0.25 and 0.5 throughout continental Europe and the Northern Mediterranean. The δ^{18}O–sea-level pressure correlation (Panel (c)) is moderate ($R \approx 0.3$–0.5), forming a broad band extending from the British Isles through Central Europe to the Eastern European Plain, with a localized maximum over the Bay of Biscay and Iberia. Evaporation–δ^{18}O correlations (Panel (d)) exhibit a complex pattern: low correlations ($R < 0.2$) dominate the North Sea, Baltic Sea, neighboring Baltic states, and the North Atlantic off Western Europe. Regions of insignificant correlation appear in the Sahel, while a pronounced local maximum recurs northwest of Galicia over the Bay of Biscay and Iberian Peninsula.

6.3.4 Evaluation of δ^{18}O Weighting Schemes

Figure 15 presents regression results comparing long-term mean speleothem δ^{18}O values from the SISAL database with simulated climatological means under four weighting schemes: (a) calcite-weighted δ^{18}O, (b) infiltration-weighted δ^{18}O, (c) precipitation-weighted δ^{18}O, and (d) unweighted δ^{18}O in precipitation. Statistical comparisons were conducted using one-sample t-tests to assess whether the mean differences significantly deviate from zero. Error bars represent measurement uncertainties.

Panel (a) displays calcite-weighted δ^{18}O values (in ‰ VSMOW), with data points closely clustering around the reference line. The mean difference is negligible (-0.0065), and the result is statistically insignificant ($t = -0.0086$, $p = 0.9933$), demonstrating a high level of concordance between simulated and observed values. Sofular Cave and Sieben Hengste Cave are strongly overestimated, Karaca Cave and Poleva Cave are slightly overestimated, and Chauvet Cave aligns closely with the ideal fit. Slight under-

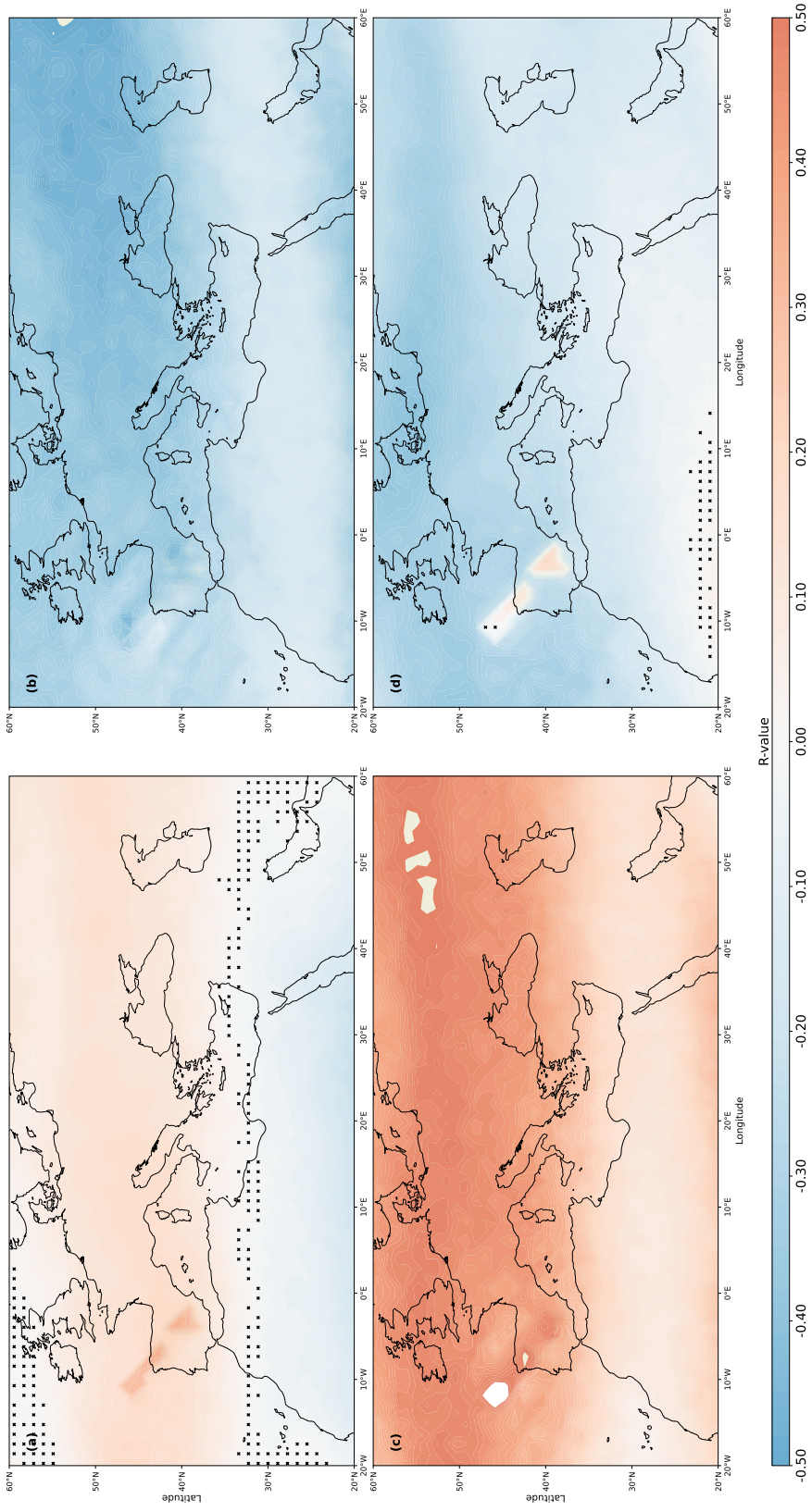

Figure 14: Spatial distribution of the coefficient of determination (R) between simulated $\delta^{18}O$ values in precipitation and selected climate variables during the Last Glacial Maximum (LGM). Panels show correlations with (a) temperature, (b) precipitation, (c) sea-level pressure, and (d) evaporation. Black dots mark regions where the regression model is not statistically significant (p-value ≥ 0.05).

estimations occur at La Mine Cave, Dim Cave, Jeita Cave, Jerusalem West Cave, and Ma'ale Efrayim Cave, while Soreq Cave, Villars Cave, Pindal Cave, and Buraca Gloriosa Cave show moderate underestimation. Panel (b) shows infiltration-weighted δ^{18}O values, where most points lie near the 1:1 line, though a slight negative bias is evident. The mean difference of -0.7185 ‰ is not statistically significant ($t = -1.2515$, $p = 0.2328$). Sofular Cave and Sieben Hengste Cave remain strongly overestimated. Karaca Cave, Poleva Cave, La Mine Cave, Dim Cave, Jeita Cave, Chauvet Cave, Jerusalem West Cave, and Ma'ale Efrayim Cave fall close to the ideal fit. Buraca Gloriosa Cave is slightly underestimated, and Pindal Cave, Soreq Cave, and Villars Cave are strongly underestimated. Panel (c) presents precipitation-weighted δ^{18}O values, with a mean difference of 0.1963 ‰. The data points are broadly distributed around the reference line, and the deviation is statistically insignificant ($t = 0.3520$, $p = 0.7305$). Sofular Cave and Sieben Hengste Cave are strongly overestimated; Poleva Cave, La Mine Cave, and Dim Cave are slightly overestimated; Karaca Cave, Jeita Cave, Chauvet Cave, Jerusalem West Cave, and Ma'ale Efrayim Cave align closely; and Buraca Gloriosa Cave is slightly underestimated. Pindal Cave, Soreq Cave, and Villars Cave exhibit strong underestimation. Panel (d) illustrates unweighted δ^{18}O values in precipitation, where a more pronounced positive deviation is observed. The mean difference of 1.2791 ‰ approaches statistical significance ($t = 2.1272$, $p = 0.0531$), suggesting a tendency for the simulation to overestimate observed values. Sofular Cave and Sieben Hengste Cave remain strongly overestimated; Karaca Cave and Poleva Cave are moderately overestimated; La Mine Cave, Dim Cave, and Jeita Cave show slight overestimation; Chauvet Cave, Jerusalem West Cave, Ma'ale Efrayim Cave, and Buraca Gloriosa Cave lie near the ideal fit; and Pindal Cave, Soreq Cave, and Villars Cave are slightly underestimated.

Overall, the results indicate that calcite-weighted and infiltration-weighted schemes yield the closest agreement with observations, while unweighted values show the largest deviation. Precipitation-weighted results fall in between, with moderate discrepancies but no significant bias.

6.4 Discussion

The comparison of *Großwetterlagen* (GWL) frequencies between the Last Glacial Maximum (LGM) and the Modern Day (MD) period reveals a profound reorganization of mid-latitude circulation over Central Europe. During the LGM, anticyclonic or weakly cyclonic westerly flows (WW, SWA, NWA) become more frequent, indicating persistent zonal regimes associated with stable, dry conditions and a muted Atlantic storm track

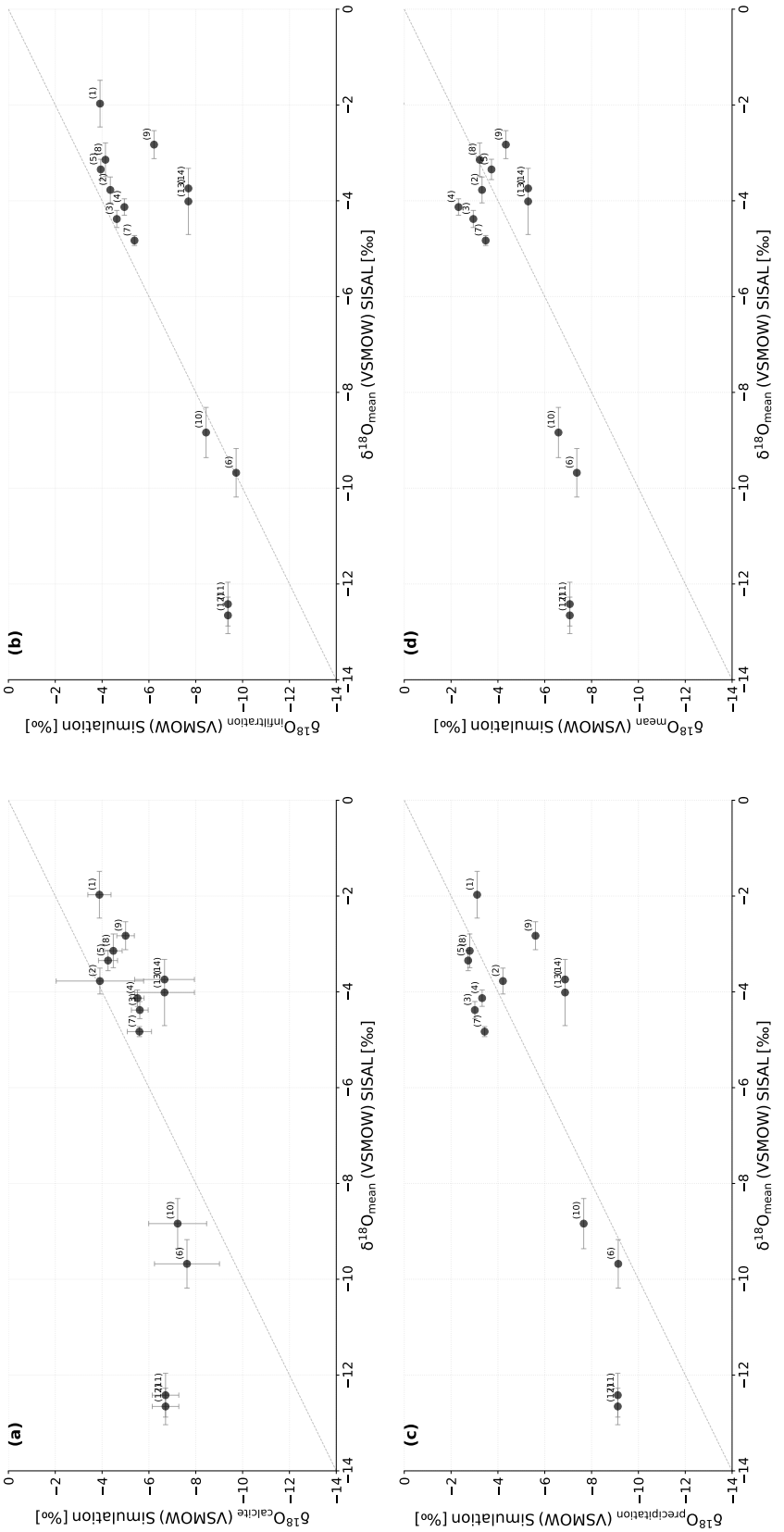

Figure 15: Regression analysis comparing mean δ^{18}O values from the SISAL database with simulated δ^{18}O values under four different weighting schemes during the Last Glacial Maximum (LGM). Panels display: (a) calcite-weighted δ^{18}O, (b) infiltration-weighted δ^{18}O, (c) precipitation-weighted δ^{18}O, and (d) unweighted δ^{18}O in precipitation. Cave site identifiers: (1) Buraca Gloriosa Cave, (2) Chauvet Cave, (3) Dim Cave, (4) Jeita Cave, (5) Jerusalem West Cave, (6) Karaca Cave, (7) La Mine Cave, (8) Ma'ale Efrayim Cave, (9) Pindal Cave, (10) Poleva Cave, (11) Sieben Hengste Cave, (12) Sofular Cave, (13) Soreq Cave, (14) Villars Cave.

[75, 79]. In contrast, other cyclonic westerly types (WA, WS, SWZ, NWZ) dominate under modern boundary conditions, reflecting intensified frontal systems. Northerly and northeasterly regimes (NZ, NEA, NEZ) diminish under glacial conditions, pointing to reduced or shifted Arctic and continental cold-air intrusions and a less amplified planetary wave pattern [79]. The unchanged frequency of NA alongside the increased occurrence of cyclonic NWA further underscores altered meridional exchange. Southern and southeastern types show nuanced shifts: SEA declines, suggesting weakened warm-air advection from the southeast, while SA increases slightly and SEZ/SZ remain stable, indicating that some Mediterranean-influenced pathways persist despite overarching atmospheric reconfiguration [39]. Stationary highs over Central Europe (HM, BM) rise in frequency, likely driven by enhanced radiative cooling and an expanded Siberian High, contributing to prolonged dry, cold spells [90]. Hybrid and transitional types (HNA, HNZ, HNFA, HFZ, HFA, TRM, TB) decrease, whereas TRW and HB gain prevalence, all pointing to fewer regime transitions and a more locked-in synoptic state. Finally, the greater share of unclassified flow patterns under interglacial conditions highlights a more variable, less predictable circulation [17].

Simulated fields from the isotope-enabled EMAC model reveal coherent spatial anomalies in isotopic composition, precipitation, temperature, and surface pressure under LGM forcing. A pronounced north–south gradient in δ^{18}O in precipitation arises from temperature-driven fractionation, characterized by strongly depleted values at high latitudes (Scandinavia, Baltic region, British Isles) and enriched values along the southern margins (Levant, North Africa, southern Arabian Peninsula, Azores) [119]. Continental rainout across the Eastern European Plain intensifies depletion toward Siberia and Central Asia. A well-defined region of low δ^{18}O values in precipitation, centered northwest of Galicia and extending over the Bay of Biscay and the Iberian Peninsula, consistently emerges across all analyzed fields. This feature is most plausibly attributed to inherent limitations in the model parametrization rather than representing a genuine paleoclimatic signal [117]. Precipitation totals exhibit alternating bands of high and low values, with pronounced maxima over the Bay of Biscay, Iberian Peninsula, Central Europe, British Isles, Sahel, Arabian Peninsula, and Persian Plateau. These patterns are indicative of substantial shifts in precipitation coherent with a southward displacement of the polar front [82, 90]. Nevertheless, the recurring high and low bands may also reflect limitations inherent to the model parametrization rather than true climatic variability. Anticyclonic ridges over western North Africa, the Azores, Western Europe, Central Asia, and the Eastern European Plain reflect anticyclonic dominance and continental aridity [93]. Temperature maps mirror the δ^{18}O gradient in precipitation, showing cold

conditions over northern Europe and the Bay of Biscay/Iberia, with Western Europe marginally warmer than Central Europe. This pattern is consistent with glacial insolation dynamics, reduced Gulf Stream influence, and a poleward shifted frontal zone [84, 111]. Surface pressure exhibits a meridional dipole: cyclonic over Central/Northern Europe and anticyclonic over the Mediterranean–Middle East (Azores), reinforcing a southward-shifted polar front and a steep meridional gradient [70].

Figure 14 demonstrates that no single climatic driver fully explains the variability in simulated monthly δ^{18}O in precipitation across Europe and adjacent regions during the Last Glacial Maximum. The temperature–δ^{18}O correlation (Panel a) is consistently weak and predominantly positive ($0 < R < 0.3$), with localized negative correlations over the Sahara and Arabian Peninsula, indicating a limited thermal coupling in the simulation [4]. Moderate correlations between precipitation and δ^{18}O in precipitation (Panel b), ranging from $0.25 < R < 0.5$, are evident over continental Europe and the northern Mediterranean, in line with the classical amount effect [104], and also reflect continental isotopic depletion in Eastern Europe [99]. The relationship between δ^{18}O in precipitation and sea-level pressure (Panel c) shows intermediate correlations ($R \approx 0.3$–0.5) extending from the British Isles through Central Europe to the Eastern European Plain, capturing the linkage between large-scale pressure patterns and moisture transport and paralleling the cyclonic westerly flow associated with a southward-displaced polar front [44]. Evaporation–δ^{18}O correlations (Panel d) are generally low ($R < 0.2$) over the North Sea, Baltic region, and North Atlantic, but exhibit a recurrent local maximum northwest of Galicia over the Bay of Biscay. The consistent appearance of this maximum across all panels suggests it likely reflects a model parametrization artifact rather than a robust paleoclimatic signal.

The regression analysis of four δ^{18}O weighting schemes against SISAL speleothem records reveals that the calcite-weighted approach most accurately reproduces observed values. Calcite-weighted results cluster tightly around the 1:1 line, with a negligible mean offset of -0.0065 ‰ ($t = -0.0086$, $p = 0.9933$), indicating near-perfect correspondence between simulated and measured δ^{18}O. Infiltration weighting induces a modest negative bias (mean offset $= -0.7185$; $t = -1.2515$, $p = 0.2328$), while most sites cluster closely along the 1:1 line, highlighting the significant role of subsurface flow processes in shaping speleothem isotope signatures. Precipitation weighting yields a slight positive offset (0.1963 ‰; $t = 0.3520$, $p = 0.7305$) with broadly scattered deviations around the 1:1 line, while the unweighted scheme exhibits the largest systematic overestimation (1.2791 ‰; $t = 2.1272$, $p = 0.0531$). All weighting approaches consistently overestimate δ^{18}O at Sofular Cave and Sieben Hengste Cave, while tending

to underestimate values at Pindal Cave, Soreq Cave, and Villars Cave [7, 121]. The close agreement achieved by calcite and infiltration weighting supports their application for reconstructing paleo-hydrological conditions in karst environments, whereas the pronounced bias of the unweighted method underscores the need for process-based weighting schemes [94, 113].

6.5 Conclusion

This study demonstrates that the Last Glacial Maximum (LGM) featured a fundamentally reorganized atmospheric circulation over Europe, marked by a pronounced decline in transitional and hybrid synoptic regimes, a reorganization of meridional flow types, and an increase in stationary anticyclonic systems over Central Europe, reflecting more stable yet less dynamically active conditions under glacial boundary forcings such as expanded ice sheets, altered sea-surface temperatures, and shifted jet-stream trajectories [79]. The spatial distribution of simulated δ^{18}O in precipitation reveals coherent depletion patterns across western and central Europe which are consistent with temperature fractionation and continental rain-out effects, while a recurring anomaly over the Bay of Biscay and the Iberian Peninsula, evident in multiple climate fields and correlation maps, points to systematic model parameterization deficiencies. Correlation analyses between δ^{18}O in precipitation and climatic variables (temperature, precipitation, sea-level pressure, evaporation) uncover robust coupling in central and northern Europe, with the δ^{18}O–SLP correlation band mirroring the cyclonic westerly drift during glacial periods and indicating directional coherence between isotopic signals and synoptic circulation, whereas southern regions exhibit more complex, heterogeneous relationships influenced by seasonal recharge, evaporative processes, and subtropical circulation [96]. A comparative evaluation of four δ^{18}O weighting schemes against SISAL speleothem records confirms the critical role of hydrological weighting in improving simulation–proxy agreement. Calcite- and infiltration-weighted approaches show the closest agreement with observed values. Calcite weighting yields a near-zero mean offset, while infiltration weighting introduces a modest negative bias but effectively captures key subsurface dynamics, as evidenced by the tight clustering of most sites along the 1:1 line. In contrast, the unweighted scheme exhibits the largest systematic overestimation. The consistent performance of process-based schemes underscores their importance for accurately reconstructing paleo-hydrological conditions in karst environments. Persistent overestimations at Sofular Cave and Sieben Hengste Cave and underestimations at Pindal Cave, Soreq Cave, and Villars Cave highlight the limitations of simplified weighting strategies.

The combined use of synoptic-scale circulation analysis, detailed spatial correlation assessments, and rigorous evaluation of isotopic weighting schemes establishes a comprehensive approach for deciphering the complex controls on $\delta^{18}O$ variability during the Last Glacial Maximum. This integrative framework enables robust reconstruction of speleothem proxy records by capturing the nuanced interactions between large-scale atmospheric patterns, local hydrological processes, and isotopic fractionation mechanisms. Such an approach not only improves the fidelity of paleoenvironmental interpretations but also guides future model developments aimed at refining isotope-enabled climate simulations.

7 Model Application to Speleothem Archives

Synoptic Controls on Speleothem $\delta^{18}O$ During the Last Glacial Maximum (manuscript in preparation)

Specific Contribution Summary

The foundational concept of the study was developed by Holger Tost and Denis Scholz. All simulation data were processed by Tim Liesenhoff and Holger Tost. Tim Liesenhoff carried out the regime classification across all datasets and developed the source code for the DSRM and the infiltration model. The interpretation of results was a joint effort by Tim Liesenhoff, Holger Tost, and Denis Scholz, with Tim Liesenhoff assuming a leading role. He also coordinated and led the writing of the manuscript.

7.1 Background and Objectives

Large-scale atmospheric circulation patterns are a fundamental driver of regional climate and isotopic variability across Europe [72, 91, 92]. During the Last Glacial Maximum (LGM), glacial boundary conditions, including expanded ice sheets, reduced greenhouse gas concentrations, and modified sea surface temperatures, fostered more persistent high-pressure systems and a stabilized atmospheric configuration over the European continent [75, 90]. To understand past climate variability, it is essential to examine synoptic-scale circulation dynamics and their imprint on hydroclimatic conditions. The *Großwetterlagen* (GWL) classification system, originally developed by Hess and Brezowsky [52], remains a cornerstone in characterizing persistent synoptic conditions over Central Europe. With 29 defined circulation types, grouped into circulation types (GT) and flow regimes (GR), the system enables detailed analysis of prevailing atmospheric directions and their climatic impacts [45, 53]. A key parameter in paleoclimate research is δ^{18}O, a stable oxygen isotope widely used to reconstruct past environmental conditions [8, 20]. Speleothem-derived δ^{18}O values integrate signals from temperature, moisture sources, and rainout histories, but their interpretation is complicated by interactions with meteorological variables such as precipitation amount, temperature variability, and circulation dynamics [65, 112].

This study investigates the direct influence of atmospheric circulation types on speleothem $\delta^{18}O$ signals during the Last Glacial Maximum (LGM) in the Mediterranean region. By analyzing the interplay between synoptic-scale weather patterns and isotopic variations recorded in speleothems, it aims to unravel the climatic and hydrological controls shaping these proxy records in this climatically complex area [2]. This regional perspective provides valuable insights into the mechanisms driving isotopic variability and helps improve the interpretation of paleoclimate archives from the Mediterranean basin. Using records from the SISAL database, isotopic variability is analyzed in relation to synoptic-scale regimes classified via a Diagnostic Synoptic Regime Model (DSRM) framework. This framework applies objective classification to daily sea-level pressure (SLP) fields from the isotope-enabled ECHAM5/MESSy Atmospheric Chemistry (EMAC) model, allowing reproducible identification of circulation types under glacial conditions and targeted comparison with proxy data. To link simulation output with speleothem records, a multi-tiered isotope modeling approach is employed. Monthly $\delta^{18}O$ means are derived using three weighting schemes: precipitation-weighted values emphasize effective rainfall contributions, infiltration-weighted values incorporate hydrological filtering such as evapotranspiration and karstic recharge, and calcite-weighted values simulate speleothem formation through temperature-dependent fractionation of infiltrated water [112].

The specific objectives of this study are:

1. To quantitatively evaluate the robustness and climatological relevance of the DSRM-based circulation types under glacial boundary conditions.

2. To determine direct linkages between objectively classified synoptic regimes and speleothem-derived $\delta^{18}O$ signals, thereby identifying circulation-dependent isotopic imprints in Mediterranean proxy records.

3. To assess the reproducibility and generalizability of the combined DSRM and infiltration modeling framework for paleoclimate applications.

By integrating synoptic diagnostics with proxy-based isotope modeling, this study aims to disentangle the climatic drivers of speleothem $\delta^{18}O$ variability and enhance understanding of glacial climate dynamics across Europe and the Mediterranean.

7.2 Methods and Data

This study employs a process-based framework that integrates climate model diagnostics, isotope modeling, and circulation classification to assess how glacial boundary conditions modulate speleothem-relevant isotopic variability. A 30-year simulation using the ECHAM5/MESSy Atmospheric Chemistry (EMAC) model, which includes the H_2OISO submodel for stable water isotopologues ($H_2^{18}O$, $H_2^{16}O$), is forced with prescribed Last Glacial Maximum (LGM) sea surface temperatures (SST), sea ice concentrations (SIC), and atmospheric trace gas levels [31, 68, 117]. The full suite of forcing parameters is summarized in Table 7, as previously detailed in Chapter 6.2.1.

Observational validation relies on ten well-dated speleothem records from the SISAL database [20], regionally grouped into Eastern and Western Mediterranean domains (Fig. 16). Eastern Mediterranean sites (Jeita Cave, Dim Cave, Ma'ale Efrayim Cave, Jerusalem West Cave, and Soreq Cave) and Western Mediterranean sites (Buraca Gloriosa, Pindal Cave, Villars Cave, Chauvet Cave, and La Mine Cave) provide high-precision oxygen isotope ratios ($\delta^{18}O$) on the VPDB scale, subsequently converted to VSMOW, with analytical precision of ± 0.15 ‰ and temporal coverage from 19–29 ka BP [6, 20, 21]. The analysis integrates three primary datasets: (i) daily and monthly output from isotope-enabled EMAC simulations under Last Glacial Maximum boundary conditions at T106 horizontal resolution (approximately 1.1°), (ii) speleothem proxy $\delta^{18}O$ records from SISAL, and (iii) synoptic regime classifications derived from the HB–GWL framework. Key meteorological and hydrological variables include air temperature (T), precipitation amount (P), infiltration rate (I) from the process-based infiltration model, and frequencies of classified *Großwetterlagen* (GWL). Isotopic parameters evaluated comprise unweighted $\delta^{18}O$ in precipiation, precipitation-weighted $\delta^{18}O$, infiltration-weighted $\delta^{18}O$, and calcite-weighted $\delta^{18}O$ values.

Daily synoptic regimes during the Last Glacial Maximum (LGM) are identified using the same Diagnostic Synoptic Regime Model (DSRM) framework described in Section 5.2.2. In short, sea-level pressure (SLP) fields are extracted from six regional subgrids covering Western Europe, Iceland, Azores, Eastern Europe, Scandinavia, and Central Europe (see Figure 1 for subgrid layout). Geostrophic flow diagnostics are then computed, including zonal and meridional components (W, S), resultant flow magnitude (F), flow direction (θ), and shear vorticity (ζ), following the classification logic illustrated in Figure 2. Based on threshold criteria shown in Table 5 and Table 6, each simulation day is assigned to one of 27 circulation types: zonal, mixed, meridional, straight, or unclassified. Monthly *Großwetterlagen* (GWL) frequencies are derived from these daily labels, enabling direct comparison with climate simulations and observational datasets.

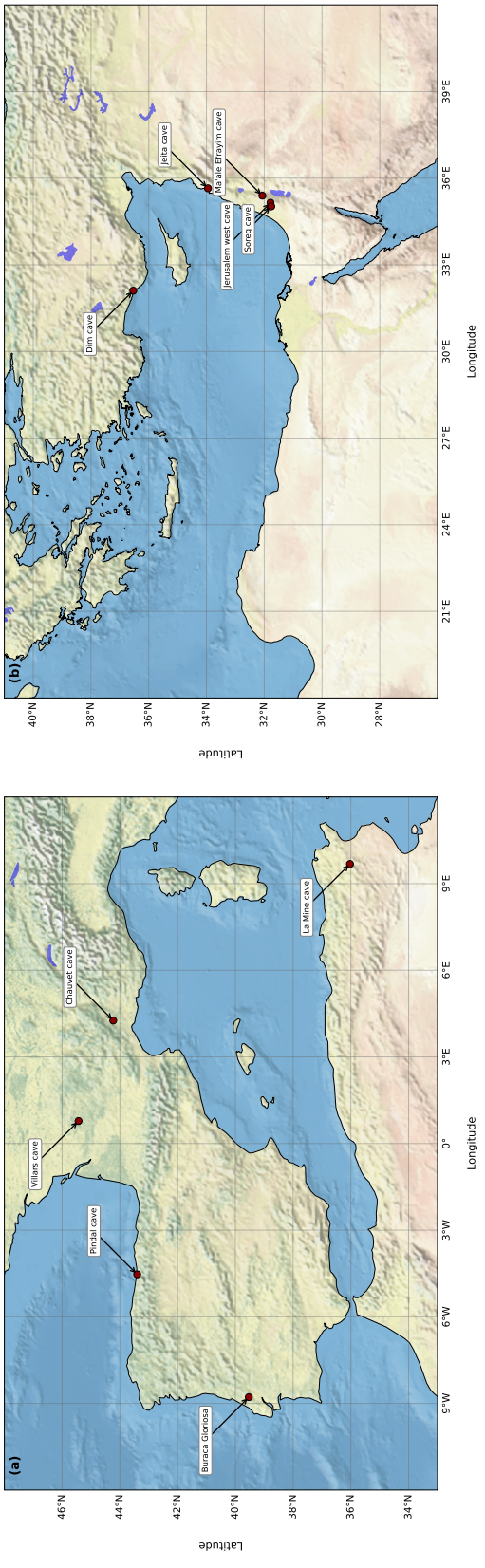

Figure 16: Panel (a): Locations of speleothem sites in the Eastern Mediterranean (EM) used in this study, including Jeita Cave, Dim Cave, Maale Efrayim Cave, Jerusalem West Cave, and Soreq Cave. Panel (b): Locations of speleothem sites in the Western Mediterranean (WM), comprising Buraca Gloriosa, Pindal Cave, Villars Cave, Chauvet Cave, and La Mine Cave.

For each identified GWL, composite fields of temperature, precipitation, and the oxygen isotope signal (δ^{18}O) are generated and evaluated using three weighting schemes (precipitation-weighted δ^{18}O, infiltration-weighted δ^{18}O, and calcite-weighted δ^{18}O) to reflect hydrological and geochemical processes relevant to speleothem formation [112]. A detailed description of the used infiltration model is provided in Section 6.2.2. All calculations are performed at each speleothem site's grid cell using bilinear interpolation of EMAC fields, ensuring spatial consistency with SISAL site locations. The resulting monthly δ^{18}O time series for each weighting scheme form the basis for evaluating synoptic-scale circulation controls on isotopic variability under LGM boundary conditions, building on prior comparisons with SISAL records. Climate Parameters, including precipitation amount, infiltration dynamics, and temperature, are also analyzed, and observational reference data from ten speleothem sites in the SISAL database support the interpretation and regional differentiation of circulation impacts [20].

7.3 Results

7.3.1 GWL Frequency Distributions (LGM)

Each segment represents a specific synoptic regime, color-coded as follows: blue and dark blue indicate zonal regimes (pure westerly flow), green denotes mixed regimes, orange represents meridional regimes, and grey corresponds to transitional or undefined regimes. As shown in Figure 17, the hierarchical distribution of *Großwetterlagen* (GWL) frequencies during the Last Glacial Maximum (LGM) is dominated by meridional regimes, which account for 37.8 % of all classified patterns. Mixed regimes follow at 28.5 %, while pure zonal flows contribute 14.6 % and straight flow patterns only 6.4 %. Transitional or ambiguous types remain unclassified and comprise 12.6 % of the distribution. The low overall frequency of the Straight Flow Regime (STR) reflects a consistently pronounced pressure gradient across Europe, indicative of a stable and persistent anticyclonic configuration under glacial boundary conditions, characterized by atmospheric blocking and reduced zonal flow. Within the mixed GWL, HM (High-pressure Central Europe) and NW (Northwest) types are most prevalent, together representing roughly 21 % of mixed regimes, whereas SW (Southwest) and TM (Low-pressure Central Europe) types are comparatively rare at about 7.5 %. Northern and Eastern flow types collectively contribute approximately 23 % to the total circulation, and Southern types account for around 14.9 %. Zonal regimes are comparatively minor, underscoring the reorganization toward meridional and mixed circulation during the LGM.

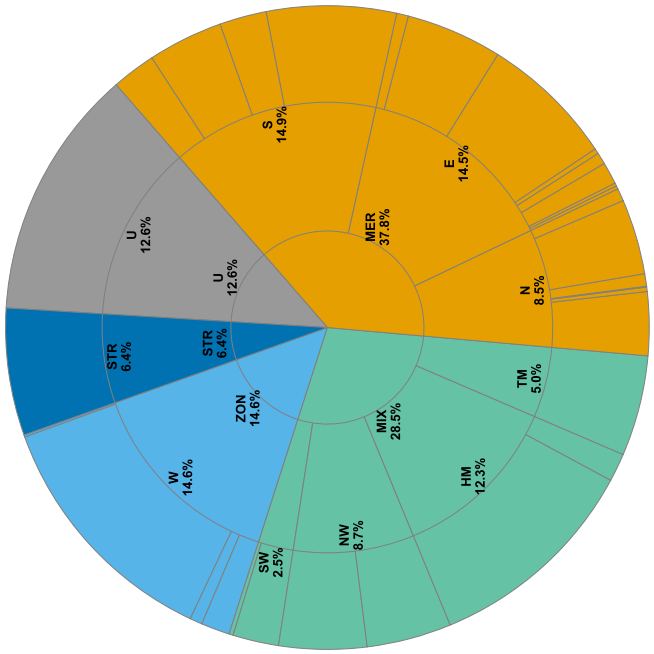

Figure 17: Hierarchical distribution of simulated *Großwetterlagen* (GWL) frequencies during the Last Glacial Maximum (LGM), based on the Hess–Brezowsky classification. Each segment represents a specific synoptic regime, color-coded as follows: blue and dark blue indicate zonal regimes (straight westerly flow), green denotes mixed regimes, orange represents meridional regimes, and grey corresponds to transitional or undefined regimes.

7.3.2 Climate Parameter Anomalies by Circulation Type

Figures 18 and 19 illustrate standardized climate anomalies for the Eastern and Western Mediterranean, respectively. These anomalies are expressed in standard deviations (σ) relative to the region-wide mean and grouped by circulation type across four parameters: (a) δ^{18}O in precipitation, (b) precipitation, (c) infiltration, and (d) temperature. Each boxplot aggregates station-specific deviations for the *Großwetterlagen* (GWL) types, with bracketed labels denoting the dominant pressure regime (H = anticyclonic, T = cyclonic) or flow direction (e.g., NW, SW).

In the Eastern Mediterranean, the δ^{18}O anomalies in precipitation are generally centered on zero, with HM (T) exhibiting a slight negative shift and SW (H) and U showing minor positive deviations. Precipitation anomalies also cluster around zero, although HM (T) displays a broad positive distribution. Infiltration anomalies trend slightly negative overall, driven by pronounced negative trends under HM (T), S (W), and N (NW). Temperature anomalies remain symmetrically distributed about the median across all regimes. Similarly, in the Western Mediterranean, δ^{18}O deviations in precipitation are close to zero; TM (W) shows a modest negative bias and U features a narrow distribution, while HM (H), TM (W), and NW (H) exhibit wider spreads. Precipitation and infiltration anomalies both tend toward slight negative means, with TM (W) and S (E) near the median and HM (H) spanning a wide range. Temperature anomalies again cluster around zero, with TM (W) slightly negative and HM (H) and S (E) slightly positive. Overall, climate anomalies in both Mediterranean regions concentrate near the climatological mean, with HM and TM regimes associated with greater variability in isotopic, hydrological, and thermal parameters.

7.3.3 δ^{18}O Anomalies by Circulation Type

Figure 20 and Figure 21 illustrates standardized δ^{18}O anomalies for the Eastern and Western Mediterranean, expressed in standard deviations (σ) relative to the region-wide mean and grouped by circulation type, across four weighting schemes: (a) calcite-weighted δ^{18}O, (b) infiltration-weighted δ^{18}O, (c) precipitation-weighted δ^{18}O, and (d) unweighted δ^{18}O in precipitation. Each boxplot aggregates station-specific deviations for the *Großwetterlagen* (GWL) types, with bracketed labels denoting the dominant pressure regime (H = anticyclonic, T = cyclonic) or flow direction (e.g., NW, SW).

In the Eastern Mediterranean, calcite-weighted δ^{18}O anomalies (Panel (a)) show the strongest depletion under northerly and southwesterly flows (NW (T) and SW (H)), both exhibiting median shifts below zero and broad interquartile ranges. E (T) and S

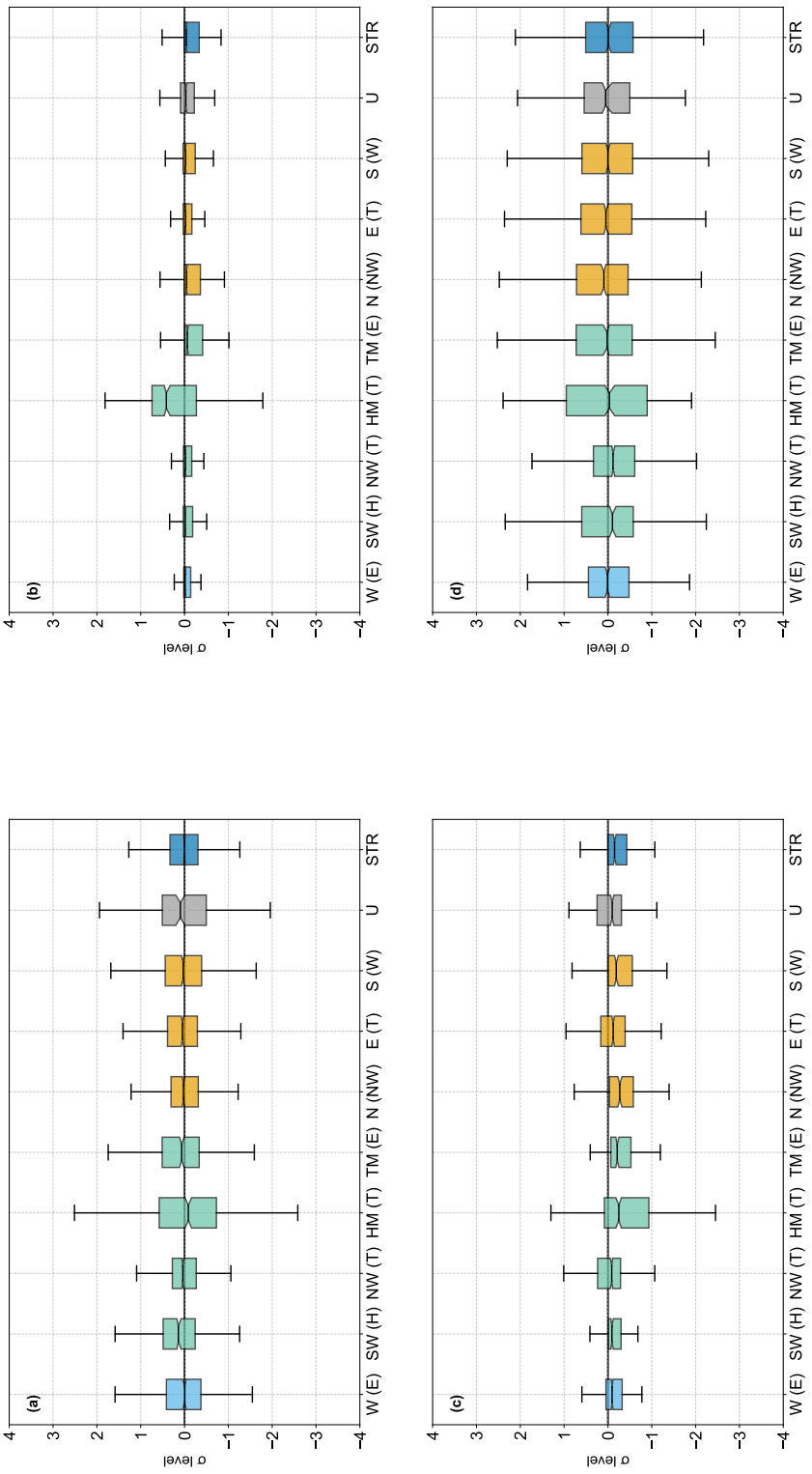

Figure 18: Boxplot distributions of standardized climate variables across different *Großwetterlagen* (GWL) types in the Eastern Mediterranean (EM). Variables are labeled as follows: (a) — δ^{18}O in precipitation, (b) — Precipitation, (c) — Infiltration, (d) — Temperature. GWL types are classified according to the Hess-Brezowsky system; bracketed labels denote the dominant regional atmospheric flow direction or pressure regime associated with each type.

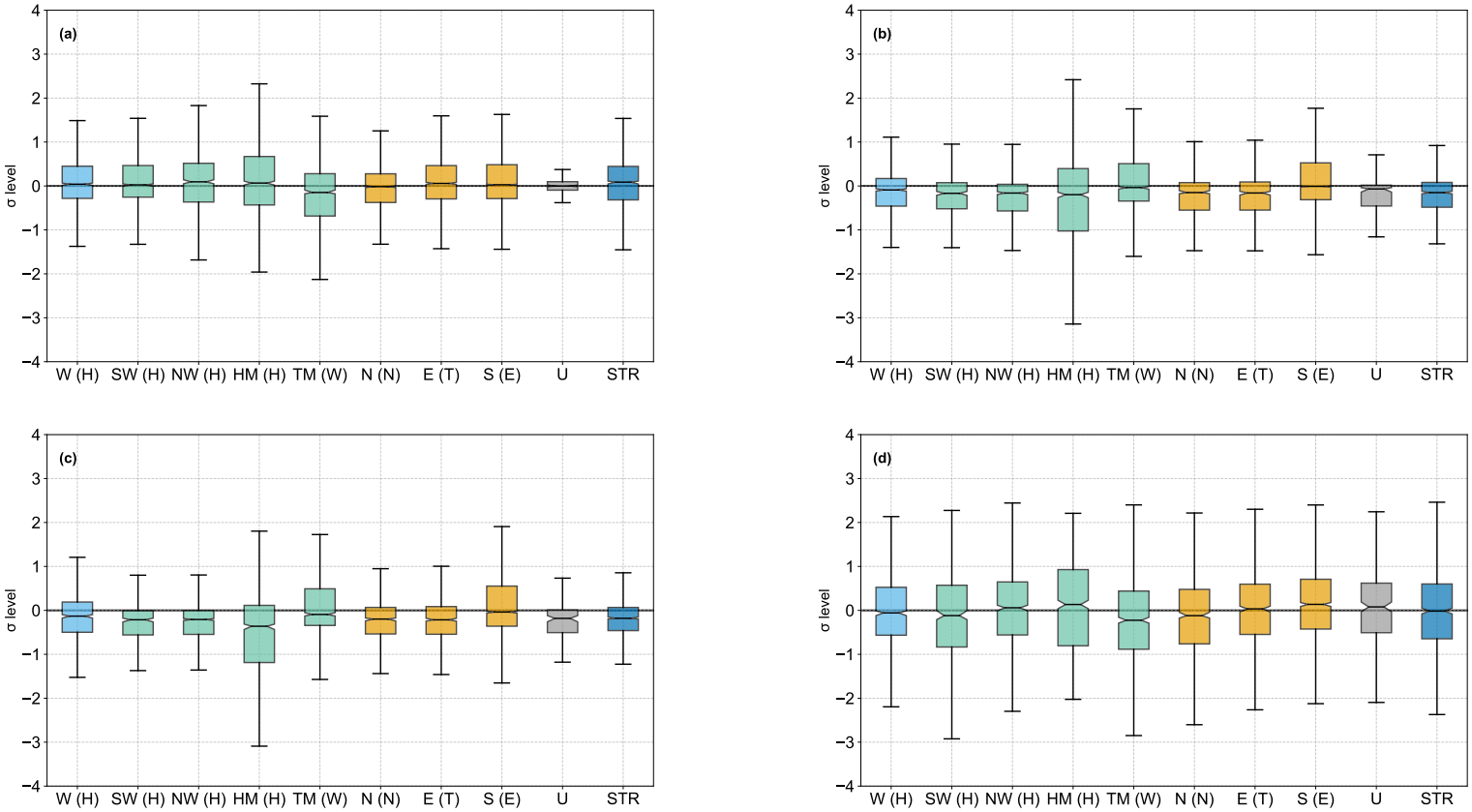

Figure 19: Boxplot distributions of standardized climate variables across different *Großwetterlagen* (GWL) types in the Western Mediterranean (WM). Variables are labeled as follows: (a) — δ^{18}O in precipitation, (b) — Precipitation, (c) — Infiltration, (d) — Temperature. GWL types are classified according to the Hess-Brezowsky system; bracketed labels denote the dominant regional atmospheric flow direction or pressure regime associated with each type.

(W) regimes also produce moderate negative deviations, while the Straight Flow regime (STR) stands out with a pronounced positive anomaly exceeding $+1\sigma$. Infiltration-weighted δ^{18}O values (Panel (b)) cluster tightly around the median for most regimes, but STR again yields a strong positive deviation and TM (E), N (NW), and E (T) display slight positive biases. Precipitation-weighted δ^{18}O anomalies (Panel (c)) remain centered near zero, although HM (T) exhibits a clear negative skew and both HM (T) and U have widened distributions. Unweighted δ^{18}O values in precipitation (Panel (d)) mirror these patterns, with HM (T) moderately depleted and SW (H) and U slightly enriched. In the Western Mediterranean, calcite-weighted anomalies (Panel (a)) shift positively under southwesterly and northwesterly flows (SW (H), NW (H)), as well as under S (E) and U regimes, indicating enriched isotope signals, whereas HM (H) aligns closely with the climatological mean. STR again produces the highest positive anomaly. Infiltration-weighted δ^{18}O anomalies (Panel (b)) show minimal spread for most regimes, with U and STR revealing moderate positive deviations and HM (H) a slight depletion. Precipitation-weighted δ^{18}O values (Panel (c)) and unweighted δ^{18}O anomalies in precipitation (Panel (d)) both concentrate around zero; HM (H) records a small negative offset, S (E) and U remain narrowly distributed, and HM (H), TM (W), and NW (H) present the largest interquartile ranges.

Overall, straight flow regimes consistently drive the most positive δ^{18}O anomalies across all weighting schemes, while meridional flows, especially under calcite-weighted conditions, yield the most pronounced negative deviations, highlighting the strong influence of synoptic-scale circulation on speleothem isotope signals.

7.4 Discussion

During the Last Glacial Maximum (LGM), European atmospheric circulation was fundamentally reconfigured by a dominant anticyclonic regime, in which meridional and mixed atmospheric flows transported cold, dry air masses from subarctic regions such as Scandinavia and Siberia, yielding a distinctly continental climate [39]. In contrast, modern conditions are governed by zonal west–east flows and Atlantic dynamics [59, 60]. The limited occurrence of zonal and straight-flow patterns, together comprising only about 20 % of synoptic types, points to a weakened Gulf Stream and reduced Atlantic influence, while the near-constant low pressure gradient across Europe, revealed by STR analysis, underscores the stability of glacial synoptic conditions [75]. Almost 40 % of circulation types fall into Mixed and Unclassified categories, indicating transitional or overlapping pressure systems and heightened atmospheric complexity. Within the Mixed regime, HM (High-pressure Central Europe) and NW (Northwest) types

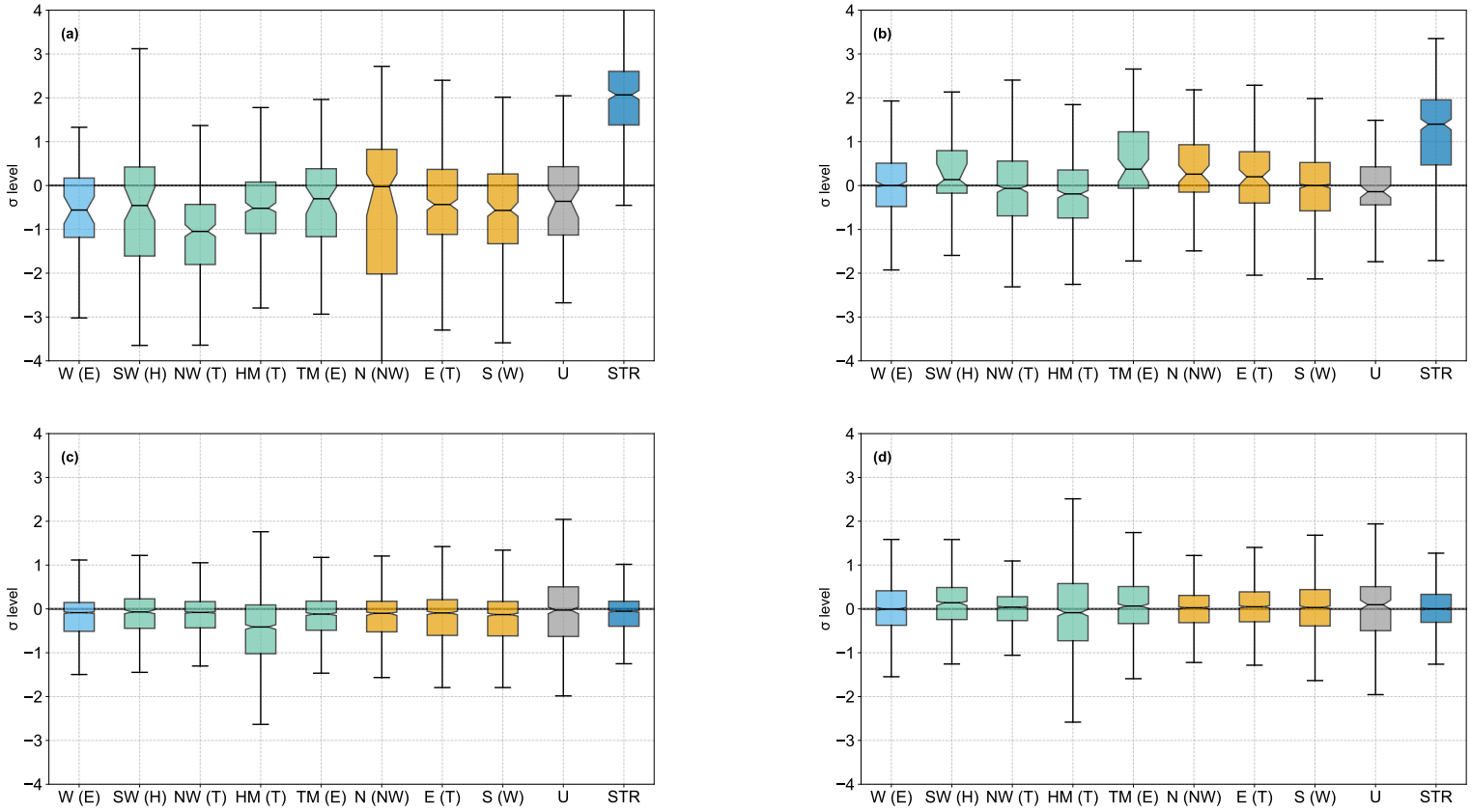

Figure 20: Boxplot distributions of standardized climate variables across different *Großwetterlagen* (GWL) types in the Eastern Mediterranean (EM). Variables are labeled as follows: (a) — Calcite-weighted δ^{18}O, (b) — Infiltration-weighted δ^{18}O, (c) — Precipitation-weighted δ^{18}O, (d) — Unweighted δ^{18}O in precipitation. GWL types are classified according to the Hess-Brezowsky system; bracketed labels denote the dominant regional atmospheric flow direction or pressure regime associated with each type.

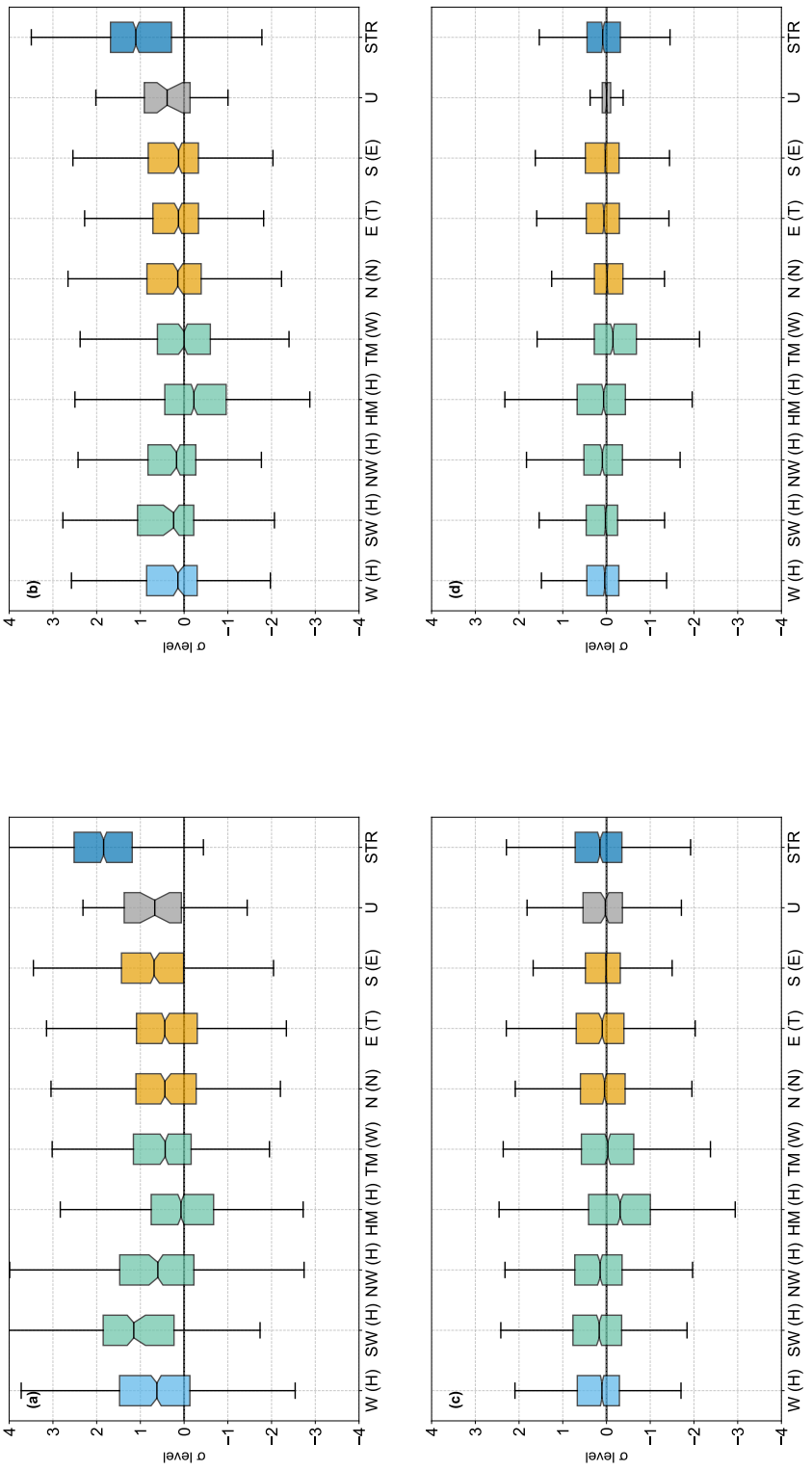

Figure 21: Boxplot distributions of standardized climate variables across different *Großwetterlagen* (GWL) types in the Western Mediterranean (WM). Variables are labeled as follows: (a) — Calcite-weighted δ^{18}O, (b) — Infiltration-weighted δ^{18}O, (c) — Precipitation-weighted δ^{18}O, (d) — Unweighted δ^{18}O in precipitation. GWL types are classified according to the Hess-Brezowsky system; bracketed labels denote the dominant regional atmospheric flow direction or pressure regime associated with each type.

dominate with roughly 21 %, suggesting persistent high-pressure centers and subarctic intrusions from the northwest. By contrast, SW (Southwest) and TM (Low-pressure Central Europe) account for only about 7.5 %, reflecting limited Atlantic air incursions. Northern and eastern flows contribute approximately 23 %, further emphasizing meridional control, and a substantial southern component (14.9 %) likely signals a southward displacement of the polar front [75, 90]. Collectively, these patterns reveal a glacial circulation structure starkly different from today's.

Standardized climate anomalies in the Mediterranean basin exhibit clear regime- and sector-specific signatures. In the Eastern Mediterranean, δ^{18}O anomalies in precipitation cluster around the median, indicating limited isotopic variation. However, HM (T) displays a slight negative anomaly and broad distribution, attributable to convective rainfall and the isotopic amount effect under cyclonic conditions [95], while SW (H) and U regimes show slight enrichment due to reduced precipitation and increased evaporation and moisture recycling under anticyclonic influence [11]. Precipitation anomalies remain low and stable, except for elevated variability under HM (T), and infiltration anomalies trend slightly negative overall, with pronounced deficits under HM (T), S (W), and N (NW). Temperature remains largely invariant across regimes, consistent with dominant subtropical anticyclonic control and weak temperature contrasts induced by flow changes [110]. In the Western Mediterranean, a modest negative δ^{18}O anomaly in precipiation under TM (W) reflects enhanced Atlantic moisture input, whereas the narrow distributions observed for the U regime indicate uniform moisture sources under this synoptic circulation type. Precipitation and infiltration anomalies both exhibit slight negative means, with HM (H) spanning a wide range due to alternating dry spells and brief convective bursts, which can occur despite the prevailing high-pressure influence. These convective events are often facilitated by boundaries between different air masses, leading to localized instability within an otherwise stable atmospheric regime [25]. Temperature anomalies are also subdued, with cooler deviations under TM (W) and slight warming under HM (H) and S (E) linked to subtropical anticyclonic centers [110]. These findings highlight the critical role of pressure regime and flow direction in modulating hydrometeorological variability across the basin.

The spatial and regime-dependent variability of standardized and weighted δ^{18}O anomalies further elucidates how circulation patterns interact with moisture sourcing and precipitation processes in each Mediterranean sector. In the Eastern Mediterranean, calcite-weighted δ^{18}O values under NW (T) and SW (H) reveal moderate to strong negative anomalies, and the broad interquartile ranges under SW (H) point to highly variable precipitation intensity [95]. The pronounced positive excursion under STR re-

flects dry spells with minimal rainfall and enhanced evaporative enrichment from local recycling or continental sources [9]. Infiltration-weighted δ^{18}O anomalies remain clustered near zero for most regimes, yet slight positive biases under TM (E), N (NW), and E (T) indicate evaporative concentration in recharge waters during low-rainfall events [37]. Precipitation-weighted δ^{18}O signals and unweighted δ^{18}O signals in precipitation consistently show moderate depletion under HM (T) and slight enrichment under SW (H) and U, underscoring the balance between isotopic amount and source effects.
In the Western Mediterranean, calcite-weighted δ^{18}O anomalies under SW (H) and NW (H) regimes indicate anticyclonic conditions characterized by scarce rainfall and strong evaporative enrichment, likely influenced by moisture sourced from the Mediterranean basin [37]. The compact distribution under U implies consistent maritime moisture, while STR again yields the highest enrichment. Infiltration-weighted δ^{18}O values are generally near zero but show moderate enrichment under U and STR [9]. Precipitation-weighted anomalies center around zero, with HM (H) slightly depleted and narrow spreads under S (E) and U. Unweighted δ^{18}O anomalies in precipitation show a slight depletion under TM (W) and display broad variability under HM (H), TM (W), and NW (H), reflecting fluctuations in storm intensity and the corresponding isotopic amount effects during precipitation events. Collectively, these spatially resolved regime signatures confirm that cyclonic regimes influenced by Atlantic or subpolar moisture lead to depleted δ^{18}O values, whereas anticyclonic conditions sourced from the Mediterranean promote enrichment through isotopically enhanced moisture sources and recycling. This highlights the nuanced hydroclimatic controls governing speleothem isotopic signals.

7.5 Conclusion

Speleothem δ^{18}O records in the Mediterranean region are governed by a multifaceted interaction of temperature, precipitation and synoptic-scale circulation regimes. While local temperature and moisture remain primary controls on isotopic composition, pressure systems and flow directions introduce additional variability that is critical for interpreting speleothem archives.
During the Last Glacial Maximum, European atmospheric circulation was reorganized under dominant meridional flows, whereas zonal and Atlantic-driven patterns declined. Persistent high-pressure centers, low pressure gradients and frequent transitional regimes limited moisture availability, reinforced a continental climate and promoted isotopic enrichment in speleothems. The observed isotopic variability reflects the interplay of circulation regimes, moisture sources and precipitation processes. Cyclonic regimes associated with Atlantic or subpolar air masses generally correspond to

δ^{18}O depletion, primarily reflecting variations in precipitation amount, temperature, and moisture source characteristics. In contrast, anticyclonic conditions dominated by Mediterranean-sourced or recycled moisture tend to be linked with δ^{18}O enrichment, driven by differences in moisture origin and recycling processes, and associated atmospheric dynamics. The spatial and regime-dependent variability of standardized δ^{18}O anomalies is particularly pronounced between the Western and Eastern Mediterranean sectors. Advective inflows from the North Atlantic dominate in the west, whereas evaporative enrichment and local recycling from the Mediterranean Sea prevail in the east, producing a distinct east–west gradient in moisture contributions.

Distinct synoptic regime types have been demonstrated to impart characteristic δ^{18}O signatures in Mediterranean speleothems during the Last Glacial Maximum. Zonal and transitional regimes are typically linked to isotopic depletion driven by subpolar moisture advection and cyclonic activity, whereas anticyclonic regimes (including zonal regimes within the Eastern Mediterranean) promote isotopic enrichment through evaporation and moisture recycling sourced from the Mediterranean Sea. Among the evaluated isotope-weighting schemes, calcite-weighted values most accurately capture these regime-dependent variations by integrating both hydrological and, to some extent, thermodynamic factors controlling speleothem formation. Precipitation-weighted anomalies reflect the isotopic amount effect prevalent under cyclonic conditions but tend to underestimate evaporative enrichment, while infiltration-weighted signals remain near neutral and exhibit limited sensitivity to regime-specific dynamics. Although calcite-weighted δ^{18}O values are derived from infiltration-weighted signals, their enhanced sensitivity arises from the temperature-dependent fractionation applied during mineral formation. This non-linear transformation amplifies regime-specific thermal contrasts, allowing calcite weighting to more effectively capture synoptic-scale hydroclimatic variability. Consequently, the calcite-weighted scheme is identified as the most robust method for reconstructing synoptic-scale hydroclimate variability from speleothem δ^{18}O records.

These findings underscore the necessity of integrating synoptic-scale circulation information into paleoclimate reconstructions. Coupling speleothem records with isotope-enabled climate model outputs, expanding synoptic classification to other regions and combining δ^{18}O data with complementary proxies will enhance the spatial resolution and interpretative power of climate reconstructions. Additionally, long-term analyses of regime frequency promise deeper insights into how atmospheric circulation shaped hydroclimate variability across glacial–interglacial transitions.

8 Discussion

In the Modern Day Scenario, the EMAC model reproduces the large-scale circulation over Central Europe with reasonable fidelity but exhibits notable classification biases. Zonal flow types are systematically underrepresented because the simulation frequently fails to resolve weak pressure gradients, relegating these days to Unclassified (U) or Straight Flow (STR) categories [53]. Although introducing the STR regime improves the detection of low-gradient conditions compared to classical HB-GWL schemes, mixed regimes (SW, NW, HM, TM) remain undercounted. By contrast, meridional regimes are well captured, underscoring the model's strength in simulating strong north–south advection patterns [12]. Validation against GNIP station data reveals a consistent overestimation of δ^{18}O in precipitation by approximately 1 ‰ to 3 ‰, indicative of simplified fractionation schemes [31]. Incorporating precipitation-weighting reduces this bias considerably [112]. Simulated temperatures tend to be too low, which may be attributed to coarse topography and simplified representations of radiative forcing and greenhouse gas parameters. Similarly, precipitation models often overestimate extremes, potentially due to rudimentary convection parameterizations [36]. Station-specific anomaly distributions show that cyclonic and mixed regimes exhibit higher medians and broader spreads, whereas meridional and undefined regimes yield more stable, narrow anomaly distributions. Furthermore, PCA of seasonal anomalies identifies four principal components explaining about 90 % of total variance. PC1 is dominated by temperature, δ^{18}O, and precipitation; PC2 by NAO index and circulation frequencies; PC3 and PC4 capture finer synoptic modulations. Bartlett's test ($\chi^2 = 139.04$) confirmed sufficient intercorrelations, while a mean KMO of 0.602 indicated moderate sampling adequacy. All p-values were highly significant ($\overline{p} = 5.06 \times 10^{-16}$), supporting the robustness of the results.

A profound synoptic reorganization was identified during the transition from the Modern Day Scenario to the LGM Scenario. Modern boundary conditions are characterized by predominantly cyclonic westerlies (WS, SWZ, NWZ), while the LGM scenario is dominated by anticyclonic or westerly flows exhibiting anticyclonic features (WW, SWA, NWA), indicative of stable, dry conditions and a weakened Atlantic storm track [75, 90]. During the Last Glacial Maximum, a reduction in northerly and northeasterly circulation types (NZ, NEA, NEZ) is observed, likely resulting from modifications in Arctic air mass intrusions. Concurrently, the frequency of stationary high-pressure systems (HM, BM) increases, attributable to intensified radiative cooling and an expansion of the Siberian High [79]. Additionally, transitional and hybrid synoptic types exhibit

a general decline, contributing to a more persistent and quasi-stationary atmospheric circulation regime [75]. In the LGM Scenario, meridional circulation dominates almost exclusively: only about 20 % of days are zonal or STR, signaling a weakened North Atlantic surface circulation and diminished Atlantic influence [75, 111]. Nearly 40 % of days fall into Mixed and Unclassified categories, with HM and NW each accounting for roughly 21 %, indicative of persistent subarctic intrusions [75]. Southwest (SW) and low-pressure central (TM) types occur only about 7.5 %, while southern flows (14.9 %) represent a distinct circulation pattern influencing the region [90]. Isotope-enabled EMAC simulations reveal a pronounced north–south gradient of δ^{18}O in precipitation: highly depleted values at high latitudes and enriched signals in southern margins (e.g., North Africa, the Levant). Precipitation totals exhibit alternating bands of enhanced and reduced values, consistent with persistent cyclonic westerlies and a southward-displaced storm track [82, 90]. However, these spatial patterns may also be affected by model parameterization uncertainties, particularly in the representation of precipitation processes. Temperature fields closely follow the isotopic gradient, showing extreme cold over northern Europe and relatively milder conditions over Western Europe due to reduced Gulf Stream forcing [84, 111]. A meridional dipole in surface pressure, cyclonic over Central Europe, anticyclonic over the Mediterranean, reinforces the notion of a southerly displaced frontal zone [70]. In the Mediterranean sector, regime-dependent hydrometeorological signatures are pronounced. In the Eastern Mediterranean, cyclonic regimes generate convective rainfall and slight negative δ^{18}O anomalies [95], whereas anticyclonic and straight regimes produce enriched signals through reduced precipitation and increased evaporation [11, 32]. Temperature anomalies remain muted under subtropical anticyclonic control [110]. In the Western Mediterranean, TM regimes lead to moderate isotopic depletion from Atlantic moisture influx, while STR regimes yield the highest enrichment through local evaporation [37].

Finally, the regression analysis of four δ^{18}O weighting schemes against SISAL speleothem records shows that the calcite-weighted approach best reproduces observed values, with a negligible mean offset (-0.0065 ‰; $t = -0.0086$, $p = 0.9933$). Infiltration weighting introduces a modest negative bias (-0.7185 ‰; $t = -1.2515$, $p = 0.2328$), precipitation weighting a slight positive offset (0.1963 ‰; $t = 0.3520$, $p = 0.7305$), while the unweighted scheme shows the largest overestimation (1.2791 ‰; $t = 2.1272$, $p = 0.0531$), highlighting the importance of process-based weighting [94, 113]. Systematic over- and underestimations occur at key cave sites (including Sofular cave, Sieben Hengste cave, Pindal cave, Soreq cave, and Villars cave) reflecting the complex interplay of local hydrology and challenging topography [7, 121].

9 Conclusion

This dissertation demonstrates that the integration of objective synoptic classification with isotope-enabled climate simulations provides a coherent and versatile framework for analyzing the variability of temperature, precipitation, and isotopic composition across diverse climatic contexts. By applying the EMAC model in conjunction with the Diagnostic Synoptic Regime Model (DSRM) scheme, and by incorporating insights from speleothem-based proxy evaluations as well as modern GNIP station data, a deeper understanding has been gained of how large-scale atmospheric circulation modulates local hydroclimatic signals under modern and glacial conditions.

> **Research Question 1:**
> *To what degree can EMAC/H2OISO simulations accurately reproduce observed δ^{18}O values in precipitation across Germany, and in what ways are these isotopic signatures influenced by objectively classified Großwetterlagen (GWL) circulation types?*

The results show that the EMAC model realistically captures spatial and seasonal δ^{18}O variability in precipitation, particularly when precipitation-weighted values are applied. Synoptic-scale circulation types exert a clear regional imprint on isotopic signals, and their integration into the modeling framework enhances the diagnostic power of simulations. These findings underscore the importance of combining circulation-type frequency with isotope diagnostics to improve simulation–data agreement and paleoclimate interpretability.

> **Research Question 2:**
> *Which mechanisms control δ^{18}O variability in precipitation during the Last Glacial Maximum, and to what extent can speleothem proxy records be reconstructed using unweighted, precipitation-weighted, infiltration-weighted, and calcite-weighted δ^{18}O?*

A fundamental reorganization of atmospheric circulation during the LGM, marked by stationary high-pressure systems and meridional flow, produces pronounced north–south gradients in temperature and isotopic composition. Among the tested weighting schemes, calcite-weighted δ^{18}O yields the highest agreement with SISAL speleothem records, highlighting the importance of integrating both hydrological and thermodynamic controls in proxy-simulation alignment. This approach enables robust reconstructions of glacial hydroclimate variability and guides future model development.

Research Question 3:
How do distinct synoptic regime types (meridional, zonal, mixed, and transitional) imprint on δ^{18}O signals in Mediterranean speleothems during the LGM, and which isotope-weighting scheme best captures these regime-dependent variations?

The analysis reveals that zonal and transitional regimes are associated with isotopic depletion driven by subpolar moisture advection, whereas anticyclonic regimes foster enrichment through Mediterranean-sourced evaporation and moisture recycling. Among the evaluated approaches, calcite- and infiltration-weighted δ^{18}O exhibit the greatest sensitivity to synoptic variability, effectively integrating hydrological and thermodynamic controls on speleothem formation. This highlights the importance of regime-specific isotope modeling for accurate Mediterranean paleoclimate reconstructions.

Main Research Question:
How can synoptic-scale circulation diagnostics and isotope-enabled modeling be integrated into a consistent framework for interpreting speleothem δ^{18}O across interglacial and glacial periods?

Particular emphasis is placed on speleothems as high-resolution archives of hydroclimatic variability, where isotopic signals in cave drip water and calcite are governed not only by local meteorological conditions but also significantly influenced by the origin, trajectory, and seasonal dynamics of moisture transport. The close agreement between calcite-weighted δ^{18}O and observed speleothem profiles validates the diagnostic value of these archives for complex climate simulations. This dissertation demonstrates that integrating objective synoptic-scale circulation diagnostics with isotope-enabled climate modeling and proxy validation provides a methodologically rigorous and scientifically insightful framework. By capturing regime-dependent isotopic variability and accounting for hydrological and thermodynamic processes, this framework enhances the robustness and interpretative power of paleoclimate reconstructions across diverse temporal and spatial scales. It thus offers a powerful toolset for interpreting speleothem δ^{18}O signals in both interglacial and glacial contexts, advancing the field of paleoclimate diagnostics.

10 Outlook and Future Research

The findings of this dissertation provide a robust foundation for understanding the interplay between synoptic-scale atmospheric circulation and the variability of $\delta^{18}O$ in precipitation under both modern and glacial climate conditions. Building on this framework, several promising avenues for future research emerge.

One important direction is the extension of the developed methodology to other paleoclimatic periods beyond the Last Glacial Maximum (LGM). Periods such as the mid-Holocene, the Last Interglacial, or abrupt climate events like Heinrich and Dansgaard–Oeschger episodes offer valuable opportunities to test the transferability of the DSRM classification and isotope-enabled modeling framework [88]. Applying these tools to different boundary conditions would allow for a more comprehensive understanding of how synoptic regimes and isotopic signals co-evolve across diverse climatic contexts.

Another key area for future work lies in improving spatial resolution. While the current simulations were conducted at T106 resolution, which is relatively high for global climate models, it may still be insufficient to resolve fine-scale topographic and hydrological features, particularly in karst regions where speleothems form. Incorporating regional climate models (RCMs) or applying statistical downscaling techniques could help better capture site-specific processes, especially in cave systems with complex hydrology and microclimatic variability [46].

The strong performance of the calcite-weighted $\delta^{18}O$ signal in matching speleothem records highlights the importance of subsurface hydrological filtering. Although the infiltration model employed in this study captures key hydrological features, it remains limited in representing karst-specific dynamics, including prior calcite precipitation (PCP) and cave-internal processes [94]. Integrating these mechanisms would enhance its realism and applicability for simulating speleothem-based paleoclimate signals. Future studies could integrate more sophisticated karst hydrology models or couple isotope-enabled climate simulations with karst system simulators to improve the realism of speleothem signal generation and interpretation [14, 108]. Furthermore, the comparison with SISAL speleothem records revealed both strengths and limitations in the simulation–proxy agreement. To address these, future research should aim to systematically quantify uncertainties in both model outputs and proxy interpretations. Bayesian data assimilation techniques or proxy system models (PSMs) could be employed to formally integrate observational and simulated data, thereby improving the robustness and credibility of paleoclimate reconstructions [35].

Although this dissertation focused on speleothems, the methodological framework developed here could be extended to other isotope-based proxy systems such as ice cores, lake sediments, or tree rings [50, 114]. Each of these archives responds differently to climatic and hydrological processes, and applying the synoptic–isotopic approach across multiple proxy types could yield a more holistic picture of past climate dynamics and enhance cross-validation between archives.

The observed shifts in GWL frequencies between the LGM and the modern period suggest that synoptic regimes are sensitive to large-scale climate forcings. This raises important questions about how these regimes may respond to anthropogenic climate change. Future studies could explore the stability and predictability of synoptic patterns under warming scenarios using CMIP6 or next-generation isotope-enabled Earth system models [85]. Such work would help assess the resilience of circulation regimes and their role in shaping future hydroclimatic variability. Finally, the DSRM developed in this dissertation has proven effective for classifying synoptic regimes in both modern and glacial contexts. Future work could focus on integrating machine learning techniques, or expanding the model to include additional circulation metrics such as jet stream position, blocking indices, or moisture transport diagnostics. These enhancements would increase the model's diagnostic power and facilitate broader applications in climate research.

In conclusion, this dissertation demonstrates the value of combining synoptic diagnostics with isotope-enabled climate modeling and proxy comparison. The framework developed here provides a scalable and transferable approach for investigating climatic controls on $\delta^{18}O$ across diverse archives. It establishes a robust foundation for future interdisciplinary research bridging paleoclimatology, hydrology, and atmospheric science.

11 Bibliography

References

[1] Abe-Ouchi, A., Saito, F., Kawamura, K., Raymo, M. E., Okuno, J., Takahashi, K., and Blatter, H. (2015). Ice-sheet configuration in the cmip5/pmip3 last glacial maximum experiments. *Geoscientific Model Development*, 8(11):3621–3637.

[2] Abrantes, F., Voelker, A. H. L., Sierro, F. J., Naughton, F., Rodrigues, T., Cacho, I., Ariztegui, D., Brayshaw, D., Sicre, M.-A., and Batista, L. (2012). Paleoclimate variability in the mediterranean region. In Lionello, P., editor, *The Climate of the Mediterranean Region: From the Past to the Future*, pages 1–86. Elsevier.

[3] Agustí, J., Oms, O., and Remacha, E. (2001). Long plio-pleistocene terrestrial record of climate change and mammal turnover in southern spain. *Quaternary Research*, 56(3):411–418.

[4] Armengaud, A., Delaygue, G., Bard, E., Mélières, M., Petit, J.-R., and Korotkevich, F. (1998). Model evaluations of the water isotope–climate relationships used in reconstructing palaeotemperatures. In *Isotope Techniques in the Study of Environmental Change*, pages 485–502, Vienna. International Atomic Energy Agency.

[5] Atkinson, G. D. and Holliday, C. R. (1977). Tropical cyclone minimum sea level pressure/maximum sustained wind relationship for the western north pacific. *Monthly Weather Review*, 105(4):421–427.

[6] Baertschi, P. (1976). Absolute ^{18}O content of standard mean ocean water. *Earth and Planetary Science Letters*, 31:341–344.

[7] Bar-Matthews, M. and Ayalon, A. (2004). Speleothems as palaeoclimate indicators, a case study from soreq cave located in the eastern mediterranean region, israel. In Battarbee, R. W., Gasse, F., and Stickley, C. E., editors, *Past Climate Variability through Europe and Africa*, volume 6 of *Developments in Paleoenvironmental Research*, pages 363–391. Springer.

[8] Bar-Matthews, M., Ayalon, A., and Kaufman, A. (1997). Late quaternary paleoclimate in the eastern mediterranean region from stable isotope analysis of speleothems at soreq cave, israel. *Quaternary Research*, 47(2):155–168.

[9] Batibeniz, F., Ashfaq, M., Önol, B., Turuncoglu, U. U., Mehmood, S., and Evans, K. J. (2020). Identification of major moisture sources across the mediterranean basin. *Climate Dynamics*, 54:4109–4127.

[10] Beniston, M. (2002). Climate modeling at various spatial and temporal scales: where can dendrochronology help? *Dendrochronologia*, 20(1–2):117–131.

[11] Bisselink, B. and Dolman, A. J. (2008). Precipitation recycling: Moisture sources over europe using era-40 data. *Journal of Hydrometeorology*, 9(5):1073–1083.

[12] Bissolli, P. and Dittmann, E. (2001). The objective weather type classification of the german weather service and its possibilities of application to environmental and meteorological investigations. *Meteorologische Zeitschrift*, 10(4):253–260.

[13] Braconnot, P., Harrison, S. P., Kageyama, M., Bartlein, P. J., Masson-Delmotte, V., Abe-Ouchi, A., Otto-Bliesner, B., and Zhao, Y. (2012). Evaluation of climate models using palaeoclimatic data. *Nature Climate Change*, 2(6):417–424.

[14] Bradley, C., Baker, A., Jex, C. N., and Leng, M. J. (2010). Hydrological uncertainties in the modelling of cave drip-water δ^{18}O and the implications for stalagmite palaeoclimate reconstructions. *Quaternary Science Reviews*, 29(17–18):2201–2214.

[15] Brock, F. V. and Richardson, S. J. (2001). Meteorological measurement systems. In *Meteorological Measurement Systems*, pages 1–21. Oxford University Press.

[16] Budyko, M. I. (1969). The effect of solar radiation variations on the climate of the earth. *Tellus A*, 21(5):611–619.

[17] Cassou, C., Terray, L., and Phillips, A. S. (2005). Tropical atlantic influence on european heat waves. *Journal of Climate*, 18(15):2805–2811.

[18] Chaturvedi, R. K., Joshi, J., Jayaraman, M., Bala, G., and Ravindranath, N. H. (2012). Multi-model climate change projections for india under representative concentration pathways. *Current Science*, 103(7):791–802.

[19] Collins, W. J., Bellouin, N., Doutriaux-Boucher, M., Gedney, N., Halloran, P., Hinton, T., Hughes, J., Jones, C. D., Joshi, M., Liddicoat, S., Martin, G., O'Connor, F., Rae, J., Senior, C., Sitch, S., Totterdell, I., Wiltshire, A., and Woodward, S. (2011). Development and evaluation of an earth-system model – hadgem2. *Geoscientific Model Development*, 4:1051–1075.

[20] Comas-Bru, L., Rehfeld, K., Roesch, C., Amirnezhad-Mozhdehi, S., Harrison, S. P., Atsawawaranunt, K., Ahmad, S. M., Ait Brahim, Y., Baker, A., Bosomworth, M., Breitenbach, S. F. M., Burstyn, Y., Columbu, A., Deininger, M., Demény, A., Dixon, B., Fohlmeister, J., Hatvani, I. G., Hu, J., Kaushal, N., Kern, Z., Labuhn, I., Lechleitner, F. A., Lorrey, A., Martrat, B., Novello, V. F., Oster, J., Pérez-Mejías, C., Scholz, D., Scroxton, N., Sinha, N., Ward, B. M., Warken, S., Zhang, H., and Group, S. W. (2020). Sisalv2: A comprehensive speleothem isotope database with multiple age-depth models. *Earth System Science Data*, 12(4):2579–2606.

[21] Craig, H. (1957). Isotopic standards for carbon and oxygen and correction factors for mass-spectrometric analysis of carbon dioxide. *Geochimica et Cosmochimica Acta*, 12(1–2):133–149.

[22] Crutzen, P. J. (2022). Defining the anthropocene. In Schmidt, N., Gierlinger, S., and Neumeier, S., editors, *Paul J. Crutzen and the Anthropocene: A New Epoch in Earth's History*, pages 19–21. Springer.

[23] Danabasoglu, G., Lamarque, J.-F., Bacmeister, J., Bailey, D. A., DuVivier, A. K., Edwards, J., Emmons, L. K., Fasullo, J., Garcia, R., Gettelman, A., Hannay, C., Holland, M. M., Large, W. G., Lauritzen, P. H., Lawrence, D. M., Lenaerts, J. T. M., Lindsay, K., Lipscomb, W. H., Mills, M. J., Neale, R., Oleson, K. W., Otto-Bliesner, B., Phillips, A. S., Sacks, W., Tilmes, S., Kampenhout, L., Vertenstein, M., Bertini, A., Dennis, J., Deser, C., Fischer, C., Fox-Kemper, B., Kay, J. E., Kinnison, D., Kushner, P. J., Larson, V. E., Long, M. C., Mickelson, S., Moore, J. K., Nienhouse, E., Polvani, L., Rasch, P. J., and Strand, W. G. (2020). The community earth system model version 2 (cesm2). *Journal of Advances in Modeling Earth Systems*, 12(2):e2019MS001916.

[24] Dansgaard, W. (1964). Stable isotopes in precipitation. *Tellus A*, 16(4):436–468.

[25] Dayan, U., Nissen, K., and Ulbrich, U. (2015). Atmospheric conditions inducing extreme precipitation over the eastern and western mediterranean. *Natural Hazards and Earth System Sciences*, 15(11):2525–2544.

[26] De Santis, V., Caldara, M., Marsico, A., and Pennetta, L. (2018). Evolution of the ofanto river delta from the 'little ice age' to modern times: Implications of large-scale synoptic patterns. *The Holocene*, 28(1):1–20.

[27] Deutscher Wetterdienst (2023). Jahrbuch 2022. `https://www.dwd.de/DE/`

leistungen/jahresberichte_dwd/jahresberichte_pdf/jahresbericht_2022.html. Zugriff am 13. September 2025.

[28] Deutscher Wetterdienst (2025). Monats- und jahreszeitenbericht deutschland. https://www.dwd.de/DE/leistungen/klimakartendeutschland/klimakartendeutschland_monatsbericht.html. Zugriff am 13. August 2025.

[29] Dore, M. H. (2005). Climate change and changes in global precipitation patterns: What do we know? *Environment International*, 31(8):1167–1181.

[30] Dunn, P. J. H., Malinovsky, D., Ogrinc, N., Potočnik, D., Flierl, L., Rienitz, O., Paul, D., and Meijer, H. A. J. (2024). Re-determination of $r(^{13}C/^{12}C)$ for vienna peedee belemnite (vpdb). *Rapid Communications in Mass Spectrometry*, 38(16):e9773.

[31] Eichinger, R., Jöckel, P., Brinkop, S., Werner, M., and Lossow, S. (2015). Simulation of the isotopic composition of stratospheric water vapour – part 1: Description and evaluation of the emac model. *Atmospheric Chemistry and Physics*, 15(10):5537–5555.

[32] Eshel, G. and Farrell, B. F. (2000). Mechanisms of eastern mediterranean rainfall variability. *Journal of the Atmospheric Sciences*, 57(19):3219–3232.

[33] Fairchild, I. J., Frisia, S., Borsato, A., and Tooth, A. F. (2007). Speleothems. In *Encyclopedia of Quaternary Science*. Wiley.

[34] Fairchild, I. J., Smith, C. L., Baker, A., Fuller, L., Spötl, C., Mattey, D., and McDermott, F. (2006). Modification and preservation of environmental signals in speleothems. *Earth-Science Reviews*, 75(1–4):105–153.

[35] Fang, M. and Li, X. (2016). Paleoclimate data assimilation: Its motivation, progress and prospects. *Science China Earth Sciences*, 59(9):1817–1826.

[36] Feldmann, H., Früh, B., Schädler, G., Panitz, H.-J., Keuler, K., Jacob, D., and Lorenz, P. (2008). Evaluation of the precipitation for south-western germany from high resolution simulations with regional climate models. *Meteorologische Zeitschrift*, 17(4):455–465.

[37] Fernández-Chacón, F., Benavente, J., Rubio-Campos, J. C., Kohfahl, C., Jiménez, J., Meyer, H., Hubberten, H., and Pekdeger, A. (2010). Isotopic composition ($\delta^{18}O$

and δD) of precipitation and groundwater in a semi-arid, mountainous area (guadiana menor basin, southeast spain). *Hydrological Processes*, 24(10):1343–1356.

[38] Field, P. R. and Wood, R. (2007). Precipitation and cloud structure in midlatitude cyclones. *Journal of Climate*, 20(2):233–254.

[39] Florineth, D. and Schlüchter, C. (2000). Alpine evidence for atmospheric circulation patterns in europe during the last glacial maximum. *Quaternary Research*, 54(3):295–308.

[40] Gao, C., Robock, A., and Ammann, C. (2008). Volcanic forcing of climate over the past 1500 years: An improved ice core-based index for climate models. *Journal of Geophysical Research: Atmospheres*, 113(D23):D23111.

[41] Garratt, J. R. (1984). The measurement of evaporation by meteorological methods. In de Vries, F. and van Laar, J., editors, *Evaporation and Environment*, volume 13 of *Developments in Agricultural and Managed Forest Ecology*, pages 3–20. Elsevier.

[42] Gat, J. R. (1996). Oxygen and hydrogen isotopes in the hydrologic cycle. *Annual Review of Earth and Planetary Sciences*, 24:225–262.

[43] Gates, W. L. (1999). An overview of the results of the atmospheric model intercomparison project (amip i). *Bulletin of the American Meteorological Society*, 80(1):29–55.

[44] Gedzelman, S. D. and Lawrence, J. R. (1982). The isotopic composition of cyclonic precipitation. *Journal of Applied Meteorology and Climatology*, 21(10):1385–1404.

[45] Gerstengarbe, F.-W. and Werner, P. C. (2010). Katalog der großwetterlagen europas (1881–2009) nach paul hess und helmut brezowsky. PIK Report 119, Potsdam-Institut für Klimafolgenforschung (PIK), Potsdam, Germany.

[46] Giorgi, F. (2019). Thirty years of regional climate modeling: Where are we and where are we going next? *Journal of Geophysical Research: Atmospheres*, 124(11):5696–5723.

[47] Gradstein, F. M., Ogg, J. G., Schmitz, M. D., and Ogg, G. M., editors (2012). *The Geologic Time Scale 2012*. Elsevier, Amsterdam.

[48] Greuell, W. and Böhm, R. (1998). 2 m temperatures along melting mid-latitude glaciers, and implications for the sensitivity of the mass balance to variations in temperature. *Journal of Glaciology*, 44(146):9–20.

[49] Grootes, P. M., Stuiver, M., White, J. W. C., Johnsen, S. J., and Jouzel, J. (1993). Comparison of oxygen isotope records from the gisp2 and grip greenland ice cores. *Nature*, 366:552–554.

[50] Hammarlund, D., Barnekow, L., Birks, H. H., Buchardt, B., and Edwards, T. W. D. (2002). Holocene changes in atmospheric circulation recorded in the oxygen-isotope stratigraphy of lacustrine carbonates from northern sweden. *The Holocene*, 12(3):339–351.

[51] Haude, W. (1955). Zur praktischen bestimmung der aktuellen und potentiellen evaporation und evapotranspiration. Berichte des Deutschen Wetterdienstes 8, Deutscher Wetterdienst, Offenbach am Main, Germany.

[52] Hess, P. and Brezowsky, H. (1969). Katalog der großwetterlagen europas. Berichte des Deutschen Wetterdienstes 33, Deutscher Wetterdienst, Offenbach am Main, Germany.

[53] Hess, P. and Brezowsky, H. (1993). Katalog der großwetterlagen europas: 1881–1992. Berichte des Deutschen Wetterdienstes 113, Deutscher Wetterdienst, Offenbach am Main, Germany.

[54] Houghton, J. T. (1997). An introduction to simple climate models used in the ipcc second assessment report. Ipcc technical paper ii, Intergovernmental Panel on Climate Change (IPCC), Geneva, Switzerland.

[55] Hourdin, F., Mauritsen, T., Gettelman, A., Golaz, J.-C., Balaji, V., Duan, Q., Folini, D., Ji, D., Klocke, D., Qian, Y., Rauser, F., Rio, C., Tomassini, L., Watanabe, M., and Williamson, D. (2017). The art and science of climate model tuning. *Bulletin of the American Meteorological Society*, 98(3):589–602.

[56] Hovan, S. A., Rea, D. K., and Pisias, N. G. (1991). Late pleistocene continental climate and oceanic variability recorded in northwest pacific sediments. *Paleoceanography*, 6(3):349–370.

[57] Hu, J., Emile-Geay, J., Tabor, C., Nusbaumer, J., and Partin, J. (2020). Deciphering oxygen isotope records from chinese speleothems with an isotope-enabled climate model. *Paleoceanography and Paleoclimatology*, 35(2):e2019PA003741.

[58] Hurrell, J. W. (2001). North atlantic oscillation: Patterns and predictability. *Science*, 291(5504):603–605.

[59] Hurrell, J. W. and Deser, C. (2024). North atlantic climate variability: The role of the north atlantic oscillation. Technical report, National Center for Atmospheric Research, Boulder, Colorado.

[60] Hurrell, J. W., Kushnir, Y., Ottersen, G., and Visbeck, M. (2003). An overview of the north atlantic oscillation. In Hurrell, J. W., Kushnir, Y., Ottersen, G., and Visbeck, M., editors, *The North Atlantic Oscillation: Climatic Significance and Environmental Impact*, volume 134 of *Geophysical Monograph Series*, pages 1–35. American Geophysical Union.

[61] International Atomic Energy Agency (IAEA) (2025). Water Isotope System for Data Analysis, Visualization and Electronic Retrieval (WISER). `https://www.iaea.org/services/networks/gnip`. Accessed: 2025-02-24.

[62] Iturbide, M., Martínez-Alvarado, J., Matthes, H., Torre, L., Gutiérrez, J. M., et al. (2020). An update of ipcc climate reference regions for subcontinental analysis of climate model data: Definition and aggregated datasets. *Earth System Science Data*, 12(4):2959–2978.

[63] James, P. M. (2007). An objective classification method for hess and brezowsky grosswetterlagen over europe. *Theoretical and Applied Climatology*, 88:17–42.

[64] Johns, T. C., Carnell, R. E., Crossley, J. F., Gregory, J. M., Mitchell, J. F. B., Senior, C. A., Tett, S. F. B., and Wood, R. A. (2003). Anthropogenic climate change for 1860 to 2100 simulated with the hadcm3 model under updated emissions scenarios. *Climate Dynamics*, 20(6):583–612.

[65] Joint Committee for Guides in Metrology (2008). International vocabulary of metrology—basic and general concepts and associated terms (vim). *Chemistry International*, 30(6):21–25.

[66] Jones, P. D., Harpham, C., and Briffa, K. R. (2013). Lamb weather types derived from reanalysis products. *International Journal of Climatology*, 33(5):1129–1139.

[67] Jones, P. D. and Kelly, P. M. (1982). Principal component analysis of the lamb catalogue of daily weather types: Part 1, annual frequencies. *Journal of Climatology*, 2(2):147–157.

[68] Jöckel, P., Kerkweg, A., Buchholz-Dietsch, J., Tost, H., Sander, R., and Pozzer, A. (2008). Technical note: Coupling of chemical processes with the modular earth

submodel system (messy) submodel tracer. *Atmospheric Chemistry and Physics*, 8:1677–1687.

[69] Kelemen, F. D., Ludwig, P., Reyers, M., Ulbrich, S., and Pinto, J. G. (2016). Evaluation of moisture sources for the central european summer flood of may/june 2013 based on regional climate model simulations. *Tellus A: Dynamic Meteorology and Oceanography*, 68:29288.

[70] Kutzbach, J. E. and Guetter, P. J. (1986). The influence of changing orbital parameters and surface boundary conditions on climate simulations for the past 18,000 years. *Journal of the Atmospheric Sciences*, 43(16):1726–1759.

[71] Lachniet, M. S. (2009). Climatic and environmental controls on speleothem oxygen-isotope values. *Quaternary Science Reviews*, 28(5–6):412–432.

[72] Lamb, H. H. (1972). *British Isles Weather Types and a Register of the Daily Sequence of Circulation Patterns 1861–1971.* Number 116 in Geophysical Memoirs. H.M. Stationery Office, London.

[73] Leng, M. J. and Marshall, J. D. (2004). Palaeoclimate interpretation of stable isotope data from lake sediment archives. *Quaternary Science Reviews*, 23(7–8):811–831.

[74] Lewis, S. L. and Maslin, M. A. (2015). Defining the anthropocene. *Nature*, 519:171–180.

[75] Ludwig, P., Schaffernicht, E. J., Shao, Y., and Pinto, J. G. (2016). Regional atmospheric circulation over europe during the last glacial maximum and its links to precipitation. *Journal of Geophysical Research: Atmospheres*, 121(3):1384–1401.

[76] Lussana, C., Tveito, O. E., and Uboldi, F. (2018). Three-dimensional spatial interpolation of 2 m temperature over norway. *Quarterly Journal of the Royal Meteorological Society*, 144(711):344–364.

[77] McMahon, T. A., Finlayson, B. L., and Peel, M. C. (2016). Historical developments of models for estimating evaporation using standard meteorological data. *WIREs Water*, 3(6):788–818.

[78] McMahon, T. A., Peel, M. C., Lowe, L., Srikanthan, R., and McArthur, T. R. (2013). Estimating actual, potential, reference crop and pan evaporation using standard meteorological data: A pragmatic synthesis. *Hydrology and Earth System Sciences*, 17:1331–1363.

[79] Merz, N., Raible, C. C., and Woollings, T. (2015). North atlantic eddy-driven jet in interglacial and glacial winter climates. *Journal of Climate*, 28(10):3977–3997.

[80] Mischel, S. A., Scholz, D., and Spötl, C. (2015). δ^{18}O values values of cave drip water: a promising proxy for the reconstruction of the north atlantic oscillation? *Climate Dynamics*, 45:3035–3050.

[81] Moreno, A., Sancho, C., Bartolomé, M., Oliva-Urcia, B., Delgado-Huertas, A., Estrela, M. J., Corell, D., López-Moreno, J. I., and Cacho, I. (2014). Climate controls on rainfall isotopes and their effects on cave drip water and speleothem growth: the case of molinos cave (teruel, ne spain). *Climate Dynamics*, 43:221–241.

[82] Nicholson, S. E. (2013). The west african sahel: A review of recent studies on the rainfall regime and its interannual variability. *ISRN Meteorology*, pages 1–32.

[83] Nusbaumer, J., Wong, T. E., Bardeen, C. G., and Noone, D. (2017). Evaluating hydrological processes in the community atmosphere model version 5 (cam5) using stable isotope ratios of water. *Journal of Advances in Modeling Earth Systems*, 9(3):949–977.

[84] Otto-Bliesner, B. L., Brady, E. C., Clauzet, G., Levis, S., Harrison, S. J., and Kutzbach, K. E. (2006). Last glacial maximum and holocene climate in ccsm3. *Journal of Climate*, 19(11):2526–2544.

[85] O'Neill, B. C., Tebaldi, C., van Vuuren, D. P., Eyring, V., Friedlingstein, P., Hurtt, G., Knutti, R., Kriegler, E., Lamarque, J.-F., Lowe, J., Meehl, G. A., Moss, R., Riahi, K., and Sanderson, B. M. (2016). The scenario model intercomparison project (scenariomip) for cmip6. *Geoscientific Model Development*, 9:3461–3482.

[86] Paillard, D. (1998). The timing of pleistocene glaciations from a simple multiple-state climate model. *Nature*, 391(6665):378–381.

[87] Paillard, D. (2001). Glacial cycles: toward a new paradigm. *Reviews of Geophysics*, 39(3):325–346.

[88] Petersen, S. V., Schrag, D. P., and Clark, P. U. (2013). A new mechanism for dansgaard–oeschger cycles. *Paleoceanography*, 28(1):24–30.

[89] Peterson, B. J. and Fry, B. (1987). Stable isotopes in ecosystem studies. *Annual Review of Ecology and Systematics*, 18:293–320.

[90] Pinto, J. G. and Ludwig, P. (2020). Extratropical cyclones over the north atlantic and western europe during the last glacial maximum and implications for proxy interpretation. *Climate of the Past*, 16:611–626.

[91] Plavcová, E. and Kyselý, J. (2011). Evaluation of daily temperatures in central europe and their links to large-scale circulation in an ensemble of regional climate models. *Tellus A: Dynamic Meteorology and Oceanography*, 63(4):763–781.

[92] Plavcová, E., Kyselý, J., and Štěpánek, P. (2014). Links between circulation types and precipitation in central europe in the observed data and regional climate model simulations. *International Journal of Climatology*, 34(9):2885–2898.

[93] Prentice, I. C., Jolly, D., and Participants, B. . (2000). Mid-holocene and glacial-maximum vegetation geography of the northern continents and africa. *Journal of Biogeography*, 27(3):507–519.

[94] Riechelmann, D. F. C., Schröder-Ritzrau, A., Scholz, D., Fohlmeister, J., Spötl, C., Richter, D. K., and Mangini, A. (2011). Monitoring bunker cave (nw germany): A prerequisite to interpret geochemical proxy data of speleothems from this site. *Journal of Hydrology*, 409(3–4):682–695.

[95] Risi, V., Bony, S., and Vimeux, F. (2008). Influence of convective processes on the isotopic composition (δ^{18}O and δD) of precipitation and water vapor in the tropics: 2. physical interpretation of the amount effect. *Journal of Geophysical Research: Atmospheres*, 113(D19).

[96] Roberts, C. N., Zanchetta, G., and Jones, M. D. (2010). Oxygen isotopes as tracers of mediterranean climate variability: An introduction. *Global and Planetary Change*, 71(3–4):141–153.

[97] Roeckner, E., Brokopf, R., Esch, M., Giorgetta, M., Hagemann, S., Kornblueh, L., Manzini, E., Schlese, U., and Schulzweida, U. (2006). Sensitivity of simulated climate to horizontal and vertical resolution in the echam5 atmosphere model. *Journal of Climate*, 19(16):3771–3791.

[98] Ropelewski, M. A. and Halpert, M. S. (1987). Global and regional scale precipitation patterns associated with the el niño/southern oscillation. *Monthly Weather Review*, 115(8):1606–1626.

[99] Rozanski, K., Araguás-Araguás, L., and Gonfiantini, R. (1993). Isotopic patterns in modern global precipitation. In Swart, P. K., Lohmann, K. C., McKenzie, J.,

and Savin, S., editors, *Climate Change in Continental Isotopic Records*, volume 78 of *Geophysical Monograph Series*, pages 1–36. American Geophysical Union.

[100] Scholz, D., Mühlinghaus, C., and Mangini, A. (2009). Modelling δ^{13}C and δ^{18}O in the solution layer on stalagmite surfaces. *Geochimica et Cosmochimica Acta*, 73(9):2592–2602.

[101] Sellers, W. D. (1969). A global climatic model based on the energy balance of the earth–atmosphere system. *Journal of Applied Meteorology*, 8(3):392–400.

[102] Shackleton, N. J. (1987). Oxygen isotopes, ice volume and sea level. *Quaternary Science Reviews*, 6(3–4):183–190.

[103] Spahni, R., Chappellaz, J., Stocker, T. F., Loulergue, L., Hausammann, G., Kawamura, K., Flückiger, J., Schwander, J., Raynaud, D., Masson-Delmotte, V., et al. (2005). Atmospheric methane and nitrous oxide of the late pleistocene from antarctic ice cores. *Science*, 310(5752):1317–1321.

[104] Steen-Larsen, H. C., Sveinbjörnsdottir, A. E., Jonsson, T., Ritter, F., Bonne, J.-L., Masson-Delmotte, V., Sodemann, H., Blunier, T., Dahl-Jensen, D., and Vinther, B. M. (2015). Moisture sources and synoptic to seasonal variability of north atlantic water vapor isotopic composition. *Journal of Geophysical Research: Atmospheres*, 120(12):5757–5774.

[105] Stensrud, D. J. and Yussouf, N. (2003). Short-range ensemble predictions of 2-m temperature and dewpoint temperature over new england. *Monthly Weather Review*, 131(10):2510–2524.

[106] Stringer, C. (2016). The origin and evolution of homo sapiens. *Philosophical Transactions of the Royal Society B: Biological Sciences*, 371(1698):20150237.

[107] Tierney, J. E., Poulsen, C. J., Montañez, I. P., Bhattacharya, T., Feng, R., Ford, H. L., Hönisch, B., Inglis, G. N., Petersen, S. V., Sagoo, N., Tabor, C. R., Thirumalai, K., Zhu, J., Burls, N. J., Foster, G. L., Goddéris, Y., Huber, B. T., Ivany, L. C., Turner, S. K., Lunt, D. J., McElwain, J. C., Mills, B. J. W., Otto-Bliesner, B. L., Ridgwell, A., and Zhang, Y. G. (2020). Past climates inform our future. *Science*, 370(6517):eaay3701.

[108] Treble, P. C., Baker, A., Abram, N. J., Hellstrom, J. C., Crawford, J., Gagan, M. K., Borsato, A., Griffiths, A. D., Bajo, P., Markowska, M., Priestley, S. C.,

Hankin, S. I., Paterson, D. L., et al. (2022). Ubiquitous karst hydrological control on speleothem oxygen isotope variability in a global study. *Communications Earth & Environment*, 3:29.

[109] Trenberth, K. E. (2011). Changes in precipitation with climate change. *Climate Research*, 47:123–138.

[110] Ulbrich, U., Lionello, P., Belušić, D., Jacobeit, J., Knippertz, P., Kuglitsch, F. G., Leckebusch, G. C., Luterbacher, J., Maugeri, M., Maheras, P., Nissen, K. M., Pavan, V., Pinto, J. G., Saaroni, H., Seubert, S., Toreti, A., Xoplaki, E., and Ziv, B. (2012). Climate of the mediterranean: Synoptic patterns, temperature, precipitation, winds, and their extremes. In Lionello, P., editor, *Climate of the Mediterranean Region: From the Past to the Future*, pages 301–346. Elsevier.

[111] Vellinga, M. and Wood, R. A. (2002). Global climatic impacts of a collapse of the atlantic thermohaline circulation. *Climatic Change*, 54:251–267.

[112] Wackerbarth, A., Langebroek, P. M., Werner, M., Lohmann, G., Riechelmann, S., Borsato, A., and Mangini, A. (2012). Simulated oxygen isotopes in cave drip water and speleothem calcite in european caves. *Climate of the Past*, 8(6):1781–1799.

[113] Wackerbarth, A. K., Scholz, D., Fohlmeister, J., and Mangini, A. (2010). Modelling the δ^{18}O value of cave drip water and speleothem calcite. *Earth and Planetary Science Letters*, 299(3–4):387–397.

[114] Walker, M., Johnsen, S., Rasmussen, S. O., Popp, T., Steffensen, J. P., Gibbard, P., Hoek, W. Z., Lowe, J., Ammann, B., Björck, L., Cwynar, L. C., Hughen, S., Müller, I., Kromer, B., Rose, I. R., Schneider, R. A., and Schwander, G. E. (2009). Formal definition and dating of the gssp for the base of the holocene using the greenland ngrip ice core, and selected auxiliary records. *Journal of Quaternary Science*, 24(1):3–17.

[115] Walker, M. J. C., Björck, S., Lowe, J. J., Cwynar, L. C., Johnsen, S., Knudsen, K.-L., Wohlfarth, B., and Group, I. (1999). Isotopic "events" in the grip ice core: a stratotype for the late pleistocene. *Quaternary Science Reviews*, 18(14–15):1143–1151.

[116] Werner, M., Heimann, M., and Hoffmann, G. (2001). Isotopic composition and origin of polar precipitation in present and glacial climate simulations. *Tellus B: Chemical and Physical Meteorology*, 53(1):53–71.

[117] Werner, M., Langebroek, P. M., Carlsen, T., Herold, M., and Lohmann, G. (2011). Stable water isotopes in the echam5 general circulation model: Toward high-resolution isotope modeling on a global scale. *Journal of Geophysical Research: Atmospheres*, 116:D15109.

[118] Wilby, R. L. and Wigley, T. M. L. (1997). Downscaling general circulation model output: a review of methods and limitations. *Progress in Physical Geography*, 21(4):530–548.

[119] Winnick, M. J., Chamberlain, C. P., Caves, J. K., and Welker, J. M. (2014). Quantifying the isotopic 'continental effect'. *Earth and Planetary Science Letters*, 406:123–133.

[120] Xu, X., Werner, M., Butzin, M., and Lohmann, G. (2012). Water isotope variations in the global ocean model mpi-om. *Geoscientific Model Development*, 5(3):809–818.

[121] Zhang, J., Genty, D., Sirieix, C., Verdet, C., Mateo, S., Devaux, L., Sgubin, G., Bujan, S., Minster, B., Régnier, E., et al. (2023). Data-model comparisons of isotopic and hydrological variabilities of the karstic vadose zone above villars cave, sw-france based on 20 years' monitoring record. *Chemical Geology*, 631:121802.

12 Appendix

12.1 Curriculum Vitae

Tim Martin Liesenhoff

Anni-Eisler-Lehmann Straße 8a

55122 Mainz, Germany

Phone: +49 157 72014602

Email: tliesenh@students.uni-mainz.de

Date of Birth: August 11, 1993

Nationality: German

Education

2022 – 2025:	PhD Candidate, Johannes Gutenberg University Mainz, Speleothem Research Group (Prof. Dr. Denis Scholz)
2015 – 2022:	B.Sc. and M.Sc. in Geosciences
2012 – 2015:	Undergraduate studies in Chemistry (transitioned to Geosciences)
2005 – 2012:	Max-von-Laue Gymnasium Koblenz, High School Diploma
2003 – 2005:	Augustschule Neuhäusel, Primary School

Work Experience

2012 – 2021:	Private Tutoring (focus on English and Chemistry)

Skills

- Advanced proficiency in English and Chemistry
- Skilled in statistical data analysis and climate simulation modeling
- Strong IT skills (Microsoft Office, Python, LaTeX)

12.2 Nutzung KI Tools / Use of AI-Based Tools

AI Tool	Task	Purpose	When
Microsoft Copilot	Keyword generation	Finding literature keywords	Literature review
Microsoft Copilot	BibTeX formatting	Clean bibliography	Literature review
Microsoft Copilot	Concept Explanation	Answering conceptual questions	Literature review
PyCharm AI Assistant	Code optimization	Improve readability & speed	Coding
Microsoft Copilot	Text refinement	Improve readability	Writing process
Microsoft Copilot	LateX formatting	Improve layout	Writing process

Artificial intelligence (AI) tools were used to assist with code optimization and linguistic refinement during the preparation of this dissertation. No scientific content or interpretations were generated by AI; all domain-specific analyses and conclusions reflect the author's own expertise.

Place, Date: _____ Signature: _____